



## **Terms and Conditions of Use of Digitised Theses from Trinity College Library Dublin**

### **Copyright statement**

All material supplied by Trinity College Library is protected by copyright (under the Copyright and Related Rights Act, 2000 as amended) and other relevant Intellectual Property Rights. By accessing and using a Digitised Thesis from Trinity College Library you acknowledge that all Intellectual Property Rights in any Works supplied are the sole and exclusive property of the copyright and/or other IPR holder. Specific copyright holders may not be explicitly identified. Use of materials from other sources within a thesis should not be construed as a claim over them.

A non-exclusive, non-transferable licence is hereby granted to those using or reproducing, in whole or in part, the material for valid purposes, providing the copyright owners are acknowledged using the normal conventions. Where specific permission to use material is required, this is identified and such permission must be sought from the copyright holder or agency cited.

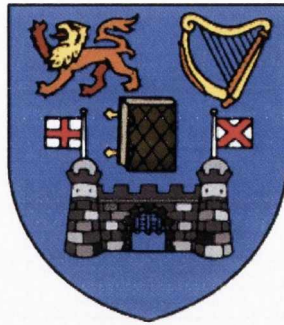
### **Liability statement**

By using a Digitised Thesis, I accept that Trinity College Dublin bears no legal responsibility for the accuracy, legality or comprehensiveness of materials contained within the thesis, and that Trinity College Dublin accepts no liability for indirect, consequential, or incidental, damages or losses arising from use of the thesis for whatever reason. Information located in a thesis may be subject to specific use constraints, details of which may not be explicitly described. It is the responsibility of potential and actual users to be aware of such constraints and to abide by them. By making use of material from a digitised thesis, you accept these copyright and disclaimer provisions. Where it is brought to the attention of Trinity College Library that there may be a breach of copyright or other restraint, it is the policy to withdraw or take down access to a thesis while the issue is being resolved.

### **Access Agreement**

By using a Digitised Thesis from Trinity College Library you are bound by the following Terms & Conditions. Please read them carefully.

I have read and I understand the following statement: All material supplied via a Digitised Thesis from Trinity College Library is protected by copyright and other intellectual property rights, and duplication or sale of all or part of any of a thesis is not permitted, except that material may be duplicated by you for your research use or for educational purposes in electronic or print form providing the copyright owners are acknowledged using the normal conventions. You must obtain permission for any other use. Electronic or print copies may not be offered, whether for sale or otherwise to anyone. This copy has been supplied on the understanding that it is copyright material and that no quotation from the thesis may be published without proper acknowledgement.



# Mechanical Properties of Advanced Nanostructured Composite Fibres Containing Carbon Nanotubes and Graphene

By

Karen Young

A thesis submitted for the degree of  
Doctor of Philosophy  
in the University of Dublin.

School of Physics,  
Trinity College Dublin,

2012



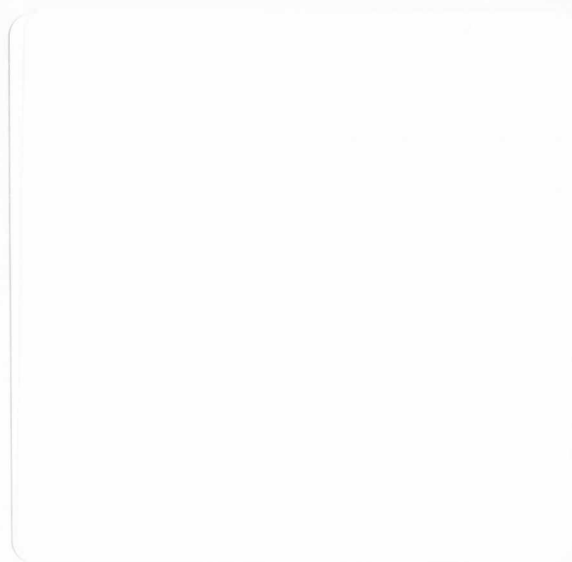
Thesis 9513

## **Declaration**

I declare that the work in this thesis has not been previously submitted as an exercise for a degree to this or any other university.

The work described herein is entirely my own, except for the assistance mentioned in the acknowledgements and the collaborative work mentioned in the list of publications.

I agree to deposit this thesis in the University's open access repository or allow the library to do so on my behalf, subject to Irish Copyright Legislation and Trinity College Library conditions of use and acknowledgement.





*Dedicated to my parents, sister  
& grandparents*



Equipped with his five senses, man explores the universe around him and calls the  
adventure science.

*Edwin Powell Hubble*

You do not really understand something unless you can explain it to your grandmother.

*Albert Einstein*

Physicists define stress as force per unit area. The rest of humanity define stress as  
physics.

*Unknown*

## Abstract

A comprehensive study of the mechanical properties of coagulation spun poly(vinyl) alcohol-nanotube composite fibres has been performed. A method has been developed to control and measure the nanotube volume fraction,  $V_f$ , in these fibres. Both the fibre modulus,  $Y$ , and strength,  $\sigma_B$ , scale linearly with  $V_f$  up to a maximum effective nanotube content of  $V_f \sim 10\%$ , after which these properties remain constant. It was found that  $dY/dV_f = 254$  GPa and  $d\sigma_B/dV_f = 2.8$  GPa in the linear region. These values correspond to the effective modulus and strength respectively, which nanotubes contributed to the composite. By drawing fibres with  $V_f < 10\%$  to a draw ratio of  $\sim 60\%$ , these values can be increased to  $dY/dV_f = 600$  GPa and  $d\sigma_B/dV_f = 7$  GPa. Raman measurements show the Herman's orientation parameter,  $S$ , to increase with drawing, indicating that significant nanotube alignment occurs. Raman spectroscopy also shows that the nanotube effective modulus,  $Y_{Eff}$ , also increases with drawing due to the increased alignment. As expected for simple composites, the undrawn samples display  $dY/dV_f = Y_{Eff}$ . However, for draw ratios above 22%,  $dY/dV_f > Y_{Eff}$ , suggesting that drawing induces polymer crystallinity. An empirical relationship between the nanotube orientation efficiency factor,  $\eta_o$ , and  $S$  has been calculated. The data for  $Y_{Eff}$  versus  $\eta_o$  was fitted showing that the fibre modulus scales linearly with  $\eta_o$ , as predicted theoretically by Krenchel. From the fit, the actual Young's modulus of the nanotubes used in this work was estimated to be  $Y_{NT} = 480$  GPa. This value is about half of the expected value of 1 TPa, suggesting that these composites are limited either by an imperfect polymer-nanotube interface or that the nanotubes are less stiff than expected. It is shown that the fibre strength also scales linearly with  $\eta_o$ . The effective interfacial stress transfer can be estimated to be  $\tau = 40$  MPa and the nanotube critical length to be  $l_c = 1250$  nm.

When normalised to nanotube volume fraction, both fibre modulus, and strength, scale strongly with fibre diameter,  $D$ :  $Y/V_f \propto D^{-1.55}$  and  $\sigma_B/V_f \propto D^{-1.75}$ . It is shown that much of this dependence is attributable to correlation between  $V_f$  and  $D$  due to details of the spinning process:  $V_f \propto D^{0.93}$ . However, by carrying out Weibull failure analysis and measuring the orientation distribution of the nanotubes, it is shown that the rest of the diameter dependence is due to a combination of defect and orientation effects. For a given nanotube volume fraction the fibre strength scales as  $\sigma_B \propto D^{-0.29} D^{-0.64}$  with the first and second terms representing the defect and orientation contributions respectively. The orientation term is present and dominates for fibres of diameter between 4 and 50  $\mu\text{m}$ .

By preparing fibres with low diameter, mean mechanical properties as high as  $Y=244$  GPa and  $\sigma_B=2.9$  GPa have been obtained.

An alternative method of composite fibre production was also introduced. A combination of solution processing and melt processing was used to form composites made from the thermoplastic polyethylene terephthalate (PET). Composite fibres based on the polyester, PET filled with both nanotubes and graphene were prepared by a combination of solution and melt processing. On addition of  $\leq 2\text{wt}\%$  filler, increases in both modulus and strength by factors of  $\times 2$  to  $\times 4$  were observed for both fillers. For the nanotube-based fibres, the mechanical properties depend strongly on fibre diameter due to a combination of orientation and defect effects. For the graphene filled fibres, the modulus is invariant with diameter while the strength is defect limited, scaling weakly with diameter. Using this method, the best fibre prepared had modulus and strength of 42 GPa and 1.2 GPa respectively. This is attributed to the excellent reinforcement predominately to the dispersion quality resulting from the solvent exfoliation of both nanotubes and graphene.

## Acknowledgements

The past four years have been a challenging but a very enjoyable experience and there are many people who I would like to thank for their help and support along the way. First and foremost I would like to thank my supervisor Prof. Jonathan Coleman who was always available for help and guidance. I cannot emphasise how reliable and supportive my supervisor has been and was always there to guide my project in the right direction.

I would also like to particularly thank several people who helped with my research. Fiona Blighe helped me greatly, from getting my project off the ground to shaping it into work that could be published. Thanks for all your help throughout my time working here. To Umar Khan who helped me a lot, especially towards the end of my PhD. I would also like to thank Shane Bergin who has been a great friend throughout this experience. I remember when I started working in the group that Shane said that “doing a PhD is a marathon and not a sprint”. This was great advice and I have always tried to work steadily throughout my four years here (with a bit of a sprint near the end)!

I would also like to thank the many friends that I have made throughout the past four years and in particular those who have proof read chapters of my thesis. Having great friends like you made the experience of doing a PhD really enjoyable. Thanks to Marguerite who started her PhD at the same time as me and has sat beside me for the four years. Also thanks to Arlene who helped me with graphene parts in the final few months. Thanks to Darren who, along with being a great friend, helped me solve the many, many computer problems I have had. Thanks also to Mustafa, Paul, Peter, Sophie, Phil, Evelyn, Anna, Trevor, Will, Grahame, Tom and Sukanta. Also thanks to the group members who have left; David Blond (thankfully neither of us were hurt while electrospinning), Yenny, Helen, David R, Paula, Niall, Eddie, Brian, Emer and Valeria. Thanks to Denise for your many kind words throughout my time here and helping me see the light at the end of the tunnel.

Thanks to the fantastic administrative and technical staff in physics, both past and present. To the technicians and the workshop who have been there for support throughout my time here. Thanks to John Kelly, David, Dave, Pa, Gordon, Mick, Jemmer, Safety Joe, Nigel and Ken. Thanks especially to Gillian and Pat who let me borrow the physics experiments when I was doing demonstrations in schools. Also thanks to Robbie (who sorted us out when we were stranded at a conference during the ash cloud when all the flights were grounded), Samantha, Marie, Ciara, Rebecca and Jeanette who are responsible for the smooth running of the school of physics. Thanks to the CMA and AML workers especially Neal and to Cathal. Thanks also to Manuel who helped with my

TGAs and saved me loads of time. Thanks also to our collaborators, especially to Juan who helped me a lot and was very welcoming on my visit to Cambridge.

I would also like to thank my friends from home who put up with me during my PhD. You've always been there to make sure I take time out. Hopefully, by now you have some idea about what I do. Thanks to Fiona Mc Ardle, Caroline, Dave Brody, Laura and Emma who have been great friends to me.

I would also like to thank my good friends from undergrad who are also finishing up PhDs. Lina Persechini has been a great friend for the past 8 years. I will miss our 4 o'clock tea breaks! Thanks to Alan Bell and also to Joe Roche and Dave Long (the astros). I think the tea breaks, especially during the last year have kept us all sane. Hopefully see you all at the summer graduation!

I would also like to thank Paul Durcan who has encouraged me in everything I wanted to do. You have been so supportive over the past few years and I really appreciate this. Thanks for listening to practice talks, for proof reading my thesis and for coming to see me give presentations as well as making me take time out.

Lastly, I would like to thank my family who have supported and encouraged me from the start, who helped me pick my college course and my subjects, listened to practice presentations and proof read my thesis. I would like to thank my mam Lorraine, my dad David and my sister Lorna. Thanks for giving me the confidence to get this far! I would also like to thank my grandparents May and Gerry for their encouragement and support.

I better finish up on my acknowledgements or they will need their own chapter! I have really enjoyed doing my PhD. I am so happy to have made such lovely friends and to have so many people around me who have made this journey a really enjoyable and rewarding experience.

## Table of Contents

### Chapter 1: Motivation and Thesis Outline

1.1	Motivation	(1)
1.2	Thesis Outline	(3)
1.3	References	(4)

### Chapter 2: Theory and Background

2.1	Introduction	(7)
2.2	Polymers	(7)
2.2.1	Mechanical Properties of Polymers	(8)
2.3	Introduction to Composites	(12)
2.3.1	Theory of Polymer Matrix Reinforcement	(13)
2.4	Carbon Nanotubes	(16)
2.4.1	Structure of Single Walled Carbon Nanotubes	(16)
2.4.2	Electronic Properties of Single Walled Carbon Nanotubes	(18)
2.4.3	Physical Properties of Single Walled Carbon Nanotubes	(21)
2.4.4	Production and Synthesis of Single Walled Carbon Nanotubes	(22)
2.4.5	Applications and Limitations of Single Walled Carbon Nanotubes	(23)
2.5	Mechanical Reinforcement in Carbon Nanotube Polymer Composites	(24)
2.5.1	Solution Processing of Composites	(24)
2.5.2	Melt Processing of Composite Films and Fibres	(26)
2.5.3	Novel Composites	(28)
2.5.4	Fibres and Fibre Composites	(31)
2.5.5	Coagulation Spun Carbon Nanotube Composite Fibres	(32)
2.6	Introduction to Graphene	(37)
2.6.1	Reinforcement of Polymers using Graphene	(38)
2.7	Conclusions	(39)
2.8	References	(40)

### Chapter 3: Materials and Methods

3.1	Introduction	(47)
3.2	Materials	(47)
3.2.1	Poly(vinyl) alcohol	(47)

3.2.2	Polyethylene Terephthalate	(48)
3.2.3	Carbon Nanotubes	(49)
3.2.4	Graphene	(49)
3.2.5	Surfactant Choice	(49)
3.2.6	Solvent Choice	(50)
3.3	Methods	(50)
3.3.1	Sonication	(51)
3.3.2	Coagulation Spinning Process	(51)
3.3.3	Melt Processing of Fibres	(52)
3.3.4	UV-Vis Spectroscopy	(53)
3.3.5	Thermogravimetric Analysis	(54)
3.3.6	Profilometry	(54)
3.3.7	Mechanical Measurements	(55)
3.3.8	Scanning Electron Microscopy	(58)
3.3.9	Raman Spectroscopy	(59)
3.3.10	Atomic Force Microscopy	(61)
3.3.11	X Ray Diffraction	(61)
3.3.12	Transmission Electron Microscopy	(62)
3.4	References	(62)

#### Chapter 4: The Effect of Nanotube Content and Orientation on the Mechanical Properties of Polymer–Nanotube Composite Fibres: Separating Intrinsic Reinforcement from Orientational Effects

4.1	Introduction	(65)
4.2	Background	(67)
4.3	Experimental Procedure	(67)
4.4	Results and Discussion	(69)
4.4.1	As Prepared Fibres	(69)
4.4.2	Fibre Drawing	(76)
4.4.3	Measurement of Nanotube Effective Modulus	(81)
4.4.4	Measurement of Polymer Orientation in PVA-NT Fibres by X-Ray Diffraction	(82)
4.4.5	Correlation of Fibre Modulus with $\eta_0$	(83)
4.4.6	Fibre Strength	(86)
4.5	Conclusions	(87)

## Chapter 5: Strong Dependence of Mechanical Properties on Fibre Diameter for Polymer–Nanotube Composite Fibres: Differentiating Defect from Orientation Effects

5.1	Introduction	(91)
5.2	Experimental Procedure	(93)
5.3	Results and Discussion	(93)
5.3.1	Fibre Formation	(93)
5.3.2	Mechanical Properties	(95)
5.3.3	Fibre Strength: Defects	(100)
5.3.4	Fibre Strength: Nanotube Orientation	(103)
5.3.5	Young’s Modulus	(106)
5.3.6	Relative Contribution of Defects and Orientation	(107)
5.4	Conclusions	(108)
5.5	Appendix. Table of Fibre Properties	(109)
5.6	References	(110)

## Chapter 6: High Strength Composite Fibres from Polyester Filled with Nanotubes and Graphene

6.1	Introduction	(113)
6.2	Background	(115)
6.3	Experimental Procedure	(116)
6.3.1	Dispersion of Graphene	(117)
6.3.2	Dispersion of Nanotubes	(117)
6.3.3	Estimation of Nanotube and Graphene Concentration	(117)
6.3.4	Melt Processing of PET Fibres	(118)
6.4	Results and Discussion	(119)
6.4.1	PET-Nanotube Fibres: Volume Fraction Dependence	(119)
6.4.2	PET-Nanotube Fibres: Diameter Dependence	(122)
6.4.3	PET-Graphene Fibres	(124)
6.4.4	PET-Graphene Fibres: Volume Fraction Dependence	(126)
6.4.5	PET-Graphene Fibres: Diameter Dependence	(129)

6.4.6	Comparison of Mechanical Properties with Previous Work on PET-Nanotube Composites	(131)
6.5	Conclusions	(133)
6.4	References	(134)

## Chapter 7: Conclusions and Future Work

7.1	Conclusions	(139)
7.2	Future Work	(140)
7.3	List of Publications	(142)
7.4	References	(142)

# Chapter 1

## Motivation and Thesis Outline

### 1.1 Motivation

Mankind's exploitation of materials has defined various ages; from primitive stone tools to early metallurgy and right through to the present day. Our ability to invent, discover and modify materials has fuelled our intellectual and technological evolution. Nanoscale materials represent a massive leap forward in materials science. Materials on the nanoscale behave very differently to materials on the macroscale. This is partially due to the increased surface area which is created when materials get smaller and also due to the quantum effects which become apparent at the nanoscale. The unique quantum and surface phenomena that nano-materials exhibit can open doors to new applications in areas such as medicine, construction and the electronics industry. Like the changes new materials brought in previous ages, nanotechnology will pave the way for significant changes in the way people live and work. Richard P. Feynman lay the foundations for nanotechnology in his lecture in 1959 entitled "There's Plenty of Room at the Bottom". He discussed the direct manipulation of matter on the atomic scale. His ideas were later realised through the use of scanning tunnelling microscopes and atomic force microscopes.

In order to provide a bridge between the nanoscale and the macroscale, composites are often used. Composites consist of two or more materials which, when combined, produce a new material with enhanced properties. The material which requires reinforcement is often

referred to as the matrix and the reinforcing agent is known as the filler. In nanotechnology research, the matrix is very often a polymer material.

Polymers are cheap, readily available, lightweight and easy to process. However, the mechanical properties of polymers are often lacking, especially for high strength applications. This is where the role of composites becomes important. A filler can be added to the polymer and can result in significant increases in the mechanical properties of the resulting material. An ideal filler for a polymer possesses good mechanical properties, is lightweight and has a high aspect ratio.

Fibreglass and carbon fibres are commonly used filler materials. Over the past 60 years, carbon fibres have been developed and are used for reinforcement in composites due to their high strength. They are currently being used to reinforce aircraft<sup>1</sup>, sports equipment<sup>2</sup> and infrastructure<sup>3</sup> along with many other materials. Carbon fibres work well because of their good strengths and high aspect ratio which is important for stress transfer. In order to progress further and achieve superior composite reinforcement, a filler with a higher aspect ratio and higher strength than carbon fibres is required. Carbon nanotubes are such a material. Not only do carbon nanotubes have a higher aspect ratio than carbon fibres, they are also stronger and less dense. Carbon nanotubes are nanoscale cylinders of carbon with remarkable mechanical, electrical and thermal properties<sup>4</sup>. They are approximately 150 times stronger than steel<sup>5,6</sup> yet they are about 5 times less dense. In order to harness the superlative properties that nanotubes possess, they are usually incorporated into a polymer. By combining carbon nanotubes with polymers, very strong composite materials can be produced; such composites will be the basis of this thesis. Carbon nanotubes have been incorporated into composite films<sup>7-13</sup> and fibres<sup>14-28</sup> for many years and have shown huge promise, particularly in the area of carbon nanotube polymer composite fibre research. Polymer-nanotube composite fibres have been prepared and investigated for over 10 years<sup>29</sup>. However, there are many issues within fibre research that are unresolved.

This work aims to confront these issues by investigating the role of filler content, nanotube orientation and the effect of diameter on the properties of a fibre. This can be done by using an established method of coagulation spinning and also, by using a novel combination of solution and melt processing for fibre production. The work presented here

aims to connect the nanoscale with the macroscale and to give some insight into what makes a fibre strong.

## **1.2 Thesis Outline**

This thesis consists of 8 chapters:

Chapter 2 introduces the theory and background of polymers and composite materials. A description is given of how composite reinforcement can be effectively achieved using materials like carbon nanotubes and graphene. The properties, production methods and applications of these materials are also discussed.

Chapter 3 describes the materials and methods used to prepare, analyse and characterise composite fibres produced. A description of coagulation spinning is presented which is the main fibre production method used throughout this thesis. The characterisation techniques used for this work, including mechanical testing and thermogravimetric analysis are also discussed.

In chapter 4, the effect of nanotube content on the mechanical properties of polymer-nanotube composite fibres is investigated. It is well known that reinforcement scales with nanotube content, however the rate of increase of fibre stiffness and strength and also the maximum achievable loading level has not been found for coagulation spun fibres. The effect of alignment on the mechanical properties of the fibre is also discussed. These properties determine the maximum strength and stiffness attainable and are very important measurements for composites.

In chapter 5, the dependence of mechanical properties on fibre diameter for polymer-nanotube composite fibres is discussed. There are two main factors which contribute to this diameter dependence; nanotube orientation and defects. These effects and their relative importance on the mechanical properties of the composite are discussed in detail in chapter 5.

In chapter 6, the properties of PET-nanotube and PET-graphene fibres produced using a combination of solution and melt processing are discussed. The variation of mechanical properties with nanotube and graphene volume fraction is also investigated. The mechanical properties of these fibres are compared with other types of fibres which are currently being produced.

Chapter 7 contains summaries of the conclusions from chapters 4, 5 and 6 along with future work that could be undertaken in this area of research. Chapter 7 also contains a list of publications.

### 1.3 References

- 1 Soutis, C. Carbon fiber reinforced plastics in aircraft construction. *Materials Science and Engineering: A* **412**, 171-176 (2005).
- 2 Tsai, C. Bicycle wheel and the manufacturing method. United States Patent. (1991).
- 3 Fu, X. & Chung, D. D. L. Self-monitoring of fatigue damage in carbon fiber reinforced cement. *Cement and Concrete Research* **26**, 15-20 (1996).
- 4 Coleman, J. N., Khan, U., Blau, W. J. & Gun'ko, Y. K. Small but strong: A review of the mechanical properties of carbon nanotube-polymer composites. *Carbon* **44**, 1624-1652 (2006).
- 5 Callister, W. D. *Materials Science and Engineering An Introduction*. (2007).
- 6 Yu, M.-F. *et al.* Strength and Breaking Mechanism of Multiwalled Carbon Nanotubes Under Tensile Load. *Science* **287**, 637-640 (2000).
- 7 Wang *et al.* The extraordinary reinforcing efficiency of single-walled carbon nanotubes in oriented poly(vinyl alcohol) tapes. Vol. 18 (*Institute of Physics*, 2007).
- 8 Shaffer, M. S. P. & Windle, A. H. Fabrication and Characterization of Carbon Nanotube/Poly(vinyl alcohol) Composites. *Advanced Materials* **11**, 937-941 (1999).
- 9 Cadek, M., Coleman, J. N., Barron, V., Hedicke, K. & Blau, W. J. Morphological and mechanical properties of carbon-nanotube-reinforced semicrystalline and amorphous polymer composites. *Applied Physics Letters* **81**, 5123-5125 (2002).
- 10 Zhang, X. *et al.* Poly(vinyl alcohol)/SWNT Composite Film. *Nano Letters* **3**, 1285-1288 (2003).
- 11 Cadek, M. *et al.* Reinforcement of Polymers with Carbon Nanotubes: The Role of Nanotube Surface Area. *Nano Letters* **4**, 353-356 (2004).
- 12 Munoz, E. *et al.* Multifunctional carbon nanotube composite fibers. *Advanced Engineering Materials* **6**, 801-804 (2004).
- 13 Coleman, J. N. *et al.* Reinforcement of polymers with carbon nanotubes. The role of an ordered polymer interfacial region. Experiment and modeling. *Polymer* **47**, 8556-8561 (2006).
- 14 Dalton, A. B. *et al.* Super-tough carbon-nanotube fibres. *Nature* **423**, 703-703 (2003).
- 15 Miaudet, P. *et al.* Hot-Drawing of Single and Multiwall Carbon Nanotube Fibers for High Toughness and Alignment. *Nano Letters* **5**, 2212-2215 (2005).
- 16 Minus, M. L., Chae, H. G. & Kumar, S. Interfacial Crystallization in Gel-Spun Poly(vinyl alcohol)/Single-Wall Carbon Nanotube Composite Fibers. *Macromolecular Chemistry and Physics* **210**, 1799-1808 (2009).
- 17 Vigolo, B. *et al.* Macroscopic Fibers and Ribbons of Oriented Carbon Nanotubes. *Science* **290**, 1331-1334 (2000).
- 18 Badaire, S. *et al.* Correlation of properties with preferred orientation in coagulated and stretch-aligned single-wall carbon nanotubes. *Journal of Applied Physics* **96**, 7509-7513 (2004).

- 19 Pichot, V. *et al.* Structural and mechanical properties of single-wall carbon nanotube fibers. *Physical Review B* **74**, 245416 (2006).
- 20 Poulin, P., Vigolo, B. & Launois, P. Films and fibers of oriented single wall nanotubes. *Carbon* **40**, 1741-1749 (2002).
- 21 Vigolo, B., Poulin, P., Lucas, M., Launois, P. & Bernier, P. Improved structure and properties of single-wall carbon nanotube spun fibers. *Applied Physics Letters* **81**, 1210-1212 (2002).
- 22 Muñoz, E. *et al.* Multifunctional Carbon Nanotube Composite Fibers. *Advanced Engineering Materials* **6**, 801-804 (2004).
- 23 Zhang, X. *et al.* Gel spinning of PVA/SWNT composite fiber. *Polymer* **45**, 8801-8807 (2004).
- 24 Minus, M. L., Chae, H. G. & Kumar, S. Single wall carbon nanotube templated oriented crystallization of poly(vinyl alcohol). *Polymer* **47**, 3705-3710 (2006).
- 25 Miaudet, P. *et al.* Thermo-electrical properties of PVA-nanotube composite fibers. *Polymer* **48**, 4068-4074 (2007).
- 26 Razal, J. *et al.* Arbitrarily Shaped Fiber Assemblies from Spun Carbon Nanotube Gel Fibers. *Advanced Functional Materials* **17**, 2918-2924 (2007).
- 27 Almecija, D., Blond, D., Sader, J. E., Coleman, J. N. & Boland, J. J. Mechanical properties of individual electrospun polymer-nanotube composite nanofibers. *Carbon* **47**, 2253-2258 (2009).
- 28 Kannan, P. & *et al.* Deformation of isolated single-wall carbon nanotubes in electrospun polymer nanofibres. *Nanotechnology* **18**, 235707 (2007).
- 29 Haggemueller, R., Gommans, H. H., Rinzler, A. G., Fischer, J. E. & Winey, K. I. Aligned single-wall carbon nanotubes in composites by melt processing methods. *Chemical Physics Letters* **330**, 219-225 (2000).



# Chapter 2

## Theory and Background

### 2.1 Introduction

This chapter begins by introducing polymers and polymer fibres. Polymers are lightweight, cheap and readily available. However for high strength applications, polymer composites are more suited. Polymer composites and the theory of polymer matrix reinforcement are introduced. Because of their exceptional mechanical and electrical properties, carbon nanotubes are ideal fillers for composite reinforcement. The remarkable properties that carbon nanotubes possess will be subsequently discussed. Mechanical reinforcement in carbon nanotube based composites and coagulation spun fibres will also be explained in detail. Graphene offers an alternative route for composite reinforcement. This chapter also includes an introduction to graphene and graphene based composites.

### 2.2 Polymers

Polymers are macromolecules consisting of long chains of repeating units joined together by covalent bonds. Polymers can be naturally occurring or can be synthesised<sup>1</sup>. They are ideal for use in composites due to their low density, low cost and ease of production. Though generally weaker than most metals or ceramics they can be mechanically reinforced using fillers like carbon nanotubes<sup>2-13</sup>. An example of a very common polymer is polyethylene. The repeating unit of polyethylene is shown in brackets in figure 2.1 and consists of a chain of carbon atoms, each of which are attached to two hydrogen atoms. The “n” in figure 2.1 indicates how many repeating units there are (degree of polymerisation).

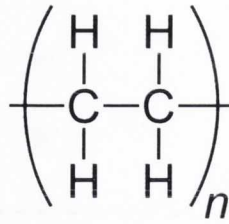


**Figure 2.1 Structure of polyethylene**

Polymers can be classified into groups based on their mechanical properties as plastics, elastomers or fibres and into further sub groups as shown in figure 2.2.

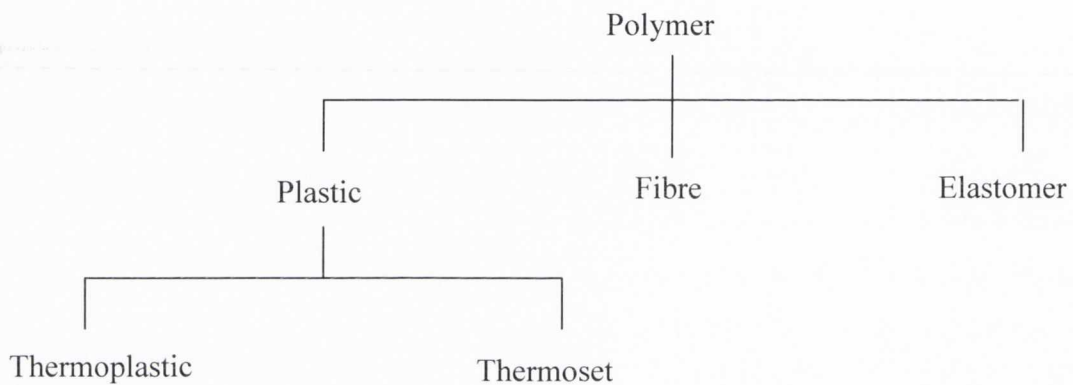


**Figure 2.2: Polymer classification**

### 2.2.1 Mechanical Properties of Polymers

The mechanical differences between various types of polymers can be examined by carrying out mechanical measurements. Samples are pulled apart at a set rate and the force per unit area (or stress) is recorded as a function of strain. The Young's modulus can be found from the slope of the stress-strain curve as the strain approaches zero and is a measure of the stiffness of the polymer. The ultimate tensile strength is found from the highest stress on the graph and the area under the curve gives the toughness. The percentage elongation can be found from the highest strain on the graph. Typical mechanical properties of some common materials along with some polymers and also carbon nanotubes are shown in table 2.1.

Material	Tensile Strength (MPa)	Young's Modulus (GPa)
Nanotubes <sup>14</sup>	63000	950
Nylon Fibre <sup>15</sup>	1000	19
Steel <sup>1</sup>	380	207
Copper <sup>1</sup>	200	110
Aluminium <sup>1</sup>	90	69
Titanium <sup>1</sup>	520	107
Bulk Polyvinyl Chloride (PVC) <sup>16</sup>	56.6	2.9
Bulk Polyester (PET) <sup>16</sup>	50	1.7
Bulk Poly(vinyl) alcohol (PVA) <sup>16</sup>	110	37

**Table 2.1: Typical mechanical properties of some common materials.**

Sample stress-strain curves for various polymer types are shown in figure 2.3.

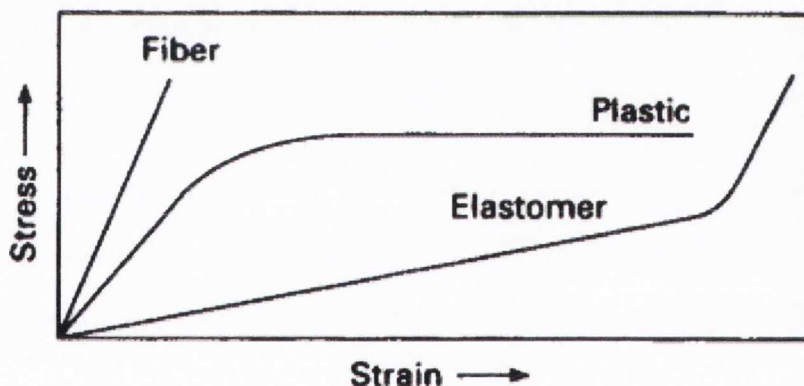


**Figure 2.3: Typical stress-strain curves for elastomers, plastics and fibres<sup>17</sup>.**

Elastomers are polymers that can undergo very large and reversible deformations. Elastomeric behaviour was first observed in natural rubber however elastomers can also be synthesised<sup>1</sup>. Natural rubber can be stretched by up to 850% before fracture. It has a tensile strength of up to 25 MPa and a Young's modulus of 2 MPa<sup>16</sup>. Polyurethane is an example of a common synthetic rubber which is used in car bumpers<sup>18</sup>, conveyor belts<sup>19</sup> and car steering wheels<sup>20</sup>. Polyurethanes have been shown to have an elongation of 2100%<sup>21</sup> and a tensile strength of 45 MPa<sup>16</sup>.

Plastics represent a large range of materials with behaviour between that of a fibre and an elastomer. Plastics can be divided up into two sub categories; thermoplastics and thermosets. Thermoplastic polymers soften when heated and harden when cooled. The heating and cooling processes can easily be repeated and reversed as required. Examples of thermoplastics are polystyrene, poly(vinyl) chloride and polyethylene terephthalate (PET). The typical strength and modulus of bulk PET is 50 MPa and 1.7 GPa respectively and its percentage elongation is approximately 180%<sup>16</sup>. Conversely, thermosets are network polymers which have crosslinks between adjacent chains. Crosslinks secure polymer chains together when heated which causes them to resist movement. Typically 10-50% of the chains are crosslinked<sup>1</sup>. Epoxies are thermosetting polymers and typical strengths of 90 MPa and a Young's modulus of 5 GPa<sup>16</sup>.

Another category of polymers are polymer fibres, which undergo low elongations. Because the polymer chains are closely packed, fibres have a high Young's modulus and tensile strength. Drawing of fibres can induce crystallisation in the fibre which enhances the mechanical strength. Fibres have become a very important part of modern life, from their use in textiles like nylon to their use in bullet proof vests<sup>22</sup>. Nylon 6,6 is a commonly used fibre due to its high strength of up to 1 GPa. It also has a modulus of elasticity of 19 GPa and an elongation to break of between 5-25%<sup>15</sup>.

Polymer based fibres offer a very promising route to producing high strength materials. The focus of this thesis is on polymer nanotube composite fibres. There are many types of high performance fibres already being produced. These fibre types will be introduced briefly here as a comparison to the fibres which will be discussed in chapters 4, 5 and 6. They can be split up into several categories:

1. Aramids
2. High performance polyethylene fibres
3. Other high strength high modulus fibres from linear polymers
4. Ceramic fibres
5. Glass fibres
6. Carbon fibres

Aromatic polyamide fibres (or aramid fibres) are strong heat resistant synthetic fibres which have polymer chains highly oriented along the fibre axis. In 1971, a new high performance fibre, Kevlar® was discovered. It is produced by Dupont and it is a

high strength organic fibre made of polyphenylene terephthalamide (PPTA) with an alternation of benzene rings and amide groups and is a type of aramid (figure 2.4).

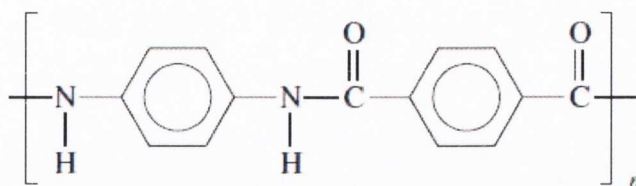


**Figure 2.4: Structure of Kevlar<sup>23</sup>.**

The maximum tensile strength and Young's modulus of Kevlar 49 is 3.6 GPa and 124 GPa respectively. The elongation to break is 2.4%. The toughness of Kevlar is approx 33 J/g<sup>24</sup>. The polymer chains align and are oriented parallel to the fibre axis. There is inter-chain hydrogen bonding between the amide groups in the polymer chains. This, along with its crystallinity contributes to Kevlar's high strength. Because of its impressive mechanical properties, Kevlar currently is being utilised in many composite applications for example in bullet proof vests<sup>22</sup>, boat sails<sup>25</sup> and in bicycle tyres<sup>26</sup>. It is twice as strong and has a modulus nine times higher than high strength nylon<sup>27</sup>.

Other high performance fibres include high performance polyethylene (PE) fibres which are produced by a gel spinning process. Dyneema® is an example of a commercially available fibre of this kind and is constructed of ultra high molecular weight polymers. These fibres have strength values of 3.6 GPa and Young's modulus values of 116 GPa<sup>23</sup>. They typically have an elongation to break of 4%. They have a low density and high energy absorption at break, so these materials are ideal for application in ballistic protection<sup>28</sup>.

Highly ordered polymers such as poly(p-phenylene-2,6-benzobisoxazol) (PBO) also have impressive fibre properties with strengths of 5.8 GPa and Young's modulus of 280 GPa. It is commonly sold under the commercial name Zylon. PBO also has remarkable thermal properties and is flame resistant. It starts to decompose at temperatures above 600 °C. In comparison, Kevlar decomposes at temperatures above 500 °C<sup>16</sup>. Nasa are particularly interested in this material due to its combination of superior strength and thermal properties. It can also be used in the protective clothing of fire fighters<sup>29</sup>.

Ceramic fibres have the advantage over other fibres as they can withstand very high temperatures above 1000 °C. Fibres constructed of 96 wt% silicon carbide have

strengths of up to 3 GPa<sup>23</sup>. Because they can withstand extreme conditions, ceramics can be used in internal combustion engines<sup>30</sup>, for aerospace applications<sup>31</sup> and in the walls of nuclear fusion reactors<sup>32</sup>.

Another type of fibre are glass fibres which are important for many industrial applications such as in optical fibres<sup>33</sup>, insulation<sup>34</sup> or for reinforcement<sup>35</sup> and have strengths of up to 3.5 GPa<sup>23</sup>.

Carbon fibres have been developed for about the last 60 years. They are fibres derived from the element carbon in which graphitic sheets are ordered parallel to the fibre axis. Polyacrylonitrile (PAN) based carbon fibres are the most popular type of carbon fibre with strengths of up to 7 GPa produced by Toray Industries Inc. Materials reinforced with carbon fibres are stronger than glass fibre reinforced materials<sup>1</sup>. They are currently being used in aircraft<sup>36</sup>, sports equipment<sup>37</sup>, infrastructure<sup>38</sup> and many other applications. Table 2.2 summaries typical ultimate tensile strength (UTS), Young's modulus (Y) and strain at break ( $\epsilon_B$ ) values for various types of fibres.

Fibre Type	UTS (MPa)	Y (GPa)	$\epsilon_B$ (%)
Toray Carbon fibres	7060	294	2
PBO	5800	280	1.7
PPTA (Kevlar)	3600	124	2.4
PE	3600	116	4
Glass fibres	3500	87	4
Ceramic fibres	3000	390	0.75

**Table 2.2: Summary of mechanical properties of high performance fibres<sup>16,23</sup>.**

### 2.3 Introduction to Composites

As discussed previously, polymers have many attractive properties. They are easy to process, have a low density and can be produced at a low cost. However, the mechanical properties in many polymers are often lacking particularly for applications where high strength and modulus are essential. This is where the role of composites becomes important. In a composite, two materials are combined and characteristics of each material contribute to produce a hybrid material with enhanced properties.

### 2.3.1 Theory of Polymer Matrix Reinforcement

The simplest way to model a fibre reinforced composite is to apply the rule of mixtures. In the most simplified situation, an elastic matrix is filled with aligned elastic fibres which span the full length of the sample. It is assumed that there is a good bond between the matrix and the fibres such that the deformation of the matrix and the fibres is the same. The Young's modulus of the composite,  $Y_C$  in the alignment direction is given by equation 2.1:

$$Y_C = Y_M(1 - V_F) + Y_F V_F \quad 2.1$$

where  $Y_F$  is the Young's modulus of the fibre,  $Y_M$  is the Young's modulus of the matrix and  $V_F$  is the fibre volume fraction. Therefore the modulus of elasticity of the composite is equal to the volume-fraction weighted average of the moduli of elasticity of the fibre and the matrix phases<sup>1</sup>.

In the perpendicular direction, the Young's modulus is given by equation 2.2:

$$Y_C = \left( \frac{Y_M Y_F}{(1 - V_F) Y_F + V_F Y_M} \right) \quad 2.2$$

However this situation is idealised. In general the length of the fibres is much shorter than the composite. For this situation, the idea of the matrix fibre stress transfer must be introduced. This scales with length and means that shorter fibres carry load less efficiently than longer fibres<sup>39</sup>. Cox et al. considered the situation using short aligned fibres and showed that the composite modulus is given by equation 2.3<sup>40</sup>.

$$Y_C = (\eta_1 Y_F - Y_M) V_F + Y_M \quad 2.3$$

where  $\eta_1 = 1 - \frac{\text{Tanh}(a \cdot l / D)}{a \cdot l / D}$  is the length efficiency factor where  $a$  is given by

$a = \sqrt{\frac{-3Y_M}{2Y_F \ln V_F}}$ .  $D$  is the fibre diameter and  $l$  is the fibre length. This approaches 1 for

$l/D > 10$ . This verifies the importance of using high aspect ratio fillers like carbon nanotubes.

This is also a simplified situation. A more probable situation is for non aligned short fibres. Here the composite modulus is given by equation 2.4.

$$Y_C = (\eta_0 \eta_1 Y_F - Y_M) V_F + Y_M \quad 2.4$$

$\eta_0$  is the orientation efficiency factor and is equal to 1 for aligned fibres. For aligned fibres in the plane parallel to the applied force,  $\eta_0$  is equal to 3/8. For randomly oriented fibres,  $\eta_0$  is equal to 1/5<sup>39</sup>.

Another model was developed by Halpin and Tsai<sup>41</sup>. This model takes randomly oriented fibres into account and also accounts for a distribution in fibre lengths. The composite modulus can be found from equation 2.5.

$$Y_C = \frac{3}{8} \left[ \frac{1 + \zeta \eta_L V_F}{1 - \eta_L V_F} \right] Y_M + \frac{5}{8} \left[ \frac{2 + \eta_T V_F}{1 - \eta_T V_F} \right] Y_M \quad 2.5$$

where  $\zeta = \frac{2l}{D}$ ,  $\eta_L = \frac{Y_F / Y_M - 1}{Y_F / Y_M + \zeta}$  and  $\eta_T = \frac{Y_F / Y_M - 1}{Y_F / Y_M + 2}$ .

What is important to note from the rule of mixtures model and the Halpin and Tsai model is that the Young's modulus is predicted to scale with both the volume fraction and aspect ratio. A linear increase in modulus with volume fraction is also predicted<sup>39</sup>. This suggests that a good measurement of composite reinforcement is given by  $\frac{dY_C}{dV_F}$  at low  $V_F$ . This shows the magnitude of the increase in Young's modulus with respect to the volume fraction of fibre added.

Using the rule of mixtures  $\frac{dY_C}{dV_F}$  is given by equation 2.6<sup>39</sup>,

$$\frac{dY_C}{dV_F} \approx \eta_0 \eta_l Y_F - Y_M \quad 2.6$$

Using the Halpin – Tsai model  $\frac{dY_C}{dV_F}$  is given by equation 2.7<sup>39</sup>,

$$\frac{dY_C}{dV_F} \approx \frac{3}{8} Y_M \eta_L (\zeta + 1) + \frac{15}{8} Y_M \quad 2.7$$

In composites where the Young's modulus of the polymer is much less than the Young's modulus of the filler, equation 2.6 can be further approximated to

$$\frac{dY_C}{dV_F} \approx \eta_0 \eta_l Y_F \quad 2.8$$

Thus for  $\eta_0$  and  $\eta_l$  values of 1, a maximum  $\frac{dY_C}{dV_F}$  value of  $Y_F$  can potentially be achieved.

A similar calculation can be carried out for composite strength,  $\sigma_B$ . For long aligned fibres the composite strength is given by equation 2.9.

$$\sigma_B = \sigma_M(1 - V_F) + \sigma_F V_F \quad 2.9$$

where  $\sigma_F$  is the strength of the fibre,  $\sigma_M$  is the strength of the matrix and  $V_F$  is the fibre volume fraction<sup>39</sup>.

As with composite modulus, this is also a simplified situation. A more probable situation is for non aligned short fibres. Here the composite strength is given by equation 2.10<sup>42</sup>.

$$\sigma_B = (\eta_0 \eta_{l\sigma} \sigma_F - \sigma_M) V_F + \sigma_M \quad 2.10$$

Where  $\eta_0$  is the orientation efficiency factor and  $\eta_{l\sigma}$  is a length efficiency factor applicable to fibre strength.

If the polymer strength is much lower than the strength of the filler, this can be approximated to

$$\sigma_B \approx \eta_0 \eta_{l\sigma} \sigma_F V_F \quad 2.11$$

A good measurement of composite reinforcement is given by  $\frac{d\sigma_B}{dV_F}$  at low  $V_F$ . For

composites where the matrix has a much lower strength than the filler,  $\frac{d\sigma_B}{dV_F}$  is given by equation 2.12<sup>42</sup>.

$$\frac{d\sigma_B}{dV_F} \approx \eta_0 \eta_{l\sigma} \sigma_F \quad 2.12$$

The maximum achievable value for  $\frac{d\sigma_B}{dV_F}$  is  $\sigma_F$ .

When the length of the filler is less than the critical length, the strength is effectively the stress required to break the matrix-filler interfaces and to fracture the polymer in cross section. In this situation, the composite strength can be written as<sup>42</sup>:

$$\sigma_B = \left( \eta_0 \frac{l}{d} \tau - \sigma_p \right) V_f + \sigma_p \approx \eta_0 \frac{l}{d} \tau V_f \quad 2.13$$

where  $l$  and  $d$  are the filler length and diameter respectively and  $\tau$  is the matrix-filler interfacial strength or the polymer shear yield strength, whichever is lower<sup>1</sup>.

## 2.4 Carbon Nanotubes

As can be seen from table 2.2, carbon fibres have a very high strength. They also have a low density and large aspect ratio. When these fibres are added to a matrix, they offer good mechanical reinforcement and they are commonly used in aircraft<sup>36</sup> and sports equipment<sup>37</sup>. However, there is another material which rivals the mechanical properties of carbon fibres. Carbon nanotubes are 1000 times smaller, less dense and have strengths an order of magnitude higher than carbon fibres. They also have a Young's modulus which is greater than that of any carbon fibre. Their smaller size means that there is a larger surface area available for stress transfer. Nanotubes can be considered as the ultimate carbon fibre. Because of their superlative properties, they are considered to be an ideal filler and are potentially useful for countless electronic and mechanical applications; for example in field effect transistors and in reinforced composites<sup>43,44</sup>. Carbon nanotube composites could provide a new class of strong lightweight materials which would revolutionalise the world around us.

### 2.4.1 Structure of Single Walled Carbon Nanotubes

A single walled carbon nanotube (SWNT) can be described as a sheet of graphene rolled seamlessly into a cylindrical tube (figure 2.5a). Multi-walled carbon nanotubes (MWNTs) consist of multiple concentric graphene cylinders (figure 2.5b).

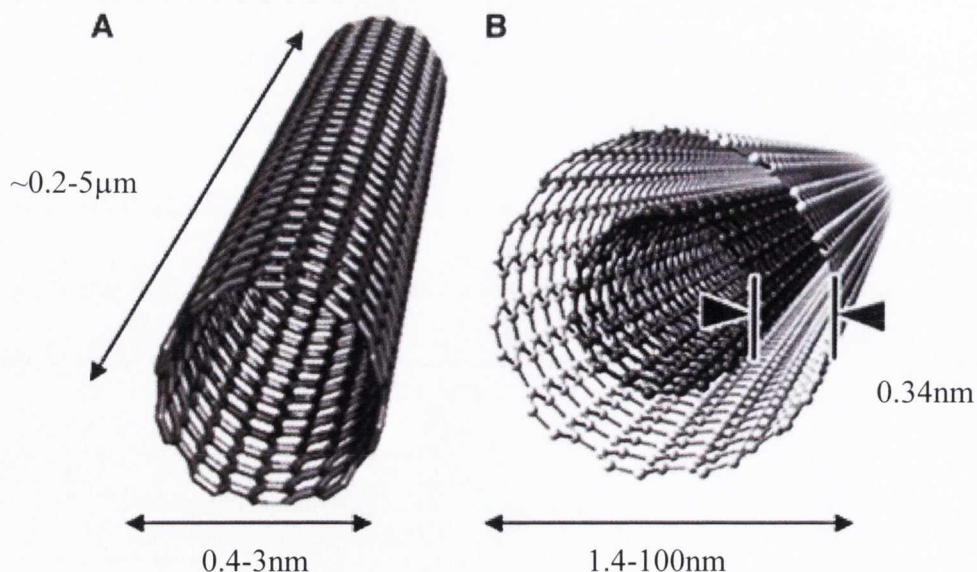


**Figure 2.5:** a) Single walled nanotube b) Multi walled nanotube

The carbon atoms in nanotubes are arranged almost entirely of  $sp^2$  bonds (which arises from the mixing of one s and two p orbitals), similar to the bonds in graphene.  $sp^2$

bonds are rigid against bond stretching deformations while flexible for bond bending deformations and therefore have a very resilient nature. There is a slight deviation from perfect  $sp^2$  hybridisation due to the curvature of the nanotube so some  $sp^3$  hybridisation is present<sup>45,46</sup>.

Carbon nanotubes are typically microns in length. The diameter of a SWNT is between 0.4–3 nm<sup>43</sup>. Carbon nanotubes have a very high aspect ratio (length/diameter) which can be  $> 1000$ <sup>47</sup>. This is higher than that for conventional carbon fibres (which is between 300 – 800)<sup>48</sup>. For MWNTs, the diameter is between 1.4 – 100 nm, depending on the number of shells present<sup>43</sup>. The nanotubes used in this thesis are formed by the HiPCO (High Pressure Carbon Monoxide) process and are 0.7 - 1.4 nm in diameter<sup>49</sup>.

Carbon nanotubes can be metallic or semi-conducting depending on the chirality of the nanotube. Figures 2.6 and 2.7 show that different chiralities of nanotubes can be formed depending on the direction in which the graphene sheet is rolled. The chiral vector of the nanotube is given by equation 2.14.

$$C_h = n\hat{a}_1 + m\hat{a}_2 \quad 2.14$$

where  $\hat{a}_1$  and  $\hat{a}_2$  are unit vectors in the two-dimensional hexagonal lattice, and  $n$  and  $m$  are integers. If  $n = m$ , the structure is described as armchair. If  $m = 0$ , the nanotubes are zigzag in structure. Otherwise, they are referred to as chiral. The integers  $n$  and  $m$  influence the electronic structure and therefore the conductivity of the nanotube. Armchair tubes are metallic and have zero bandgap. Tubes with  $n - m = 3x$  ( $x =$  any positive integer) and also including  $(3n, 0)$  zigzag tubes, are semiconducting and have a small bandgap. Chiral tubes with  $n - m \neq 3x$  are semiconducting and have a finite bandgap<sup>43,50</sup>.

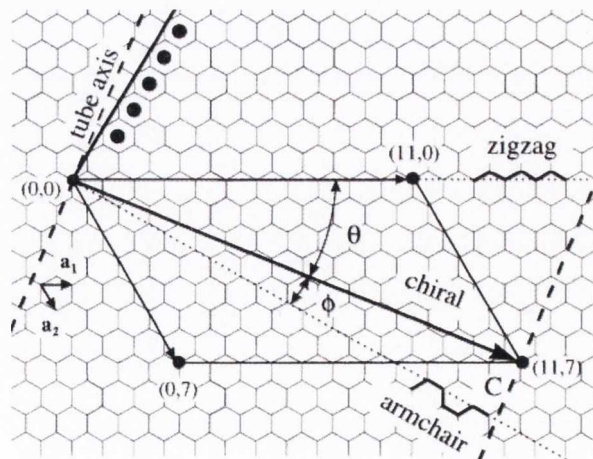


**Figure 2.6: Unrolled lattice of a nanotube (graphene sheet). The sheet can be rolled along the wrapping vector  $C$  to form a nanotube<sup>51</sup>.**

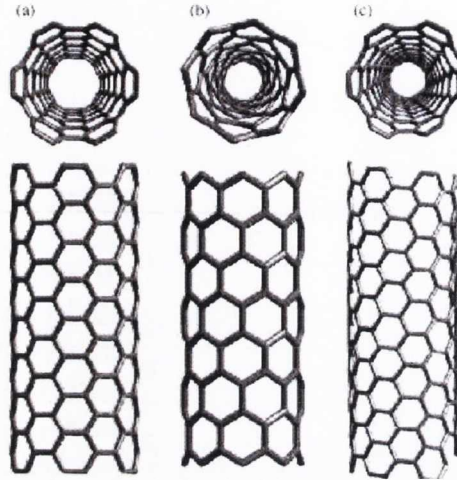


**Figure 2.7: Chirality of nanotubes**  
**a) armchair, b) zigzag, c) chiral**

Nanotubes can also be characterised by their diameter,  $d$  and chiral angle  $\theta$ . Both  $d$  and  $\theta$  can be expressed in terms of the indices  $n$  and  $m$  as shown in equations 2.15 and 2.16.

$$d = \frac{\sqrt{3}a_{C-C}}{\pi} \sqrt{n^2 + nm + m^2} \quad 2.15$$

$$\theta = \text{Tan}^{-1} \left( \frac{\sqrt{3}m}{2n + m} \right) \quad 2.16$$

where  $a_{C-C}$  is the carbon-carbon separation which is 0.142nm.<sup>52</sup>

## 2.4.2 Electronic Properties of Single Walled Carbon Nanotubes

The electronic properties of carbon nanotubes can be studied using various methods including Raman spectroscopy,<sup>53</sup> photoluminescence spectroscopy,<sup>54</sup> scanning tunnelling microscopy<sup>51</sup> and scanning tunnelling spectroscopy<sup>55</sup>. These properties can be explained more easily by examining the corresponding properties of graphene. The unit cell for graphene containing two carbon atoms is shown by the dotted rhombus in figure 2.8a. The reciprocal lattice of graphene can be constructed using the vectors  $a_1$  and  $a_2$ <sup>52</sup>. The first Brillouin zone in the reciprocal lattice is shown by the shaded section in figure 2.8b.  $a_i$  and  $b_i$  are basis vectors and reciprocal lattice vectors respectively.  $b_1$  and  $b_2$  can be found using the equation 2.17

$$b_1 = \left( \frac{2\pi}{\sqrt{3}a}, \frac{2\pi}{a} \right) \text{ and } b_2 = \left( \frac{2\pi}{\sqrt{3}a}, -\frac{2\pi}{a} \right) \quad 2.17$$

where  $a = 2.46 \text{ \AA}$  (lattice constant of graphene)

It is important to examine the reciprocal lattice to find the high symmetry points in the Brillouin zone. The points in figure 2.8b labelled  $\Gamma$ , K and M are high symmetry points.

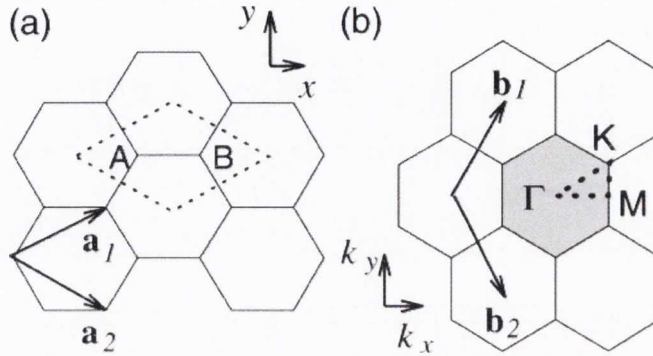


**Figure 2.8: a) Unit cell of graphene and b) First Brillouin zone of graphene showing the high symmetry points  $\Gamma$ , K and M<sup>56</sup>.**

The electronic band structure around these high symmetry points is shown in figure 2.9. Near the Fermi energy in graphene there is an occupied  $\pi$  band and an unoccupied  $\pi^*$  band. These bands meet at the point K showing that graphene is a zero gap semiconductor. Optical transitions occur at the K points where the valence and conduction bands are touching.

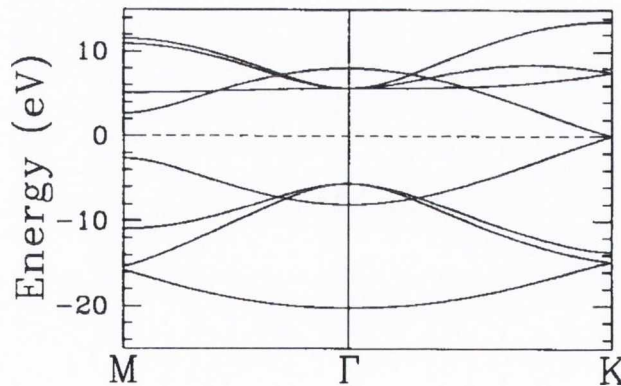


**Figure 2.9: Electronic band structure of graphene showing high symmetry points<sup>56</sup>.**

When a graphene sheet is rolled to form a nanotube, the boundary conditions which occur at the circumference mean that only a particular set of wavevectors are allowed. Examples of these are shown by the lines in figure 2.10. If the allowed

wavevector in these diagrams crosses the K point, the system is a metal with a non zero density of states at the Fermi energy.

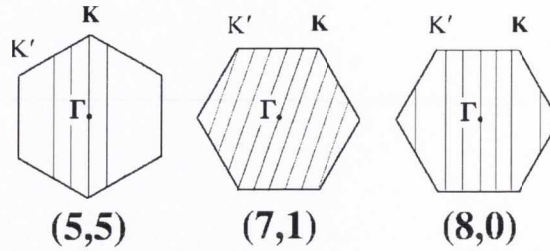


**Figure 2.10: Brillouin zone of graphene showing allowed wavevectors of (5,5), (7,1) and (8,0) nanotubes<sup>56</sup>.**

In figure 2.10, the (5,5) tube is metallic and the (8,0) tube is semiconducting. The (7,1) tube satisfies the relation  $n - m = 3x$  and is metallic also; in reality this tube has a very small gap but is considered to be metallic at room temperature.

Figure 2.11 shows the density of states of the three sample tubes examined above. Carbon nanotubes exhibit electronic behaviour of one dimensional structures and show features such as Van Hove singularities. Van Hove singularities are local maxima in the electronic density of states. These occur in regions of the Brillouin zone where the bands are parallel and are called critical points. In these regions, the photon energy  $E$  does not depend on the wavevector  $k$  and so  $dE/dk=0$ <sup>57</sup>.

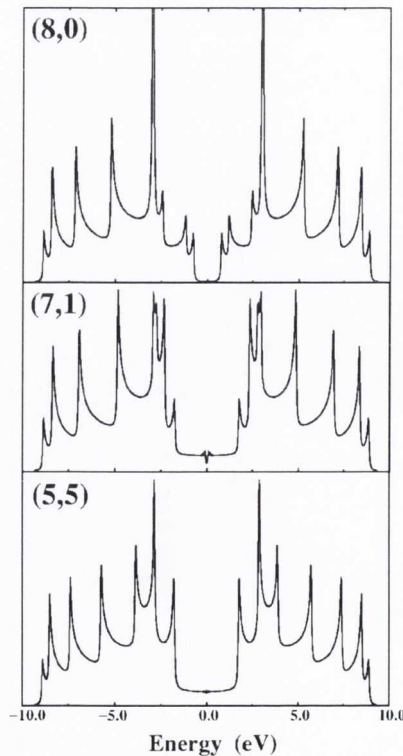


**Figure 2.11: Density of states of (5,5), (7,1) and (8,0) nanotubes<sup>56</sup>.**

### 2.4.3 Physical Properties of Single Walled Carbon Nanotubes

Carbon nanotubes exhibit remarkable mechanical, electrical and thermal properties. Mechanical measurements on individual tubes are difficult due to their size. The Young's modulus of carbon nanotubes was predicted theoretically to be 1TPa, similar to that of in-plane graphene<sup>1,39</sup>. Direct mechanical measurements of SWNT bundles have shown Young's modulus values of up to 1470 GPa<sup>58</sup>. This is high when compared to carbon fibres which have a typical Young's modulus of 800 GPa<sup>59</sup>. Measurements of nanotube moduli were carried out on individual MWNTs inside an electron microscope by Yu et al. in 2000 and Young's modulus values of 270-950 GPa were reported<sup>14</sup>.

However what really sets nanotubes apart from other materials is their strength. They are over 150 times stronger than steel and over 500 times stronger than common plastics (see table 2.1). Measurements of SWNT bundles have shown strengths between 13-52 GPa<sup>58</sup> and measurements on individual MWNTs showed strengths between 11-63 GPa<sup>14</sup> (figure 2.12).

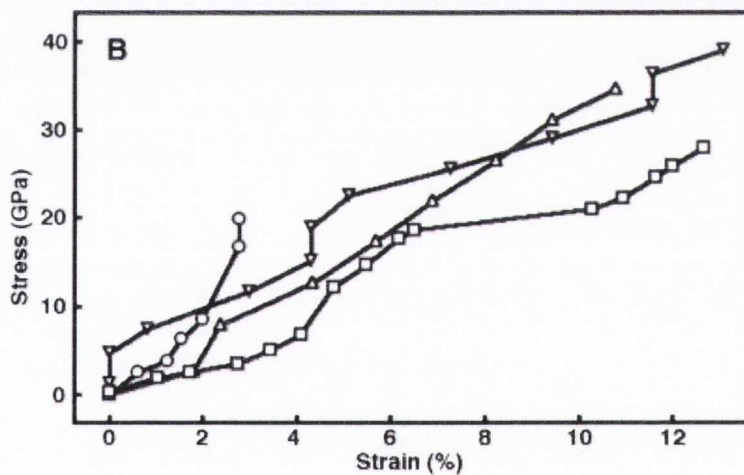


Figure 2.12: Stress-strain curves for individual MWNTs<sup>14</sup>.

The unique combination of properties found in carbon nanotubes means that they are very promising for applications in reinforcement and can be incorporated into plastics forming structural materials with increased modulus and strength.

Along with these remarkable mechanical properties, carbon nanotubes also have extraordinary transport properties. The thermal conductivity of carbon nanotubes is about twice that of diamond while their current carrying capacity is 1000 times greater than copper wires<sup>60</sup>. In conjunction with their exceptional physical properties carbon

nanotubes are exceptionally lightweight and have a density of  $1500 \text{ kg/m}^3$ <sup>61</sup>. All of these properties combined make carbon nanotubes model fillers for incorporating into polymers.

#### **2.4.4 Production and Synthesis of Single Walled Carbon Nanotubes**

Various methods can be used for nanotube production. The three main methods are arc discharge, laser ablation and chemical vapour deposition.

Carbon nanotubes were originally discovered using the arc discharge method by Sumio Ijima in 1991<sup>62</sup>. A direct current is passed through two graphite electrodes which are of a high purity. Low pressure helium or another inert atmosphere is needed for this type of production. A deposit is made on the cathode while the anode is consumed during the process. The inner core of this deposit contains the carbon nanotubes<sup>59</sup>. Synthesis can be performed by evaporation of pure graphite or by the evaporation of graphite and a metal. Nanotube yields of 48% have been reported<sup>63</sup>.

Laser ablation can also be used for carbon nanotube production. In this process a graphite target is vaporised by laser irradiation. This is carried out in an inert atmosphere inside a silica tube at  $\sim 1200 \text{ }^\circ\text{C}$ <sup>59</sup>. The resulting soot contains carbon nanotubes. This method has a nanotube yield of about 70% but is more expensive than both chemical vapour deposition and arc discharge<sup>44</sup>.

Chemical vapour deposition (CVD) is the most attractive method for carbon nanotube production. Using this method, a catalyst material is heated to high temperatures (600-1000  $^\circ\text{C}$ ) in a tube furnace through which a gas mixture containing a hydrocarbon gas is flowing<sup>64</sup>. The hydrocarbon decomposes forming a metastable carbide with the catalyst nanoparticle leading to the precipitation of carbon nanotubes<sup>65</sup>. This is the most widely used method for carbon nanotube synthesis because it is the method best suited for mass production of nanotubes.

HiPCO (High Pressure Carbon Monoxide) processing was discovered by Smalley's team in 1998<sup>49</sup>. In this process, a carbon monoxide gas is mixed with a gaseous catalyst precursor at a high temperature (800–1200  $^\circ\text{C}$ ) and pressure. The catalyst precursor decomposes and nanometre-sized metal particles develop from the decomposition products. Carbon monoxide molecules react with these metal particles to form carbon dioxide and carbon atoms, which bond together to form carbon nanotubes<sup>49</sup>. This process selectively produces 100% single walled carbon nanotubes.

## 2.4.5 Applications and Limitations of Single Walled Carbon Nanotubes

There is a large range of potential applications for carbon nanotubes ranging from semiconductors to drug delivery systems and from automobile body panels to uses in plastics<sup>43</sup>. Because of their conductive nature, nanotubes can be used as scanning probes on electron and atomic force microscope tips<sup>66</sup>. Other applications include their use in flat panel displays<sup>67</sup>. They have advantages over liquid crystal displays (which are currently being used) due to their low power consumption, high brightness and fast response rate. Nanotube based lamps could replace mercury based fluorescent lamps (used in stadium displays). They have lifetime expectancies of >8000 hours<sup>43</sup>, while the mercury based lamps only last up to 3000 hours<sup>68</sup>. Because carbon nanotubes have a current carrying capacity of up to  $10^9$  A/cm<sup>2</sup> (compared to metals which have current carrying capacities of about  $10^5$  A/cm<sup>2</sup>), carbon nanotubes could be used for downsizing electrical circuits<sup>69</sup>. Other applications could include uses in electrochemical devices and for energy storage<sup>43</sup>.

However there are some limitations which inhibit nanotube research such as nanotube dispersibility, the cost of production and nanotube toxicology. Nanotube aggregation is the major stumbling block in realising the potential applications of carbon nanotubes. Van der Waals forces cause all types of carbon nanotubes to clump together and form bundles or ropes that are difficult to separate. These bundles are weak because of slippage between the nanotubes. This hampers the use of nanotubes for electronic applications and also reduces their mechanical strength. Although individual nanotubes are very strong, bundles are weak and hence their presence limits nanotube applications. Extensive research is being carried out to overcome this problem and to find a way to disperse nanotubes using solvents and other methods<sup>70-73</sup>. In this thesis, nanotubes are effectively separated using surfactants and sonication and in some cases, using solvents. Along with this problem, the cost of nanotube production remains very high. The cost depends on the production process. The purified nanotubes used in this work were made using the HiPCO process and cost €405 per gram.

In conjunction with high costs and difficulties with dispersions, there are also concerns over the possible hazards associated with carbon nanotubes. Carbon nanotubes are a relatively new material and so the safety measures that need to be taken when using them are being constantly modified. Carbon nanotubes are now thought of as an irritant upon skin exposure and harmful upon inhalation; granulomas (inflammation) formed in tests conducted in rat lungs even at low concentration ( $0.1\mu\text{g}$ )<sup>74</sup>. Little is known on the adverse

effects of ingestion of nanotubes. In a composite, the nanotubes are bound to other materials and so could pose a lower health risk.

## **2.5 Mechanical Reinforcement in Carbon Nanotube Polymer**

### **Composites**

For effective reinforcement in carbon nanotube composites there are certain requirements which must be met. These are a large aspect ratio, good dispersion, alignment of the filler or reinforcing material and also good interfacial stress transfer between the filler and the matrix within the composite<sup>39</sup>. Carbon nanotubes have a large surface area which acts as an interface for stress transfer<sup>75</sup>. They also have a large aspect ratio. It has been shown that aligning carbon nanotubes in composites can increase its thermal and electrical conductivity<sup>76</sup>. Because of their unique properties, carbon nanotubes have the potential to improve the mechanical, electrical and physical properties of polymers. Polymer composites have shown a large improvement in mechanical properties when even a small amount of carbon nanotubes has been added to them. However this improvement is dependant on good nanotube dispersion<sup>39</sup>.

#### **2.5.1 Solution Processing of Composites**

There are many ways to incorporate carbon nanotubes into a polymer matrix. One way is to mix the polymer and nanotube in a suitable solvent, after which the solvent is evaporated. This is called solution processing. The main methods to produce a composite by solution processing are:

1. Mix nanotubes and polymers in a suitable solvent and mix by energetic agitation.
2. Use of surfactants instead of solvents as in method 1.
3. Nanotubes dispersed in polymer solutions.
4. Controlled evaporation of the solvent.

When using method 1, the nanotubes and polymer can be mixed using a range of methods including magnetic stirring, mixing, refluxing or most commonly by sonication. Mild sonication can be carried out using a sonic bath while more vigorous sonication can be carried out using a sonic tip. For this method to be effective, the solvent used for dispersion of the nanotubes must also be suitable for the polymer that is being used. After sonication, the solvent is then evaporated in a controlled manner in a method known as drop casting to produce a composite film.

In 2002, Cadek et al. used high powered sonication in solvents along with low powered sonication to produce drop cast films<sup>77</sup>. Using this method, a large increase in stiffness was obtained. They observed an increase in Young's modulus by a factor of 1.8 upon addition of 1wt% arc discharged MWNTs to PVA and an increase by a factor of 2.8 in poly(9-vinyl carbazole) (PVK) composites. In PVA composites, nanotube templated crystallinity was observed which increased the mechanical properties of the composites by enhancing nanotube matrix stress transfer. For PVK composites, this corresponds to a  $dY/dV_f$  value of 75 GPa. For the PVA composites a  $dY/dV_f$  value of 280 GPa can be given accounting for the crystallinity in the sample<sup>9</sup>. In a more recent study, Khan et al. studied the effect of solvent choice on the mechanical properties of drop cast films. Three different solvents, water, dimethyl sulfoxide (DMSO) and N-Methyl-2-pyrrolidone (NMP) were investigated. This study found that both strength and modulus were reduced upon the addition of double walled nanotubes to PVA in an NMP based system. In water or DMSO based systems, these properties were increased upon the addition of nanotubes; however in the water systems some of this increase can be attributed to nanotube templated crystallinity. Values of  $dY/dV_f=105$  GPa and  $d\sigma/dV_f=3.1$  GPa were obtained for water samples showing no crystallinity. For the DMSO samples  $dY/dV_f=105$  GPa and  $d\sigma/dV_f=5$  GPa was observed<sup>78</sup>. Ruan et al. used a method of magnetic stirring along with sonication to disperse 1 wt% MWNTs in xylene. This dispersion was then added to a mixture of ultrahigh molecular weight polyethylene (PE) in xylene and mixed by refluxing followed by drop casting to form films. Both drawn and undrawn films were prepared with an undrawn film showing enhancements in modulus and strength by 38% and 50% respectively. For high draw ratios, enhancements on the toughness of up to 150% were also observed<sup>79</sup>. For these composites  $dY/dV_f=57$  GPa. Surfactants can also be used instead of solvents to aid in the dispersion of nanotubes. Dalmas et al. used surfactants and high powered sonication to disperse MWNTs which was then mixed with an aqueous suspension of the polymer latex. This was then drop cast in Teflon moulds followed by controlled evaporation of the water. When mechanically tested, these films showed an increase in modulus and a 170% increase in strength<sup>80</sup>.

Alternative processing methods that have been reported include roll casting. In this process, functionalised nanotubes were added to isopropanol and mixed with a solution of PEO in methanol. This was then dropped onto a Teflon roller. The roll cast system was comprised of two parallel rollers made of Teflon and stainless steel. The gap

between these rollers was adjustable allowing films of varying thicknesses to be prepared. A 145% increase in modulus was observed for 1wt% nanotube composites<sup>81</sup>.

A spin casting method was used by Safadi et al. in 2001. In the spin casting process, the MWNT-polystyrene dispersion is placed in the centre of a disk. As the disk is spun, a thin film is formed as the fluid evaporates. A comparison was made with composites produced by spin casting and by drop casting showing little difference in composite strength between the two methods<sup>82</sup>. The highest strength obtained was 30.6 MPa and the highest modulus was 3.4 GPa for drop cast films. The corresponding  $dY/dV_f$  value for these composites was 122 GPa.

Large values of  $dY/dV_f$  were obtained by Coleman et al. and Cadek et al. Cadek et al. examined the optimum tube type for reinforcing poly(vinyl) alcohol. From this paper, it was found that DWNTs proved to provide a  $dY/dV_f$  value of 1244 GPa at 0.2vol% nanotubes in drop cast films<sup>7,39</sup>. However at high concentrations, the nanotubes bundled together. They also found that  $dY/dV_f$  scaled with inverse nanotube diameter for all nanotubes except the SWNTs. All samples in this study had a crystalline polymer nanotube interface. Coleman et al. obtained a  $dY/dV_f$  value of 754 GPa for poly(vinyl) alcohol composites containing 0.6vol% CVD MWNTs<sup>8</sup>. In conjunction with this, an increase in strength from 81 MPa to 348 MPa was observed. In these composites, nanotube templated crystallinity also played a role in mechanical reinforcement.

## 2.5.2 Melt Processing of Composite Films and Fibres

Not all polymers are soluble so an alternative method for composite production is necessary. Melt processing is a common method used. It is particularly suitable for use with thermoplastics as they soften when heated. This technique is beneficial as it is suited to industrial techniques and is also a quick and easy process to prepare composites<sup>39</sup>. It can also be used to produce bulk composites and composite fibres. A polymer is heated until it forms a viscous liquid. If a composite is being produced using this method, the filler can be added at this stage and the blend can become uniform by shear mixing. Composite films can be produced in a number of ways including compression moulding and extrusion.

Anand et al. used compression moulding to make composites of poly(ethylene terephthalate) (PET) and SWNTs. The tensile strength of these composites increased from 195 MPa to 509 MPa upon the addition of 2wt% nanotubes and by drawing fibres

by four times their original length. This increase was accompanied by an increase in Young's modulus from 2.21 GPa to 11.69 GPa giving  $dY/dV_f=668$  GPa. They also showed that composites were electrically conductive at concentrations above 2 wt%<sup>3</sup>.

A combination of compression moulding and shear mixing can also be used. Machado et al. used this method. In this work, shear mixing was carried out on polypropylene (PP) at 190 °C. When the polymer was melted, nanotubes were added to it and the mixture was compressed at 200 °C. An increase in modulus from 885 MPa to 1187 MPa was observed along with an increase in strength from 30.8 MPa to 35.5 MPa for composites containing 0.75% nanotubes<sup>83</sup>.  $dY/dV_f$  values for this work correspond to 68 GPa.

Using a combination of extrusion and hot pressing, Li et al. produced composites of MWNTs with the thermoplastic elastomer poly[styrene-b-(ethylene-co-butylene)-b-styrene] (SEBS). They showed an impressive 1040% increase in modulus along with a 228% increase in strength for films containing 15wt% nanotubes. These films also stretch by 600% or more before breaking<sup>84</sup>.

Impressive increases in mechanical properties for melt processed composites were observed by Liu et al. in 2004 for their Nylon 6 MWNT composites<sup>85</sup>. Large increases in moduli from 0.4 GPa to 1.24 GPa were observed upon the addition of 2wt% nanotubes. They also achieved increases in strength from 18 MPa to 47 MPa. This gives  $dY/dV_f=64$  GPa.

For many applications, fibres are more useful than bulk material. Composite fibres can also be produced by melt processing. In 2000, Haggenueller et al. reinforced the thermoplastic PMMA with SWNTs to produce composite fibres by extrusion. A value of reinforcement for these fibres is approximately  $dY/dV_f=57$  GPa. The highest strength and modulus achieved was 125 MPa and 7 GPa respectively for fibres drawn by 400%<sup>86</sup>.

Fibres displaying high reinforcement values were produced by Kearns et al.<sup>87</sup> In this study, polypropylene (PP) was reinforced with SWNTs. Solvents and sonication were used to achieve a nanotube dispersion in PP. This dispersion was placed in a vacuum oven and once the solvent was evaporated, the resultant powder was extruded as shown in figure 2.13. The advantage of this method over solution processing of fibres is that the take up speed of the fibres is much quicker and so this process is much more suited to industrial applications. These fibres showed an increase in modulus from 6.3 GPa to 9.8 GPa at 1wt% SWNTs. This gives a  $dY/dV_f$  value of 530 GPa.

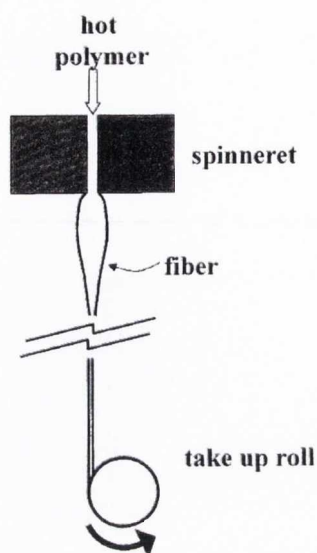


**Figure 2.13: Method for extrusion of fibres by Kearns et al.<sup>87</sup>**

Studies with MWNTs have also been completed. Andrews et al. used a combination of shear mixing and a hot pressed extrusion of a MWNT-PS composite through a 0.3 mm diameter die<sup>88</sup>. This resulted in fibres with a maximum Young's modulus of 3 GPa upon the addition of 5wt% MWNTs and  $dY/dV_f=36$  GPa.

In 2007, fibres showing a 400% increase in strength and a 270% increase in Young's modulus upon the addition of 1 wt% nanotubes were produced by Jose et al.<sup>89</sup> Polymer crystallinity was observed for these fibres. A value of reinforcement of  $dY/dV_f=210$  GPa was obtained.

### 2.5.3 Novel Composites

There are also various other methods of composite preparation; for example buckypaper preparation, electrospinning and coagulation spinning.

In the buckypaper method, a polymer nanotube dispersion is filtered through a filter paper leaving an entanglement of nanotubes and polymer behind<sup>5</sup>. Either solvents or surfactants can be used for dispersion of nanotubes for buckypaper formation. Buckypapers can also be made by a similar process where an existing nanotube network is soaked in a polymer solution to form a composite. This technique was first demonstrated by Coleman et al. in 2003<sup>90</sup>. In this study, the polymers poly(vinyl alcohol), poly(vinyl pyrrolidone) and poly(styrene) were investigated. The mechanical properties of these sheets significantly improved upon the addition of polymers. The maximum Young's modulus of composites for all polymer types was 6.9 GPa for a buckypaper

which was soaked for 64 hours. The strength of PVA composites increased by a factor of 9 to 57 MPa. The toughness of PS composites increased by a factor of 30 to  $39 \times 10^4 \text{ J/m}^3$ . Buckypapers have also been shown to demonstrate high conductivities<sup>91</sup> and actuation properties<sup>92</sup>.

Electrospinning is another composite preparation method. In this method, a high voltage is applied to a polymer-nanotube dispersion and this is placed at a set distance from a grounded plate or drum. The composite solution becomes charged and nanometre sized fibres are attracted to the plate or drum. Plate collection is used to form a mesh of fibres while using a rotating drum results in aligned fibres. In 2008, Blond et al. used both plate and drum collection methods for the production of PVA-SWNT composites. Mechanical improvement was seen upon aligning the fibres and also by drawing. This method resulted in strong tough composites with a maximum Young's modulus of 1.2 GPa, a strength of 40 MPa and a toughness of  $13 \text{ J/g}$ <sup>6</sup>.

Other methods of composite production such as in situ polymerisation, nanotube functionalisation and composites based on thermosets are possible. In situ polymerisation results in polymers being grafted to the walls of nanotubes. This method is suited to polymers which are thermally unstable or insoluble. High nanotube loading can also be achieved using this method and it is suitable for almost any polymer type. In situ polymerisation was used by Jin et al. to produce PET-MWNT composites. In this study, the strength of composites increased by 350% in comparison with neat PET samples. PET-MWNT composites achieved a strength of 140 MPa<sup>93</sup>.

In general, composites based on functionalisation show good reinforcement because the functionalisation improves dispersion and stress transfer<sup>39</sup>. Dispersion of these nanotubes also tends to be good, as the functional groups help the nanotubes to disperse in the presence of solvents or polymers.

Composites based on thermosets can also be produced. The most common thermosets are epoxy resins. These composites have a large range of industrial applications. In 2003, Bai et al. showed very good mechanical reinforcement in epoxy based composites. An impressive  $dY/dV_f$  value of 330 GPa was observed for these composites. At 1 wt% MWNT loading, they had strengths of 41 MPa along with Young's modulus values of  $2.4 \text{ GPa}$ <sup>4</sup>.

Coagulation spinning is also another composite production method. It is the main method of composite preparation used in this thesis and will be described in detail in Section 2.5.5.

$dY/dV_f$  values for various composites were calculated by Coleman et al. in 2006<sup>39</sup>. Some of these values along with others from literature are shown in table 2.3.

Reference	NT Type	Polymer	Method	UTS (MPa)	Y (GPa)	$dY/dV_f$ (GPa)
Cadek et al. <sup>77</sup>	MWNT	PVA	Drop casting	N/A	12.5	280
Cadek et al. <sup>77</sup>	MWNT	PVK	Drop casting	N/A	6	75
Khan et al. <sup>78</sup>	SWNT	PVA	Drop casting	49	1.43	105
Ruan et al. <sup>79</sup>	MWNT	PE	Drop casting	12.4	1.35	57
Safadi et al. <sup>82</sup>	MWNT	PS	Spin casting	30.6	3.4	122
Cadek et al. <sup>7</sup>	DWNT	PVA	Drop casting	N/A	3.6	1244
Coleman et al. <sup>8</sup>	MWNT	PVA	Drop casting	348	7.04	754
Manchado et al. <sup>83</sup>	SWNT	PP	Melt processing	36	1.19	68
Li et al. <sup>84</sup>	MWNT	SEBS	Melt processing	14	0.19	974
Liu et al. <sup>85</sup>	MWNT	Nylon 6	Melt processing	47	1.27	64
Anand et al. <sup>3</sup>	SWNT	PET	Fibre extrusion	509	11.69	668
Haggenmueller et al. <sup>86</sup>	SWNT	PMMA	Fibre extrusion	125	7	57
Kearns et al. <sup>87</sup>	SWNT	PP	Fibre extrusion	1027	9.8	530
Andrews et al. <sup>88</sup>	MWNT	PS	Fibre extrusion	40	3	36
Jose et al. <sup>89</sup>	MWNT	PP	Fibre extrusion	420	305	210
Minus et al. <sup>94</sup>	SWNT	PVA	Coagulation spun	2600	71	3175
Blond et al. <sup>6</sup>	SWNT	PVA	Electrospun	40	1.2	24
Xu et al. <sup>95</sup>	GO	PVA	Buckypaper	110	6.1	110
Bai et al. <sup>4</sup>	MWNT	Epoxy	Thermosetting	41	2.4	330

**Table 2.3:  $dY/dV_f$  values of various composites. N/A indicates that this value was not available in the literature.**

As can be seen from table 2.3, solution based drop cast composites show good mechanical reinforcement. However, in some cases, much of the mechanical reinforcement can be attributed to nanotube templated crystallinity<sup>9,78</sup>. It can also be seen

that melt processed fibres produced by fibre extrusion methods show better mechanical properties than bulk melt processed composites. In general, composite fibres show the greatest strength of all composite types. Further discussion on fibres and composite fibres will be included in the next section.

#### 2.5.4 Fibres and Fibre Composites

Because of their impressive mechanical properties, there have been many attempts to produce carbon nanotube only fibres. These fibres can be produced in several ways.

1. Wet spinning
2. Spinning from nanotube carpets
3. Spinning from nanotube plume directly from a CVD as they are being produced.

In the wet spinning process, the nanotubes are dispersed in superacids. Using this process, nanotubes can be produced at high enough concentrations so that they join together in ordered domains<sup>96</sup>. This dispersion is injected through an air gap and into a solution where coagulation occurs. Ericsson et al. produced fibres using this method. They dispersed SWNTs in fuming sulfuric acid and used a coagulation bath of 5% diethyl ether, aqueous sulphuric acid or water<sup>97</sup>. These fibres displayed maximum strengths of 116 MPa and Young's modulus values of 120 MPa. Razal et al. used a similar method by dispersing nanotubes using hyaluronic acid which was injected into a coagulation bath of 5% acetic acid<sup>98</sup>. An alternative method was used by Kozlov et al. They used either acidic or basic coagulation baths to collapse surfactant dispersed carbon nanotubes. Either solid or hollow fibres could be produced depending on the spinning parameters<sup>99</sup>.

Carbon nanotube fibres can also be formed by drawing yarns out of carbon nanotube forests. This process was discovered by Jiang et al. who made carbon nanotube only fibres of about 30 cm in length and 200  $\mu\text{m}$  wide<sup>100</sup>. Zhang et al. used a similar method and spun MWNTs into a twisted fibre with strengths of 1.91 GPa and Young's modulus values of 330 GPa for fibres which were 3 $\mu\text{m}$  in diameter. Zhang et al. also showed that fibre strength increases upon increasing nanotube length and decreasing diameter<sup>101</sup>. Fibres made using this method are shown in figure 2.14. The strongest individual fibre produced using this method was 3.3 GPa<sup>102</sup>.

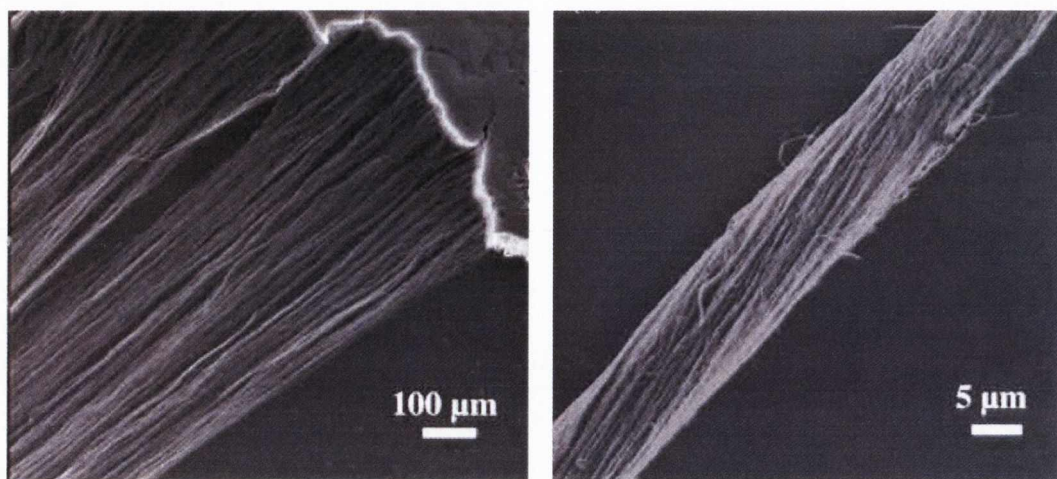


**Figure 2.14: a) MWNT being pulled out of a nanotube forest and b) MWNTs twisted into a fibre<sup>101</sup>.**

The last main method for nanotube only fibre production is from an aerogel of MWNTs and SWNTs as they are being produced in a CVD. This method was first used by Li et al. They could produce fibres of unlimited length with strengths of 1 GPa<sup>103</sup>. Very impressive mechanical properties were observed in fibres made by Koziol et. al by producing MWNT fibres from a CVD aerogel<sup>104</sup>. A UTS value of 9 GPa was obtained for fibres which were tested at a 1 mm gauge length along with a Young's modulus value of 360 GPa and a toughness of 300 J/g.

For many applications, composite fibres are more attractive. Composite fibres can be processed using solution based methods or by melt processing. In these materials, the nanotubes (or other fillers) along with the polymer chains themselves can be aligned along the direction of the fibre thus improving its mechanical properties. One such method of composite production is coagulation spinning which will be introduced below.

### **2.5.5 Coagulation Spun Carbon Nanotube Composite Fibres**

Coagulation spinning offers a promising route for the development of high-performance carbon nanotube composites. In this process, a nanotube dispersion is injected into a polymer solution and coagulates upon contact. This process can be carried out in a rotating bath as shown below but more effectively by flowing through a glass tube. Due to processing parameters, the nanotubes are partially aligned in the fibre during processing. This alignment improves the mechanical properties of the composite. As will be discussed further in chapters 4 and 5, further alignment is possible through drawing.

Coagulation can occur for various reasons from injection into non solvents, pH variations in a coagulation bath, temperature variations etc.

The mechanism for the collapse of the nanotube dispersion and fibre formation is not fully understood. It is difficult to interpret the mechanism for fibre formation as it occurs so quickly and because of fibre movement. It is thought that the polymer displaces some of the surfactant molecules causing collapse of the nanotube dispersion to form a fibre<sup>105,106</sup>. Some attempts have been made to understand the process. In experiments conducted by Mercader et al. in 2010, it was found that fibre strength increases with increasing time in the coagulation tube indicating that the polymer needs time to diffuse through the fibre to bind the nanotubes together<sup>107</sup>. For this reason, the pipe in which the polymer flows must be of sufficient length to avoid breakage of the fibre.

Along with this, in order for a fibre to form, there are some important conditions which must be met. Firstly, the nanotube dispersion must be of a very high quality. The nanotubes should be dispersed from their bundles and single nanotubes should be present in dispersion. Otherwise slippage will occur in the nanotube bundles reducing the mechanical properties of the fibre. As it is difficult to disperse the nanotubes completely at high concentrations, the nanotubes may be in small bundles. Secondly, the flow in the tube must be laminar. In laminar flow, the fluid velocity at the centre of the tube is approximately twice the average velocity of the fluid. Turbulent flow would interfere with fibre formation. Laminar flow in a pipe occurs for a Reynold's number lower than 2000. The Reynolds number is given by equation 2.18.

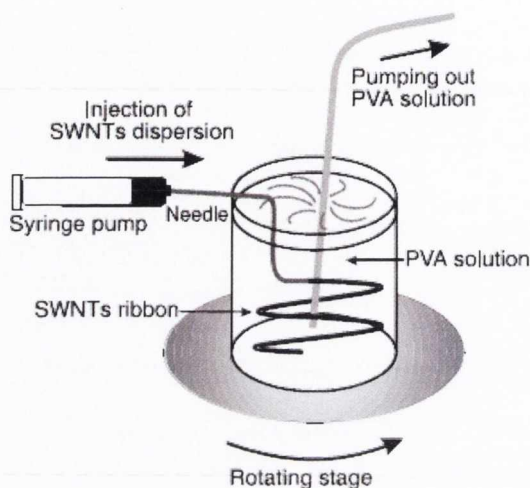
$$R_e = \frac{2Rv_{av}\rho}{\eta} \quad 2.18$$

where  $R$  is the radius of the pipe,  $\rho$  is the fluid density,  $\eta$  is the fluid viscosity and  $v_{av}$  is the average flow velocity which can be found by dividing the polymer flow rate by the cross sectional area of the pipe<sup>12</sup>.

The nanotube dispersion must be injected into the centre of the glass tube so that it is carried along smoothly. This can be ensured by inserting the needle through 3 spacers, around which the polymer flows. In order to produce mechanically strong fibres, PVA is usually the polymer of choice.

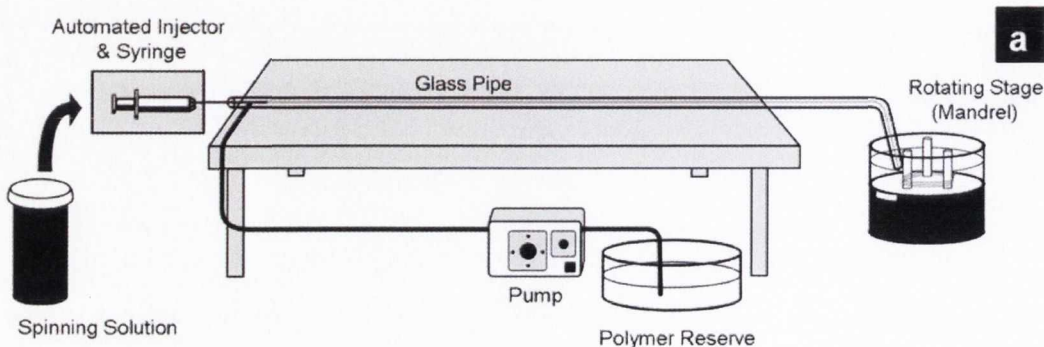
The technique used in this thesis was first used by Vigolo et al. in 2000<sup>105</sup>. This method involved the injection of a SWNT-sodium dodecyl sulphate (SDS) dispersion into a rotating bath of poly(vinyl alcohol) solution, (figure 2.15). The fibres created had

strengths of approximately 150 MPa but only short fibres could be obtained as they tangled very easily.



**Figure 2.15: Original coagulation spinning apparatus<sup>105</sup>.**

Continuous fibres were produced by Dalton et al. in 2003<sup>10</sup>. A specialised spinning apparatus was developed. The nanotube-lithium dodecyl sulfate (LDS) dispersion was injected into the centre of a cylindrical pipe of flowing poly(vinyl) alcohol (PVA) and fibres were collected in a rotating bath. These fibres contained 60% nanotubes by weight and had strengths of 1.8 GPa. More recently, the spinning technique was developed further by processing the fibres post spinning. Razal et al. also used an LDS-nanotube dispersion<sup>12</sup>. The resulting fibres were wound and unwound on mandrels, passed over rollers through an acetone wash bath and dried at a strain of 400%. Using this method, density normalised strengths of  $1.3\text{GPa cm}^3/\text{g}$  were obtained. Fibres were also tested while drawn in hot steam resulting in strengths of 497 MPa and an exceptionally high toughness value of 152 J/g. The more advanced spinning set up is shown in figure 2.16.



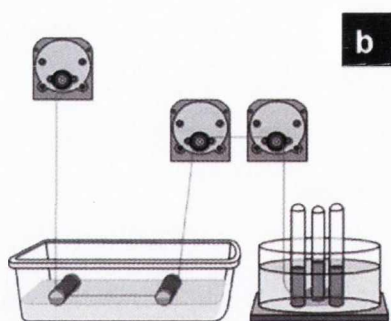


**Figure 2.16: a) Coagulation spinning set up and b) mandrels used for drying fibres<sup>12</sup>.**

Hot drawing was a technique used by Miaudet et al.<sup>108</sup>. SDS was used as a surfactant in this SWNT-PVA system. Untreated fibres had strengths of 570 MPa while those drawn by 850% in hot air at 180°C had strengths of 1.6 GPa. Munoz et al. produced even stronger fibres<sup>109</sup>. This system consisted of PVA, SWNTs and LDS. These continuous fibres had an ultimate tensile strength of 1.8 GPa and a very large toughness of over 600 J/g. PVA-nanotube composites can also be produced using a methanol coagulation bath. This method was used by Zhang et al. in 2004<sup>13</sup>. In this study, a spinning solution of SWNTs in PVA, DMSO and H<sub>2</sub>O was injected into a coagulation bath of methanol. The fibres were then hot drawn and displayed strengths of 1.1 GPa. A similar method was used by Xu et al. in 2010 producing fibres with strengths of 2.2 GPa<sup>110</sup>.

The strongest fibres produced were those made by Minus et al. using this method<sup>94</sup>. These fibres were drawn at high temperature and had impressive strengths of 2.6 GPa. Some of this mechanical strength can be attributed to nanotube templated crystallinity which was observed for these fibres.

In another study, Munoz et al. used polyethyleneimine as a coagulant<sup>111</sup>. While these composites are not as strong or tough as those produced by Minus et al., they have far superior electrical properties than similar SWNT-PVA composites.

Polymer free coagulation spinning has also recently been developed. In 2008, Razal et al. produced highly conductive carbon nanotube biofibres using carbon nanotubes dispersed in biomolecules<sup>98</sup>. Instead of using a polymer as a coagulation medium, the coagulation bath was altered by pH control. The use of a polymer free coagulation solution results in fibres containing only carbon nanotubes and biomolecules. (In polymer based systems, the surfactants, polymer and nanotubes would remain in the

fibres). These biomolecules have been shown to contribute to a wide range of applications including nerve regeneration, wound dressing and biosensors. They have excellent electrical and capacitive behaviour. These carbon nanotube biofibres may have potential use in the biomedical industry.

Table 2.4 summarises literature results for nanotube only and composite fibres produced by the method of coagulation spinning. The results in this table have been arranged by decreasing strength.

Reference	Coagulation solution	Spinning solution	UTS (MPa)	T (J/g)	$\epsilon_B$ (%)	Y (GPa)
Minus et al. <sup>94</sup>	Methanol	SWNT-PVA-DMSO	2600	59	6.2	71
Xu et al. <sup>110</sup>	Methanol	SWNT-PVA-DMSO	2200	N/A	10	36
Munoz et al. <sup>109</sup>	PVA	SWNTs in LDS	1800	600	102	80
Dalton et al. <sup>112</sup>	PVA	SWNT in LDS	1800	600	30	N/A
Dalton et al. <sup>10</sup>	PVA	SWNTs in LDS	1800	570	30	80
Miaudet et al. <sup>108</sup>	PVA	SWNT in SDS	1600	55	11.2	45
Zhang et al. <sup>13</sup>	Methanol	SWNT-PVA-DMSO-H <sub>2</sub> O	1100	N/A	8.8	35.8
Neri et al. <sup>113</sup>	PVA	Oxidised MWNTs	500	500	200	5-10
Razal et al. <sup>12</sup>	PVA	SWNT in LDS	497	152	54	N/A
Granero et al. <sup>114</sup>	Gellan Gum-SWNT	Chitosan	183	4.2	5.6	6.9
Vigolo et al. <sup>105</sup>	PVA	SWNT in SDS	150	N/A	3	9-15
Barisci et al. <sup>115</sup>	PVA	SWNTs in DNA	125	N/A	N/A	18.7
Razal et al. <sup>98</sup>	Acetic Acid	HA-SWNT	123	6-10	7	12
Ericson et al. <sup>97</sup>	Diethyl ether/H <sub>2</sub> SO <sub>4</sub>	SWNT fuming H <sub>2</sub> SO <sub>4</sub>	116	N/A	N/A	120
Munoz et al. <sup>111</sup>	Polyethyleneimine	SWNT in LDS	N/A	5-6	7-13	N/A
Steinmetz et al. <sup>116</sup>	Ethanol/ glycerol	SWNT in SDS	N/A	N/A	4.5	2

**Table 2.4: Mechanical properties of nanotube only and composite fibres produced by coagulation spinning. N/A implies that no data was available.**

## 2.6 Introduction to Graphene

Alongside nanotubes, graphene has been the focus of vast amounts of research in recent years due to its remarkable mechanical and electronic properties<sup>117</sup>. One of the advantages it has over carbon nanotubes is its low cost of production. This makes it a very promising material for many industrial applications.

Graphene is a one atom thick, sheet of carbon atoms which are arranged in a hexagonal pattern. It was once thought that these 2D materials would be too unstable to exist however rippling occurs in the third dimension which stabilises the structure. This has been seen experimentally in suspended graphene<sup>118</sup> (figure 2.17).

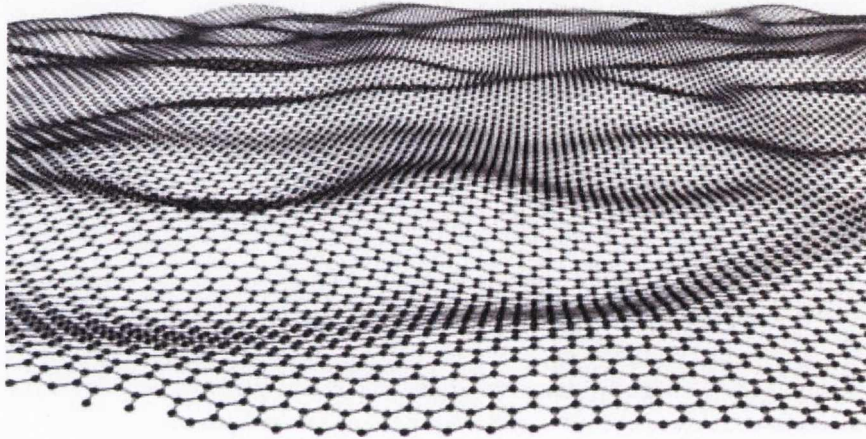


**Figure 2.17: Rippling surface of graphene**

The properties that this structure possesses have intrigued scientists and have sparked an explosion of publications in this area in recent years.

The charge carriers in graphene mimic the behaviour of relativistic particles and can be described using the Dirac equation (rather than the Schrödinger equation). The mobilities of these charge carriers can be greater than  $15,000 \text{ cm}^2\text{V}^{-1}\text{s}^{-1}$  even at room temperature<sup>117</sup>. The charge carriers can move for several micrometers without being scattered<sup>119</sup>. Unlike carbon nanotubes, chirality does not affect the electrical properties of graphene. Along with its exceptional electronic properties, graphene also possesses very impressive mechanical properties.

Graphene is the strongest material ever measured. The strength of graphene is difficult to measure because of defects and grain boundaries; however Lee et al. managed to measure the mechanical properties of graphene using an AFM and the method of nanoindentation. They reported strengths of 130 GPa and Young's modulus values of

1 TPa<sup>120</sup>. Because of its superlative properties, applications in reinforcement are very promising but before this can be achieved, production methods need to be optimised and improved to facilitate advances in research.

Graphene was first produced by Novoselov in 2004 by mechanical exfoliation<sup>121</sup>. Graphene was exfoliated from the parent material graphite using the scotch tape method whereby layers of graphene were peeled off. This method of producing graphene was used during early research into the structure, however it has a low yield and is not suitable for large scale applications but can currently produce single graphene flake sizes of up to one millimetre<sup>119</sup>. Alternative methods for graphene production are epitaxial growth where graphene is grown on top of other crystals or graphene functionalisation<sup>122,123</sup>. However, these methods alter the electronic properties of graphene. Graphene can also be produced by chemical vapour deposition with properties similar to that of graphene produced by micro-cleaving<sup>124</sup>. The disadvantage of this method is the small scale production. It is also possible to exfoliate graphene using solution based techniques. This technique is particularly suited for composite production. The graphene flakes produced are sub micrometer sized but can be produced at a much higher yield than micromechanical cleavage methods<sup>125,126</sup>. Along with using solvents, surfactants can also be used to exfoliate graphene with concentrations of 0.3mg/ml being achieved with 20% of flakes containing only one layer<sup>127</sup>. The graphene used in chapter 6 of this thesis was processed using liquid phase exfoliation in solvents.

Research into graphene is in its early stages and because of this the applications of graphene are still being developed. Graphene based electronics have been the focus of large amounts of research from companies such as Intel and IBM<sup>117</sup>. This is mainly due to its high mobility of charge carriers. It also has potential applications in field effect transistors or for hydrogen storage.

### **2.6.1 Reinforcement of Polymers using Graphene**

To date, polymer-graphene composites have not shown exceptional mechanical results. It has been suggested in some papers that this is due to poor stress transfer. This is in stark contrast with many nanotube composite papers which have described very good stress transfer<sup>77,128,129</sup>.

Poly lactide-graphene composites have been produced by Kim et al. by the process of melt processing. The strength was increased from 62 MPa to 70 MPa upon the addition

of 0.5wt% graphene. The Young's modulus increased from 3 GPa to 4.3 GPa. Along with this, the electrical resistivity decreased from  $\sim 10^{16} \Omega/\text{cm}$  to  $\sim 10^6 \Omega/\text{cm}$ <sup>130</sup>.

Khan et al. added graphene to elastomers showing that graphene is a more promising filler for elastomers than nanotubes<sup>131</sup>. They incorporated graphene of mass fractions of up to 90% into polyurethane (PU) to produce drop cast films. The Young's modulus increases from 0.01 GPa up to 1.5 GPa for mass fractions above 50 wt%. A maximum strength of 36 MPa was also achieved. The strain at break and toughness decreases as expected, however the rate of this decrease was slower than the rate of increase of the Young's modulus and strength. These results were compared to similar systems containing nanotubes and it was concluded that this graphene system provided better reinforcement.

Some good mechanical results have also been shown for graphene oxide (GO) composites. While graphene oxide improves dispersion of graphene, it significantly decreases its electronic properties. In a study by Xu et al., PVA-GO composites were made by vacuum filtration and showed a  $dY/dV_f$  value of 110 GPa<sup>95</sup>. A Young's modulus of 4.8 GPa and a strength of 110 MPa was obtained along with a large elongation to break of 36%.

Reinforcement of fibres using graphene nanoplatelets (approx 40 layers) has also been seen. In 2005, polyacrylonitrile (PAN)-nanoplatelet composites were prepared by the electrospinning process. An AFM was used to measure the mechanical properties of the fibres produced. The Young's modulus of these composites doubled upon the addition of 4wt% graphene nanoplatelets<sup>132</sup>.

## 2.7 Conclusions

Carbon nanotubes and graphene can be considered as ideal fillers for incorporating into polymers due to their remarkable mechanical and electrical properties along with their low density. Carbon nanotubes can reinforce polymers even at a low volume fraction which results in a stronger, more elastic composite without any compromise to the overall density. Composite fibres show great promise, generally showing greater mechanical properties than any other composite types. Development of such fibres warrant further research thus development and advancement in fibre composites will be the focus of this thesis.

## 2.8 References

- 1 Callister, W. D. *Materials Science and Engineering. An Introduction.* (2007).
- 2 Almecija, D., Blond, D., Sader, J. E., Coleman, J. N. & Boland, J. J. Mechanical Properties of Individual Electrospun Polymer-Nanotube Composite NanoFibers. *Carbon* **47**, 2253-2258 (2009).
- 3 Anand K, A., Agarwal, U. S. & Joseph, R. Carbon nanotubes-reinforced PET nanocomposite by melt-compounding. *Journal of Applied Polymer Science* **104**, 3090-3095 (2007).
- 4 Bai, J. Evidence of the reinforcement role of chemical vapour deposition multi-walled carbon nanotubes in a polymer matrix. *Carbon* **41**, 1325-1328 (2003).
- 5 Blighe, F. M., Blau, W. J. & Coleman, J. N. Towards tough, yet stiff, composites by filling an elastomer with single-walled nanotubes at very high loading levels. *Nanotechnology*, 415709 (2008).
- 6 Blond, D. *et al.* Strong, Tough, Electrospun Polymer-Nanotube Composite Membranes with Extremely Low Density. *Advanced Functional Materials* **18**, 2618-2624 (2008).
- 7 Cadek, M. *et al.* Reinforcement of Polymers with Carbon Nanotubes: The Role of Nanotube Surface Area. *Nano Letters* **4**, 353-356 (2004).
- 8 Coleman, J. N. *et al.* High Performance Nanotube-Reinforced Plastics: Understanding the Mechanism of Strength Increase. *Advanced Functional Materials* **14**, 791-798 (2004).
- 9 Coleman, J. N., Khan, U. & Gun'ko, Y. K. Mechanical Reinforcement of Polymers Using Carbon Nanotubes. *Advanced Materials* **18**, 689-706 (2006).
- 10 Dalton, A. B. *et al.* Super-tough carbon-nanotube fibres - These extraordinary composite fibres can be woven into electronic textiles. *Nature* **423**, 703-703 (2003).
- 11 Muñoz, E. *et al.* Multifunctional Carbon Nanotube Composite Fibers. *Advanced Engineering Materials* **6**, 801-804 (2004).
- 12 Razal, J. M. *et al.* Arbitrarily shaped fiber assemblies from spun carbon nanotube gel fibers. *Advanced Functional Materials* **17**, 2918-2924 (2007).
- 13 Zhang, X. *et al.* Gel spinning of PVA/SWNT composite fiber. *Polymer* **45**, 8801-8807 (2004).
- 14 Yu, M.-F. *et al.* Strength and Breaking Mechanism of Multiwalled Carbon Nanotubes Under Tensile Load. *Science* **287**, 637-640 (2000).
- 15 Gogolewski, S. & Pennings, A. J. High-modulus fibres of nylon-6 prepared by a dry-spinning method. *Polymer* **26**, 1394-1400 (1985).
- 16 Mark, J. E. *Polymer data handbook.* (Oxford University Press, 1999).
- 17 Lampman, S. *Characterization and Failure Analysis of Plastics.* (ASM International, 2003).
- 18 Verzelli, A. & Rossi, M. High performance car bumper module. United States Patent (1994).
- 19 Eroskey, R. E. & Worchester, W. Process of making a conveyor belt. United States Patent (1988).
- 20 Werner, H., Grothe, K. & Kreuzer, M. Safety Steering Wheel. United States Patent. (1989).
- 21 Pattanayak, A. & Jana, S. C. Properties of bulk-polymerized thermoplastic polyurethane nanocomposites. *Polymer* **46**, 3394-3406 (2005).
- 22 Samowich, J. J. Bullet proof protective shielding and garments and methods of making the same and use thereof. (1985).

- 23 Hearle, J. W. S. High Performance Fibres. (Woodhead Publishing, 2001).
- 24 Dalton, A. B. *et al.* Super-tough carbon-nanotube fibres. *Nature* **423**, 703-703 (2003).
- 25 Nicolson, I. *Boat Data Book*. (Adlard Coles Nautical, 2009).
- 26 Yang Ming, Y. Bicycle Tyre structure. (2003).
- 27 Zachariades, A. E. & Porter, R. S. *The Strength and Stiffness of Polymers*,. p327 (Marcel Dekker, New York, 1983).
- 28 Jacobs, M. J. N. & Van Dingenen, J. L. J. Ballistic protection mechanisms in personal armour. *Journal of Materials Science* **36**, 3137-3142 (2001).
- 29 Thiriot, L. Multilayer material for heat protective garments. (2008).
- 30 Berneburg, P. L. Ceramic composite valve for internal combustion engines and the like. USA patent (1990).
- 31 Naslain, R. *et al.* Boron-bearing species in ceramic matrix composites for long-term aerospace applications. *Journal of Solid State Chemistry* **177**, 449-456 (2004).
- 32 Hopkins, G. R. & Price, R. J. Fusion reactor design with ceramics. *Nuclear Engineering and Design. Fusion* **2**, 111-143 (1985).
- 33 Giallorenzi, T. G. *et al.* Optical Fiber Sensor Technology. *Microwave Theory and Techniques, IEEE Transactions on* **30**, 472-511 (1982).
- 34 Porter, R. M. Glass fiber compositions. United States Patent (1991).
- 35 Kalnin, U. L. Glass fiber reinforced composite article exhibiting enhanced longitudinal tensile and compressive moduli. United States Patent (1971).
- 36 Soutis, C. Carbon fiber reinforced plastics in aircraft construction. *Materials Science and Engineering: A* **412**, 171-176 (2005).
- 37 Tsai, C. Bicycle wheel and the manufacturing method. United States Patent (1991).
- 38 Fu, X. & Chung, D. D. L. Self-monitoring of fatigue damage in carbon fiber reinforced cement. *Cement and Concrete Research* **26**, 15-20 (1996).
- 39 Coleman, J. N., Khan, U., Blau, W. J. & Gun'ko, Y. K. Small but strong: A review of the mechanical properties of carbon nanotube-polymer composites. *Carbon* **44**, 1624-1652 (2006).
- 40 Cox, H. L. The elasticity and strength of paper and other fibrous materials. *British Journal of Applied Physics*, 72 (1952).
- 41 J. C. Halpin Affdl, J. L. K. The Halpin-Tsai equations: A review. *Polymer Engineering & Science* **16**, 344-352 (1976).
- 42 Rosenthal, J. A model for determining fiber reinforcement efficiencies and fiber orientation in polymer composites. *Polymer Composites* **13**, 462-466 (1992).
- 43 Baughman, R. H., Zakhidov, A. A. & de Heer, W. A. Carbon Nanotubes--the Route Toward Applications. *Science* **297**, 787-792 (2002).
- 44 Popov, V. N. Carbon nanotubes: properties and application. *Materials Science and Engineering: R: Reports* **43**, 61-102 (2004).
- 45 Omata, Y., Yamagami, Y., Tadano, K., Miyake, T. & Saito, S. Nanotube nanoscience: A molecular-dynamics study. *Physica E: Low-dimensional Systems and Nanostructures* **29**, 454-468 (2005).
- 46 Ebbesen, T. W. & Takada, T. Topological and SP3 defect structures in nanotubes. *Carbon* **33**, 973-978 (1995).
- 47 Silva, G. G. *et al.* Thermoplastic Polyurethane Nanocomposites Produced via Impregnation of Long Carbon Nanotube Forests. *Macromolecular Materials and Engineering* **296**, 53-58 (2011).

- 48 Naji, H., Zebarjad, S. M. & Sajjadi, S. A. The effects of volume percent and aspect ratio of carbon fiber on fracture toughness of reinforced aluminum matrix composites. *Materials Science and Engineering: A* **486**, 413-420 (2008).
- 49 Nikolaev, P. *et al.* Gas-phase catalytic growth of single-walled carbon nanotubes from carbon monoxide. *Chemical Physics Letters* **313**, 91-97 (1999).
- 50 Maiti, A. Carbon nanotubes: Bandgap engineering with strain. *Nat Mater* **2**, 440-442 (2003).
- 51 Wilder, J. W. G., Venema, L. C., Rinzler, A. G., Smalley, R. E. & Dekker, C. Electronic structure of atomically resolved carbon nanotubes. *Nature* **391**, 59-62 (1998).
- 52 Samsonidze, G. G. S., A.R.; Jorio, D.A.; Pimenta, E.M.A.; Souza Filho, E.A.G.; Grüneis, F.A.; Dresselhaus, D.G.; Dresselhaus, M.S. The Concept of Cutting Lines in Carbon Nanotube Science. *Journal of Nanoscience and Nanotechnology* **3**, 431-458(428) (2003).
- 53 Jorio, A. *et al.* Structural (n, m) Determination of Isolated Single-Wall Carbon Nanotubes by Resonant Raman Scattering. *Physical Review Letters* **86**, 1118 (2001).
- 54 O'Connell, M. J. *et al.* Band Gap Fluorescence from Individual Single-Walled Carbon Nanotubes. *Science* **297**, 593-596 (2002).
- 55 Lemay, S. G. *et al.* Two-dimensional imaging of electronic wavefunctions in carbon nanotubes. *Nature* **412**, 617-620 (2001).
- 56 M S Dresselhaus, G. D., A Jorio. Unusual Properties and Structure of Carbon Nanotubes. *Annual Review of Materials Research* **34**, 247-278 (2004).
- 57 Fox, M. (Oxford Master Series in Condensed Matter Physics, 2006).
- 58 Yu, M.-F., Files, B. S., Arepalli, S. & Ruoff, R. S. Tensile Loading of Ropes of Single Wall Carbon Nanotubes and their Mechanical Properties. *Physical Review Letters* **84**, 5552 (2000).
- 59 Terrones, M. Carbon nanotubes: synthesis and properties, electronic devices and other emerging applications. *International Materials Reviews* **49**, 325-376 (2004).
- 60 Thostenson, E. T., Ren, Z. & Chou, T.-W. Advances in the science and technology of carbon nanotubes and their composites: a review. *Composites Science and Technology* **61**, 1899-1912 (2001).
- 61 Coleman, J. N. *et al.* Reinforcement of polymers with carbon nanotubes. The role of an ordered polymer interfacial region. Experiment and modeling. *Polymer* **47**, 8556-8561 (2006).
- 62 Iijima, S. Helical microtubules of graphitic carbon. *Nature* **354**, 56-58 (1991).
- 63 Cadek, M. *et al.* Optimisation of the arc-discharge production of multi-walled carbon nanotubes. *Carbon* **40**, 923-928 (2002).
- 64 Charlier, J.-C. & Iijima, S. in *Carbon Nanotubes* Vol. 80 *Topics in Applied Physics* 55-81 (2001).
- 65 Esconjauregui, S., Whelan, C. M. & Maex, K. The reasons why metals catalyze the nucleation and growth of carbon nanotubes and other carbon nanomorphologies. *Carbon* **47**, 659-669 (2009).
- 66 Hafner, J. H., Cheung, C. L. & Lieber, C. M. Growth of nanotubes for probe microscopy tips. *Nature* **398**, 761-762 (1999).
- 67 Lee, N. S. *et al.* Application of carbon nanotubes to field emission displays. *Diamond and Related Materials* **10**, 265-270 (2001).
- 68 Koedam, M. Lighting in the Nineties. *Journal of Light & Visual Environment* **15** (1991).

- 69 Yao, Z., Kane, C. L. & Dekker, C. High-Field Electrical Transport in Single-Wall Carbon Nanotubes. *Physical Review Letters* **84**, 2941 (2000).
- 70 Giordani, S. *et al.* Debundling of Single-Walled Nanotubes by Dilution: Observation of Large Populations of Individual Nanotubes in Amide Solvent Dispersions. *The Journal of Physical Chemistry B* **110**, 15708-15718 (2006).
- 71 Bergin, S. D. *et al.* Large Populations of Individual Nanotubes in Surfactant-Based Dispersions without the Need for Ultracentrifugation. *The Journal of Physical Chemistry C* **112**, 972-977 (2008).
- 72 Bergin, S. D. *et al.* Exfoliation in ecstasy: liquid crystal formation and concentration-dependent debundling observed for single-wall nanotubes dispersed in the liquid drug  $\gamma$ -butyrolactone. *Nanotechnology*, 455705 (2007).
- 73 Bergin, S. D. *et al.* Towards Solutions of Single-Walled Carbon Nanotubes in Common Solvents. *Advanced Materials* **20**, 1876-1881 (2008).
- 74 Service, R. F. Nanomaterials Show Signs of Toxicity. *Science* **300**, 243 (2003).
- 75 Fiedler, B., Gojny, F. H., Wichmann, M. H. G., Nolte, M. C. M. & Schulte, K. Fundamental aspects of nano-reinforced composites. *Composites Science and Technology* **66**, 3115-3125 (2006).
- 76 Wang, Q., Dai, J., Li, W., Wei, Z. & Jiang, J. The effects of CNT alignment on electrical conductivity and mechanical properties of SWNT/epoxy nanocomposites. *Composites Science and Technology* **68**, 1644-1648 (2008).
- 77 Cadek, M., Coleman, J. N., Barron, V., Hedicke, K. & Blau, W. J. Morphological and mechanical properties of carbon-nanotube-reinforced semicrystalline and amorphous polymer composites. *Applied Physics Letters* **81**, 5123-5125 (2002).
- 78 Khan, U., Ryan, K., Blau, W. J. & Coleman, J. N. The effect of solvent choice on the mechanical properties of carbon nanotube-polymer composites. *Composites Science and Technology* **67**, 3158-3167 (2007).
- 79 Ruan, S. L., Gao, P., Yang, X. G. & Yu, T. X. Toughening high performance ultrahigh molecular weight polyethylene using multiwalled carbon nanotubes. *Polymer* **44**, 5643-5654 (2003).
- 80 Dalmas, F. *et al.* Multiwalled carbon nanotube/polymer nanocomposites: Processing and properties. *Journal of Polymer Science Part B: Polymer Physics* **43**, 1186-1197 (2005).
- 81 Geng, H. Z. *et al.* Fabrication and Properties of Composites of Poly(ethylene oxide) and Functionalized Carbon Nanotubes. *Advanced Materials* **14**, 1387-1390 (2002).
- 82 Safadi, B., Andrews, R. & Grulke, E. A. Multiwalled carbon nanotube polymer composites: Synthesis and characterization of thin films. *Journal of Applied Polymer Science* **84**, 2660-2669 (2002).
- 83 Manchado, M. A. L., Valentini, L., Biagiotti, J. & Kenny, J. M. Thermal and mechanical properties of single-walled carbon nanotubes-polypropylene composites prepared by melt processing. *Carbon* **43**, 1499-1505 (2005).
- 84 Li, Y. & Shimizu, H. Toward a Stretchable, Elastic, and Electrically Conductive Nanocomposite: Morphology and Properties of Poly[styrene-*b*-(ethylene-co-butylene)-*b*-styrene]/Multiwalled Carbon Nanotube Composites Fabricated by High-Shear Processing. *Macromolecules* **42**, 2587-2593 (2009).
- 85 Liu, Phang, I. Y., Shen, L., Chow, S. Y. & Zhang, W.-D. Morphology and Mechanical Properties of Multiwalled Carbon Nanotubes Reinforced Nylon-6 Composites. *Macromolecules* **37**, 7214-7222 (2004).

- 86 Haggenueller, R., Gommans, H. H., Rinzler, A. G., Fischer, J. E. & Winey, K. I. Aligned single-wall carbon nanotubes in composites by melt processing methods. *Chemical Physics Letters* **330**, 219-225 (2000).
- 87 Kearns, J. C. & Shambaugh, R. L. Polypropylene fibers reinforced with carbon nanotubes. *Journal of Applied Polymer Science* **86**, 2079-2084 (2002).
- 88 Andrews, R., Jacques, D., Qian, D. & Rantell, T. Multiwall Carbon Nanotubes: Synthesis and Application. *Accounts of Chemical Research* **35**, 1008-1017 (2002).
- 89 Jose, M. V., Dean, D., Tyner, J., Price, G. & Nyairo, E. Polypropylene/carbon nanotube nanocomposite fibers: Process-morphology-property relationships. *Journal of Applied Polymer Science* **103**, 3844-3850 (2007).
- 90 Coleman, J. N. *et al.* Improving the mechanical properties of single-walled carbon nanotube sheets by intercalation of polymeric adhesives. *Applied Physics Letters* **82**, 1682-1684 (2003).
- 91 Blighe, F. M., Hernandez, Y. R., Blau, W. J. & Coleman, J. N. Observation of Percolation-like Scaling – Far from the Percolation Threshold – in High Volume Fraction, High Conductivity Polymer-Nanotube Composite Films. *Advanced Materials* **19**, 4443-4447 (2007).
- 92 Vohrer, U., Kolaric, I., Haque, M. H., Roth, S. & Detlaff-Weglikowska, U. Carbon nanotube sheets for the use as artificial muscles. *Carbon* **42**, 1159-1164 (2004).
- 93 Jin, S. H., Park, Y.-B. & Yoon, K. H. Rheological and mechanical properties of surface modified multi-walled carbon nanotube-filled PET composite. *Composites Science and Technology* **67**, 3434-3441 (2007).
- 94 Minus, M. L., Chae, H. G. & Kumar, S. Interfacial Crystallization in Gel-Spun Poly(vinyl alcohol)/Single-Wall Carbon Nanotube Composite Fibers. *Macromolecular Chemistry and Physics* **210**, 1799-1808 (2009).
- 95 Xu, Y., Hong, W., Bai, H., Li, C. & Shi, G. Strong and ductile poly(vinyl alcohol)/graphene oxide composite films with a layered structure. *Carbon* **47**, 3538-3543 (2009).
- 96 Chou, T.-W., Gao, L., Thostenson, E. T., Zhang, Z. & Byun, J.-H. An assessment of the science and technology of carbon nanotube-based fibers and composites. *Composites Science and Technology* **70**, 1-19.
- 97 Ericson, L. M. *et al.* Macroscopic, Neat, Single-Walled Carbon Nanotube Fibers. *Science* **305**, 1447-1450 (2004).
- 98 Razal, J. M., Gilmore, K. J. & Wallace, G. G. Carbon nanotube biofiber formation in a polymer-free coagulation bath. *Advanced Functional Materials* **18**, 61-66 (2008).
- 99 Kozlov, M. E. *et al.* Spinning Solid and Hollow Polymer-Free Carbon Nanotube Fibers. *Advanced Materials* **17**, 614-617 (2005).
- 100 Jiang, K., Li, Q. & Fan, S. Nanotechnology: Spinning continuous carbon nanotube yarns. *Nature* **419**, 801-801 (2002).
- 101 Zhang, X. *et al.* Strong Carbon-Nanotube Fibers Spun from Long Carbon-Nanotube Arrays. *Small* **3**, 244-248 (2007).
- 102 Li, Q. W. *et al.* Sustained Growth of Ultralong Carbon Nanotube Arrays for Fiber Spinning. *Advanced Materials* **18**, 3160-3163 (2006).
- 103 Li, Y.-L., Kinloch, I. A. & Windle, A. H. Direct Spinning of Carbon Nanotube Fibers from Chemical Vapor Deposition Synthesis. *Science* **304**, 276-278 (2004).
- 104 Koziol, K. *et al.* High-Performance Carbon Nanotube Fiber. *Science* **318**, 1892-1895 (2007).

- 105 Vigolo, B. *et al.* Macroscopic fibers and ribbons of oriented carbon nanotubes. *Science* **290**, 1331-1334 (2000).
- 106 Everett, D. H. in *Basic Principles of Colloid Science* 191-201 (The Royal Society of Chemistry, 2009).
- 107 Mercader, C. *et al.* Kinetics of fiber solidification. *Proceedings of the National Academy of Sciences* **107**, 18331-18335 (2010).
- 108 Miaudet, P. *et al.* Hot-drawing of single and multiwall carbon nanotube fibers for high toughness and alignment. *Nano Letters* **5**, 2212-2215 (2005).
- 109 Munoz, E. *et al.* Multifunctional carbon nanotube composite fibers. *Advanced Engineering Materials* **6**, 801-804 (2004).
- 110 Xu, X. *et al.* Fabrication of high strength PVA/SWCNT composite fibers by gel spinning. *Carbon* **48**, 1977-1984.
- 111 Munoz, E. *et al.* Highly conducting carbon nanotube/polyethyleneimine composite fibers. *Advanced Materials* **17**, 1064 (2005).
- 112 Dalton, A. B. *et al.* Continuous carbon nanotube composite fibers: properties, potential applications, and problems. *Journal of Materials Chemistry* **14**, 1-3 (2004).
- 113 Neri, W. *et al.* Surfactant-free spinning of composite carbon nanotube fibers. *Macromolecular Rapid Communications* **27**, 1035-1038 (2006).
- 114 Granero, A. J., Razal, J. M., Wallace, G. G. & Panhuis, M. I. H. Spinning Carbon Nanotube-Gel Fibers Using Polyelectrolyte Complexation. *Advanced Functional Materials* **18**, 3759-3764 (2008).
- 115 Barisci, J. N. *et al.* Properties of carbon nanotube fibers spun from DNA-stabilized dispersions. *Advanced Functional Materials* **14**, 133-138 (2004).
- 116 Steinmetz, J., Glerup, M., Paillet, M., Bernier, P. & Holzinger, M. Production of pure nanotube fibers using a modified wet-spinning method. *Carbon* **43**, 2397-2400 (2005).
- 117 Geim, A. K. & Novoselov, K. S. The rise of graphene. *Nat Mater* **6**, 183-191 (2007).
- 118 Meyer, J. C. *et al.* The structure of suspended graphene sheets. *Nature* **446**, 60-63 (2007).
- 119 Geim, A. K. Graphene: Status and Prospects. *Science* **324**, 1530-1534 (2009).
- 120 Lee, C., Wei, X., Kysar, J. W. & Hone, J. Measurement of the Elastic Properties and Intrinsic Strength of Monolayer Graphene. *Science* **321**, 385-388 (2008).
- 121 Novoselov, K. S. *et al.* Electric Field Effect in Atomically Thin Carbon Films. *Science* **306**, 666-669 (2004).
- 122 Oshima, C. & Nagashima, A. Ultra-thin epitaxial films of graphite and hexagonal boron nitride on solid surfaces. *Journal of Physics: Condensed Matter* **9**, 1 (1997).
- 123 Dimiev, A. *et al.* Layer-by-Layer Removal of Graphene for Device Patterning. *Science* **331**, 1168-1172 (2011).
- 124 Reina, A. *et al.* Large Area, Few-Layer Graphene Films on Arbitrary Substrates by Chemical Vapor Deposition. *Nano Letters* **9**, 30-35 (2008).
- 125 Hernandez, Y. *et al.* High-yield production of graphene by liquid-phase exfoliation of graphite. *Nat Nano* **3**, 563-568 (2008).
- 126 Khan, U., O'Neill, A., Lotya, M., De, S. & Coleman, J. N. High-Concentration Solvent Exfoliation of Graphene. *Small* **6**, 864-871 (2010).
- 127 Lotya, M., King, P. J., Khan, U., De, S. & Coleman, J. N. High-Concentration, Surfactant-Stabilized Graphene Dispersions. *ACS Nano* **4**, 3155-3162 (2010).

- 128 Qian, D., Dickey, E. C., Andrews, R. & Rantell, T. Load transfer and deformation mechanisms in carbon nanotube-polystyrene composites. *Applied Physics Letters* **76**, 2868-2870 (2000).
- 129 Bower, C., Rosen, R., Jin, L., Han, J. & Zhou, O. Deformation of carbon nanotubes in nanotube--polymer composites. *Applied Physics Letters* **74**, 3317-3319 (1999).
- 130 Kim, I.-H. & Jeong, Y. G. Polylactide/exfoliated graphite nanocomposites with enhanced thermal stability, mechanical modulus, and electrical conductivity. *Journal of Polymer Science Part B: Polymer Physics* **48**, 850-858 (2010).
- 131 Khan, U., May, P., O'Neill, A. & Coleman, J. N. Development of stiff, strong, yet tough composites by the addition of solvent exfoliated graphene to polyurethane. *Carbon* **48**, 4035-4041 (2010).
- 132 Mack, J. J. *et al.* Graphite Nanoplatelet Reinforcement of Electrospun Polyacrylonitrile Nanofibers. *Advanced Materials* **17**, 77-80 (2005).

# Chapter 3

## Materials and Methods

### 3.1 Introduction

This chapter introduces the main materials used in this thesis. The methods used to produce and characterise composite fibres are also outlined.

### 3.2 Materials

#### 3.2.1 Poly(vinyl) alcohol

Poly(vinyl) alcohol (PVA) was chosen as the matrix for spinning composite fibres as it is a well studied polymer in the field of coagulation spinning and is water soluble. It is also readily available and can be processed at a low cost. PVA is a chemically resistant plastic with good film forming properties. Its structure is shown in figure 3.1. PVA was purchased from J. T. Baker and was 99.0-99.8% hydrolysed. The average molecular weight of this PVA was 77,000-79,000g/mol. The maximum strength of bulk PVA is approximately 110 MPa and the Young's modulus is 37 GPa<sup>1</sup>.

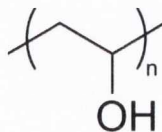


**Figure 3.1: Structure of PVA**

Wet spinning, crosslinking and drawing of PVA fibres can be carried out to produce crystalline fibres with strengths of 1.82 GPa and modulus values of 51.8 GPa<sup>2</sup>.

Another fibre production method is dry spinning of high concentrations of aqueous PVA in a controlled atmosphere followed by fibre cooling. Several drawing steps are also used as part of this method, producing fibres with strengths of up to 2 GPa<sup>3</sup>.

Organic solutions have been used as a spinning dope instead of aqueous solutions in order to improve the mechanical properties of PVA fibres. This was thought to improve fibre strength as fibres could be drawn to high draw ratios in these solvent blends. This was completed by adding PVA to an 80:20 mixture of dimethyl sulfoxide (DMSO) and water and by using a coagulation bath of methanol at -20 °C. This mixture yielded the highest obtainable drawing of fibres. Hot drawing at 160 °C and 200 °C was used for post processing of fibres and strengths of 2.8 GPa and Young's modulus values of 64 GPa were obtained for fibres showing polymer crystallinity<sup>4</sup>.

### 3.2.2 Polyethylene Terephthalate

Polyethylene terephthalate (PET) is a transparent thermoplastic polyester commonly used in synthetic fibres and bottle production. Bulk PET has a breaking strength of approximately 50 MPa and a Young's modulus of 1.7 GPa. It provides a barrier to water, carbon dioxide and oxygen, can be purchased at a low cost and is readily available. The structure of PET is shown in figure 3.2<sup>1</sup>.

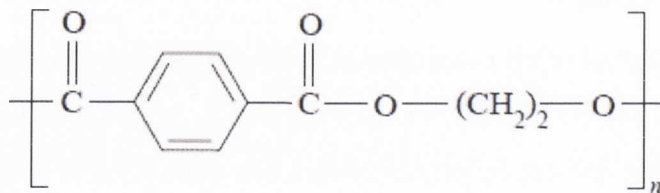


**Figure 3.2: Structure of PET**

One method of PET fibre production is through the use of hot pressing followed by fibre extrusion. Using this method, Chang et al produced fibres with strengths of 46 MPa which could be increased to 51 MPa upon fibre drawing<sup>5</sup>. PET fibres can also be produced from recycled PET bottles. The PET pellets from these bottles were melted, extruded and drawn to form fibres. These fibres had a diameter of 700µm and strengths of over 450 MPa<sup>6</sup>.

PET fibres are widely used in the textile industry and are a very common type of polyester. Several of these commercial fibres such as those produced by “Diolen” were tested by Yeh et al. and strengths of up to 1 GPa and Young's modulus values of up to 17 GPa were measured<sup>7</sup>. PET only fibres were also measured by another source and found to

have strengths and Young's moduli of 931 MPa and 6 GPa respectively with an elongation to break of 17%<sup>8</sup>. The PET used for this work was purchased from SP Deyn Plastics Ltd.

### **3.2.3 Carbon Nanotubes**

Purified SWNTs (HiPCO, Unidym) were used for this work. Individual single nanotubes from this supplier have a diameter range between 0.7-1.4 nm and a length range between 100-1000 nm. When purchased, they are in a black powder form with the nanotubes bundled in ropes which must be debundled before use in composites.

### **3.2.4 Graphene**

Graphite powder was purchased from Sigma Aldrich (product number 332461, batch number 06106DE). In order to use this graphite effectively for composite formation, the graphite layers must be separated into graphene flakes. This was achieved by sonicating graphite in a suitable solvent.

### **3.2.5 Surfactant Choice**

Perhaps the most successful dispersion technique to date, in terms of harnessing the full potential from debundled SWNTs has been through the noncovalent attachment of surfactants<sup>9</sup>. Surfactants have been found to form micelles around SWNTs, following a high power sonication step, forming a protective sheath around the SWNTs that shields them from the solvent. This prevents rebundling of the SWNTs that normally occurs due to the large surface energy difference between surface and solvent<sup>10-12</sup>. A sufficient amount of surfactant must be present in order to disperse the nanotubes efficiently; otherwise large aggregates will remain in the dispersion. However, if the concentration of the surfactant is too large, clusters of surfactant and nanotubes will form. For this reason, a concentration of 10 mg/ml (1 wt%) was chosen<sup>13</sup>.

Various types of surfactants were tested and compared to investigate which one provided fibres with the best mechanical properties<sup>14</sup>. These were sodium dodecylbenzenesulfonate (SDBS), sodium dodecyl sulphate (SDS), lithium dodecyl sulfate (LDS) and sodium cholate (SC). These four inexpensive, readily available surfactants had already been found to be very effective dispersants of SWNT<sup>14</sup>. Sodium cholate was found to be the most effective surfactant for fibre reinforcement and so this was the choice of surfactant for the fibres that will be discussed in chapters 4 and 5.

Sodium cholate was purchased from Sigma Aldrich and its structure is shown in figure 3.3:

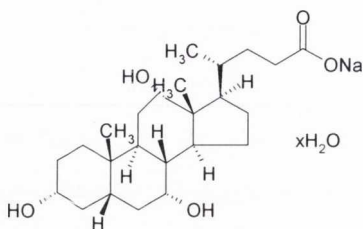


**Figure 3.3: Structures of Sodium Cholate**

### 3.2.6 Solvent Choice

PET-nanotube and PET-graphene fibres will be described in chapter 6. The solvent of choice for use in this system was N-methyl-2-pyrrolidone (NMP). In 2006, Giordani et al. used this solvent successfully to debundling SWNTs. In this study, nanotubes were debundled without the need for centrifugation at low concentrations and good dispersions could be obtained at higher concentrations with the use of centrifugation<sup>15</sup>. Many other researchers have found NMP very effective for dispersion of nanotubes and graphene<sup>16-19</sup>. Along with this, PET is also compatible with the use of NMP.

### 3.3 Methods

Methods are described below for the preparation and characterisation of fibres produced using two processing methods; coagulation spinning and melt processing. Methods are described for the preparation of nanotube and graphene dispersion for use in fibre production. The coagulation spinning process and the method of melt processing are described. Fibres were characterised using a range of methods. This included profilometry to determine fibre diameter accurately. Tensile testing was also carried out to determine the mechanical properties of the fibres. Scanning electron microscopy was used to find the cross section and uniformity of fibres. Other methods such as Raman spectroscopy, atomic force microscopy, X-ray diffraction and transmission electron microscopy were also characterisation methods used and will be described below.

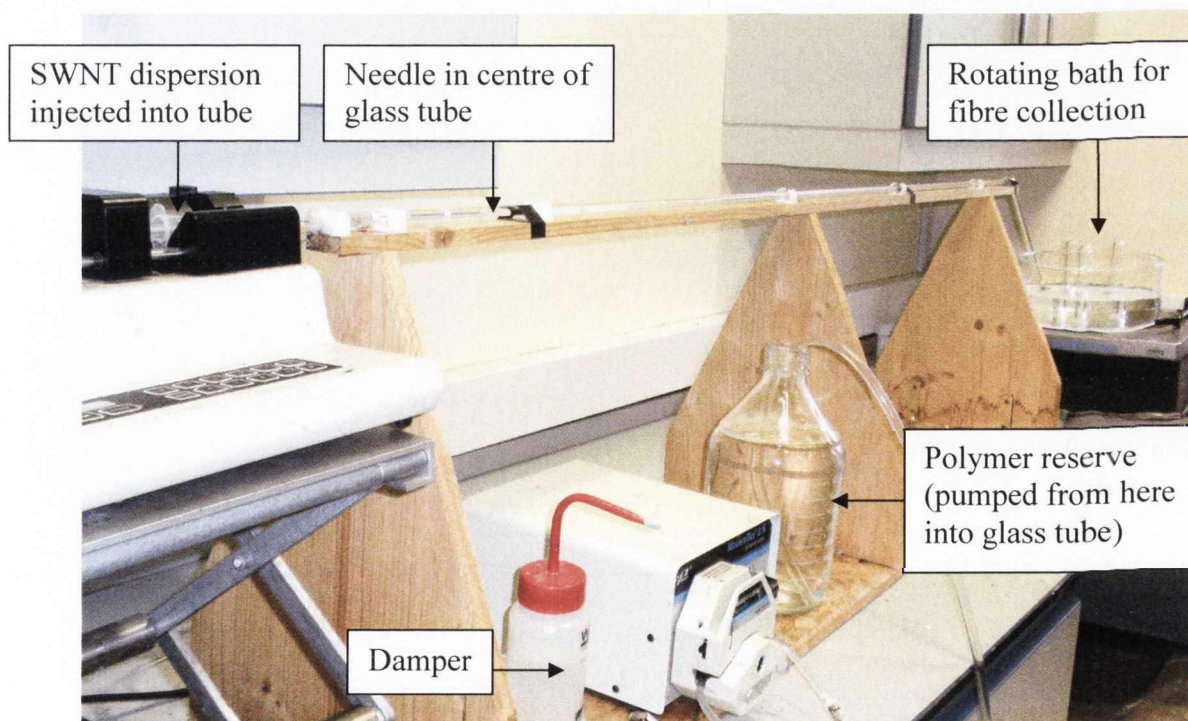
### 3.3.1 Sonication

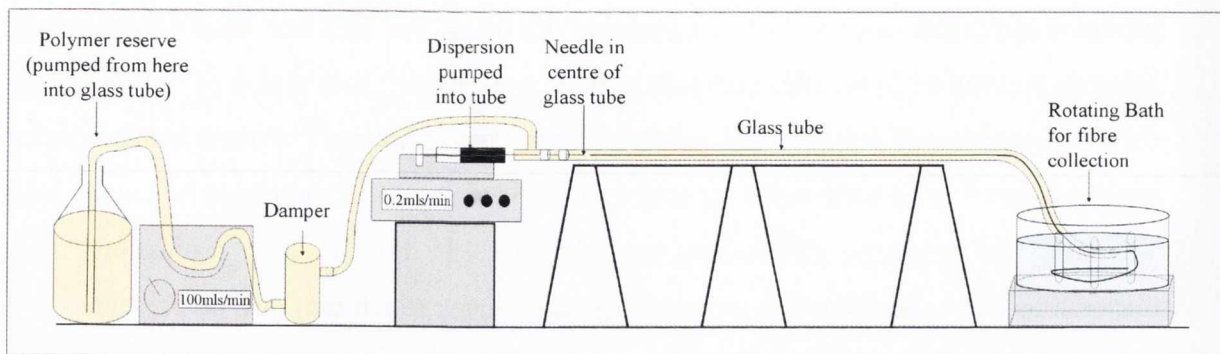
Nanotube and graphene dispersions were prepared using sonication. A sonic tip provides sufficient energy to the nanotubes to break the van der Waals interactions between nanotubes in bundles and aids in their separation<sup>15</sup>. It is also a useful technique for the dispersion of graphite into mono and few layer graphene<sup>17</sup>. Pulsed sonication for several hours was typically used for nanotube dispersions. Mild sonication in a sonic bath was used for graphene dispersions typically for 144 hours. After sonication, most dispersions were centrifuged to remove large aggregates which may still be present.

### 3.3.2 Coagulation Spinning Process

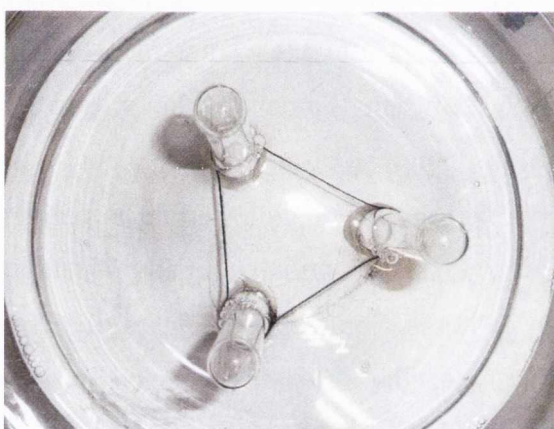
To prepare the fibres, the surfactant-dispersed single-walled nanotubes (SWNTs) were injected at known flow rates into the centre of a cylindrical glass pipe (inner diameter 5 mm) in which the poly(vinyl) alcohol solution flowed. Contact with the PVA solution causes collapse of the nanotube dispersion into a continuous nanotube-PVA fibre which then travelled down the pipe to be collected on a mandrel in a water bath. The fibres were removed from the bath for drying, initially at ambient conditions and then under vacuum at 60°C for 48 hours. Some experiments were performed on as-spun fibres that were undrawn. In other cases, the wet-state precursor fibres were drawn by attaching them to two rollers on a custom built rack.

Figure 3.4 shows a photograph and a schematic of the coagulation spinning setup used for this work. Figure 3.5 shows the rotating bath which was used for fibre collection.





**Figure 3.4: Photograph and schematic of coagulation spinning setup.**



**Figure 3.5: Rotating bath for fibre collection.**

### 3.3.3 Melt Processing of Fibres

Melt processing is particularly suitable for use with thermoplastics as they soften when heated. This technique is a quick and easy way to prepare fibres and can readily be used in large scale industrial preparation of fibres<sup>20</sup>. It can also be used to produce composite fibres. PET fibres in this work are produced using melt processing. PET is heated until it forms a viscous liquid. In previous studies, fillers were added to the PET by shear mixing with some reporting aggregation and low mechanical properties of resulting fibres<sup>21-24</sup>. The method used in this thesis aims to address this problem. The nanotube/graphene dispersions were first prepared in NMP by sonication as described above. This leads to well dispersed nanotubes/graphene with minimum aggregates and should result in fibres with improved mechanical properties. The nanotube/graphene dispersion can be added to the PET melt and constantly stirred as the NMP evaporates. This produces a uniform blend. Fibres could be formed from either a PET or composite

melt by inserting a fine needle to which the melt adhered strongly. The needle was drawn out of the melt at to give a fibre. A schematic of this process is seen in figure 3.6.

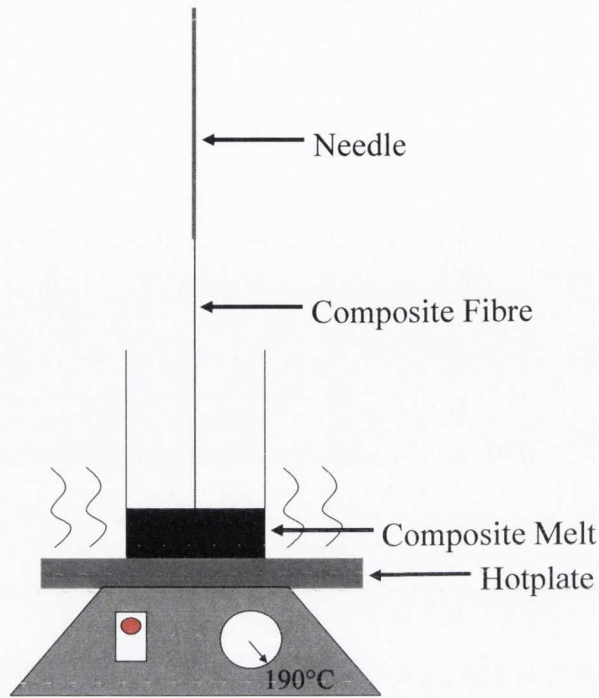


**Figure 3.6: Schematic of melt processing setup.**

### 3.3.4 UV-Vis Spectroscopy

A (Cary 6000i) UV-Vis-IR spectrometer was used to calculate the concentration of dispersions. It is important to know the starting concentration so that composites can be prepared with varying nanotube and graphene volume fractions. In UV-Vis-IR spectroscopy, a double beam spectrometer compares the light intensity between two light paths. Light from a source is split and travels through two substances. One of the paths contains a reference sample such as the solvent or surfactant solution, and the other contains the dispersion. A detector converts the incoming light into a current and plot of absorbance versus wavelength is produced.

The absorption spectra measured before and after centrifugation were compared to calculate the concentration of nanotubes or graphene in the stock. This was calculated using the Beer-Lambert law, (equation (3.1)) which states that the absorbance of the solution is directly proportional to the solutions concentration:

$$\frac{I}{I_0} = e^{-A} \quad 3.1$$

where  $A = \alpha Cl$ .

$\alpha$  is the extinction coefficient at 660nm. Its value for a carbon nanotube dispersion is  $3264\text{ml mg}^{-1}\text{m}^{-1}$  and  $3620\text{ml mg}^{-1}\text{m}^{-1}$  for a graphene dispersion<sup>15,25</sup>.  $C$  is the concentration and  $l$  is the length of the cuvette (1mm).

### 3.3.5 Thermogravimetric Analysis

Thermogravimetric analysis (TGA) is a technique used to determine the thermal stability of a sample by measuring the temperature at which different components of a sample degrade. In this work, the composition of the PVA-nanotube fibres was investigated using a Perkin Elmer Pyris TGA. 1 g of the each of the samples was heated from 30 °C-900 °C at rate of 10 °C/min. As the temperature increases, the mass of the sample decreases and the resulting curve shows mass versus temperature. The derivative of this curve usually shows more than one peak in composite materials. Each peak may be assigned to a different component of the composite and the area under the curve can be used to calculate the filler to matrix mass ratio of the material. If peaks overlap, as in the case with composites in this thesis, an alternative method can be used to calculate the mass fraction of various components.

For these samples, the derivative of the PVA powder curve shows a distinct trough at 387°C which corresponds to a significant loss of sample weight. Approximately 70% of PVA is lost at this point. The same trough is also present in the derivative curves of the composite fibres. The loss observed for the nanotube soot and the sodium cholate at this temperature is negligible. Taking the loss in PVA occurring between  $T_1$  &  $T_2$  and dividing the total composite mass at  $(T_3-T_1)$  allows the PVA and subsequently the nanotube mass fraction to be found using equation 3.2.

$$\frac{M_{T_1} - M_{T_2}}{M_{T_3} - M_{T_1}} = 70\% \text{ of PVA in sample} \quad 3.2$$

### 3.3.6 Profilometry

Dried fibre diameters were measured at typically 20 positions along their lengths using a profilometer (Dektak 6M Stylus Profile, Veeco Instruments Inc.). A  $12.5\mu\text{m}$  tip was scanned across fibre samples with a tip-sample interaction force of  $29.4\mu\text{N}$  to measure their height and hence diameter. In each scan, 3,900 data points were taken. The accuracy of these measurements is  $\pm 0.128\mu\text{m}$ .

### 3.3.7 Mechanical Measurements

Tensile testing is a fundamental mechanical test used to find the Young's modulus, tensile strength, toughness and strain at break of a sample. Mechanical testing was performed with a Zwick Z100 tensile tester using a 100 N load cell and a Textechno Favimat tensile tester with a 2N load cell. Stress-strain curves were obtained from these measurements.

The section of the curve where stress,  $\sigma$ , and strain,  $\epsilon$ , are proportional to each other illustrates the elastic deformation of the material. This is represented by the linear region in figure 3.7 (before point P). The slope of this linear region corresponds to the Young's modulus of the material. The Young's modulus ( $Y$ ), (equation 3.3) is a measure of stiffness. It has units of Pa and is defined as:

$$Y = \frac{d\sigma}{d\epsilon} \text{ as } \epsilon \rightarrow 0 \quad 3.3$$

Elastic deformation is non-permanent meaning the sample returns to its original shape when the applied stress is released. For metallic materials, the elastic deformation occurs only to strains of approximately  $0.005^{26}$ . Beyond this, plastic deformation occurs. Plastic deformation is permanent and the stress is no longer proportional to the strain. Plastic deformation occurs when the bonds of original atom neighbours are broken and when bonds with new neighbours are formed. The stress level at which plastic deformation begins is known as the yield point and is shown by point P in figure 3.7.

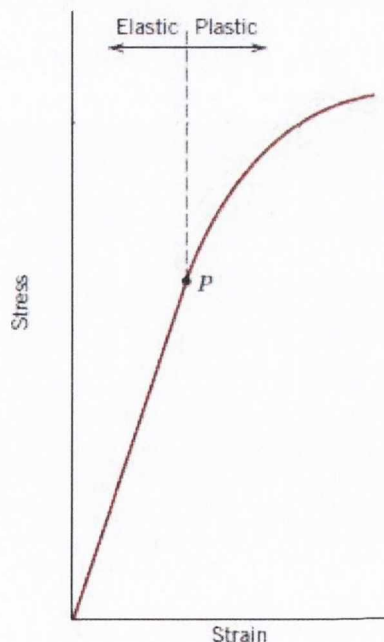
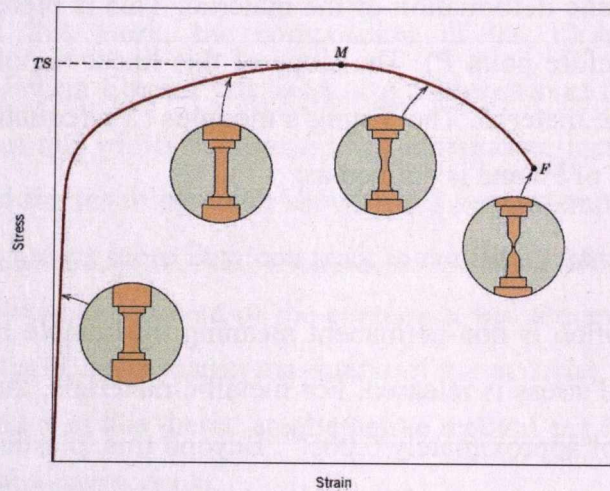


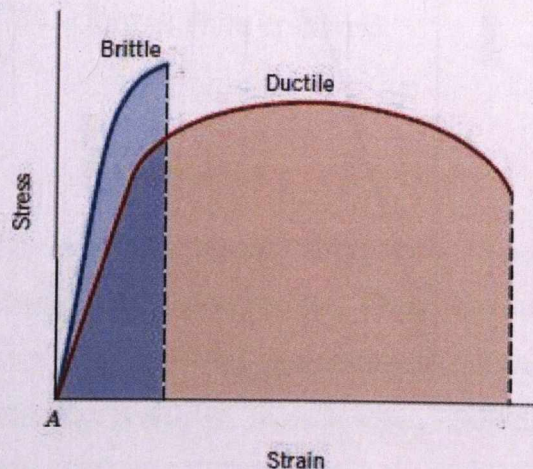
Figure 3.7: Stress-strain curve showing regions of elastic and plastic deformation for a typical metal

After yielding, the substance continues to deform plastically and in some substances (for example in metals) the stress increases to a maximum. This is known as the ultimate tensile stress (force per area,  $\text{N/m}^2$  or Pa) and is shown by point M in figure 3.8. At point M, a small neck begins to form and all subsequent deformation occurs at this point. The geometry of the specimen is shown in the circular insets of figure 3.8. After point M, the stress then decreases until the specimen fractures at point F<sup>26</sup>.



**Figure 3.8: Typical stress-strain curve to fracture. The circular insets represent the geometry of the specimen<sup>26</sup>.**

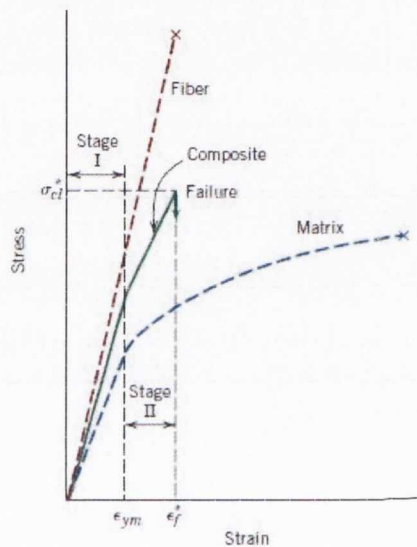
Ductility is another important mechanical property. A material that does not deform plastically or experiences only a small amount of plastic deformation is termed brittle. Examples of stress-strain curves of brittle (blue curve) and ductile (pink curve) materials are shown in figure 3.9. Ductility can be expressed as a percentage elongation. Brittle materials break at strains of 5% or less.



**Figure 3.9: Stress-strain curves for brittle and ductile materials<sup>26</sup>.**

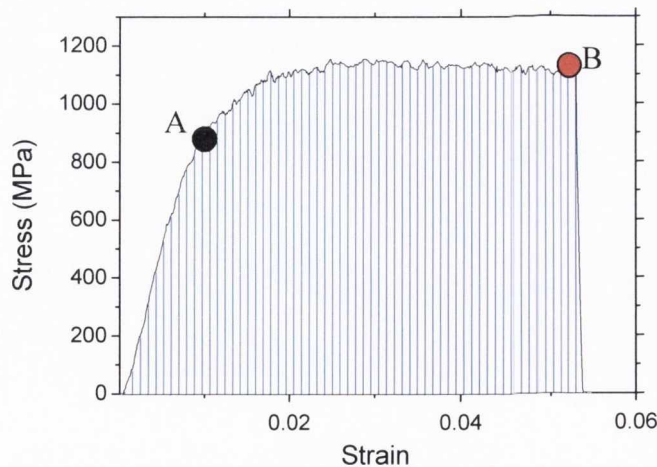
The toughness of a substance can be described as its resistance to fracture when stressed or the amount of energy that can be absorbed by a sample before it breaks. It is measured in  $J/m^3$  or  $J/g$ . It is found from the area under a stress-strain curve. For a material to be tough, it must also have high strength and high ductility.

Figure 3.10 shows typical stress-strain curves of a brittle fibre (for example a nanotube), a matrix and an aligned fibre reinforced composite. In region I both the fibre and the matrix deform elastically. The matrix yields and deforms plastically at point  $\epsilon_{ym}$ . The fibres continue to deform elastically in stage II while the matrix deforms plastically. When the fibres start to fracture, the composite begins to fail.



**Figure 3.10: Typical stress-strain curves of a brittle fibre, a matrix and an aligned fibre reinforced composite <sup>26</sup>.**

Figure 3.11 shows a typical stress strain curve for a typical coagulation spun fibre.



**Figure 3.11: Sample stress-strain curve of a polymer-nanotube fibre of volume fraction 0.23.**

Point A on figure 3.11 is the yield point. Below this point, the substance is deforming elastically. Point B on the graph shows the point at which the sample breaks. The area under the curve, marked in blue, gives the toughness. The sample shown above is a polymer-nanotube fibre of volume fraction 0.23. It was made at a nanotube injection rate of 0.214ml/min and a PVA flow rate of 135ml/min and was 4.6 $\mu$ m in diameter.

### 3.3.8 Scanning Electron Microscopy

SEM was performed on a Carl Zeiss Ultra Plus Field Emission Scanning Electron Microscope. A scanning electron microscope images a sample surface by scanning it with a high energy beam (2-40keV) of electrons. When the electron beam interacts with the sample, secondary electrons (SE), back scattered electrons (BSE), Auger electrons and X-rays are produced, collected in various detectors and an image is produced<sup>27</sup>. Secondary electrons and backscattered electrons are responsible for most imaging performed using this SEM. Figure 3.12 shows the main types of electrons that can be detected. They are split into several groups depending on their origin and their range.

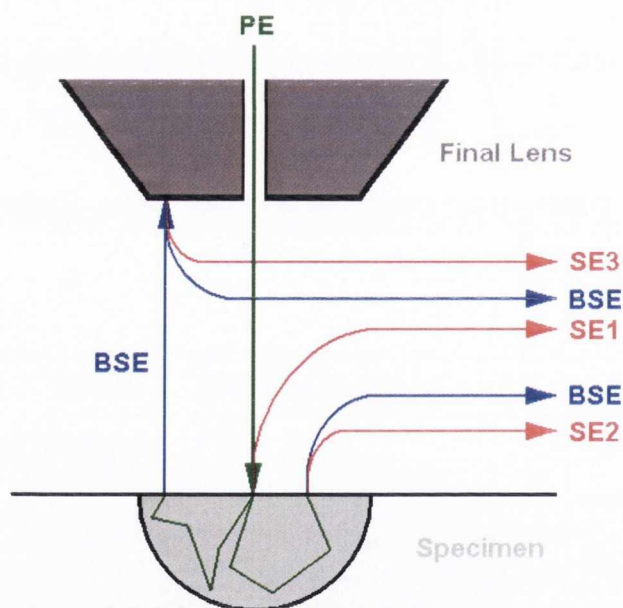


**Figure 3.12: Various types of electrons produced using the scanning electron microscope.**

When electrons are scattered from the inner core or from the electrons of the sample, inelastic scattering occurs resulting in secondary electrons. These are low energy electrons (<50 eV). SE1 electrons come from the spot centre, SE2 electrons undergo some scattering and these leave the sample further from the spot centre, SE3 electrons are

not generally used for imaging and these electrons come from backscattered electrons. Secondary electrons can be detected using the in-lens detector on this machine which is ideal for surface imaging.

Electrons with energies higher than this are known as backscattered electrons. These occur from the elastic scattering off the sample at a much deeper range. The backscattered electron (BSE) detector is useful for seeing elemental contrast between different parts of a sample. Both secondary and backscattered electrons can be detected using the SE2 detector. The secondary electrons account for 90% of the electrons with the backscattered electrons contributing to the rest. This detector can be used at a higher voltage range than the in-lens detector and is effective for looking at material contrast. This detector was most commonly used for this thesis.

### 3.3.9 Raman Spectroscopy

Raman spectroscopy is a technique which relies on the inelastic scattering of laser light off a sample. When monochromatic light interacts with a sample, the majority of photons are elastically (Rayleigh) scattered. However a small portion ( $\sim 1$  in  $10^7$ ) are shifted in wavelength through interactions with the sample material. This is referred to as the Raman effect. During this process, the frequency of the photons is either shifted up or down in comparison with the frequency of the original light. The incident photons excite the molecules in the sample and change them into oscillating dipoles. Rayleigh scattering occurs if the excited molecule returns back to its original vibrational state. If the excited molecule returns to a higher energy level, then the photon loses energy on interaction with the sample. This is known as Stokes Raman scattering. Similarly, Anti-Stokes scattering occurs when an excited molecule returns to a lower energy level, meaning the photon gains energy. The energy distribution gives us information on the chemical bonds present and is like a fingerprint of the material<sup>28</sup>.

A Raman spectra shows Raman scattering intensity (number of scattered photons detected) as a function of wavenumber. It is particularly useful for the analysis of nanotubes and graphene. Some features are prominent in the spectra for these materials. In graphene, the D peak occurs at  $1350\text{ cm}^{-1}$  and is associated with defects and also edge effects<sup>29</sup>. In graphene, the G band occurs at around  $1582\text{ cm}^{-1}$  and this occurs because of vibrations between neighbouring carbon atoms. An upshift of  $5\text{ cm}^{-1}$  occurs if single layer graphene is present. Upshifts show a  $1/n$  dependence where  $n$  is the number of graphene layers<sup>30</sup>. At  $2700\text{ cm}^{-1}$ , the 2D band is present. This is also known as the G' band. This band is seen for all  $sp^2$  hybridised carbon materials. The 2D peak changes shape width

and position with increasing number of graphene layers<sup>31</sup>. For graphene, only one peak is seen here but for graphite two distinct peaks  $G'_1$  and  $G'_2$  will be present. For graphene, the intensity of the 2D band is much larger than the G band with a ratio of 4<sup>30</sup>. This is in contrast with graphite in which the G band is larger than the 2D band (figure 3.13) which is also the case for nanotubes.

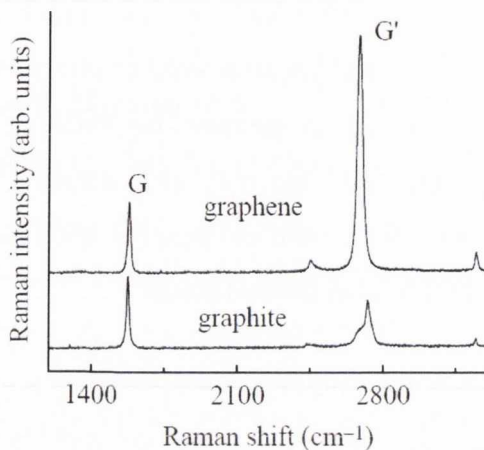


**Figure 3.13: Raman spectra for graphite and graphene showing the G and G' bands<sup>30</sup>.**

Raman measurements were carried out on graphene samples described in chapter 6 using a Horiba Jobin Yvon LabRAM HR spectrometer with a 100X objective lens and 633 nm laser excitation. Five spectra on each sample were taken and their average was found. This was compared with the spectra of bulk graphite.

In nanotubes, the D band is present between 1250 and 1450 $\text{cm}^{-1}$  and is also associated with defects<sup>32</sup>. The G band occurs at around 1580 $\text{cm}^{-1}$  and is always present. Radial breathing modes (RBM) can also feature in the range 100 - 350  $\text{cm}^{-1}$  and gives evidence that SWNTs are present in the sample<sup>33,34</sup>. RBMs are due to coherent vibrations in the radial direction and as such their position can be related to the diameter of the SWNT being probed. The 2D band is also present in the spectra of nanotubes at 2700  $\text{cm}^{-1}$ .<sup>35</sup> This feature is useful to probe the stress transferred from polymer to nanotube<sup>36</sup>. These measurements were carried out for the nanotube-PVA fibres described in chapters 4 and 5. The basis of this measurement is that, as the fibre is strained, the nanotube 2D Raman band tends to shift linearly to a lower wavenumber (at low strain) with the strain on the nanotube. The rate of change of 2D peak position with strain is related to the nanotube effective modulus. (For example a shift rate of -13 $\text{cm}^{-1}/\%$  implies that the nanotube modulus is 260 GPa. This is calculated by using the calibration of -5 $\text{cm}^{-1}/\text{GPa}$ ). The nanotube effective modulus,  $Y_{\text{Eff}}$  is defined by equation 3.4.

$$Y_{Eff} = \eta_0 \eta_l Y_{NT} \quad 3.4$$

In the ideal case,  $Y_{Eff}$  should be identical to  $dY/dV_f$ .  $Y_{Eff}$  was measured as a function of draw ratio for the fibres described above.

A Renishaw 2000 system equipped with a 633 nm He-Ne laser was used to record Raman spectra of the nanotube-PVA fibres. The laser spot size was 2  $\mu\text{m}$  in diameter, and the power was 1 mW when the laser was focused on the fibre. A custom-made tensile rig was used for stretching the paper card on which the fibre was mounted. The strain was recorded using a micrometer which was attached to the rig. The strain was increased stepwise and Raman spectra were taken at each strain level. These measurements were taken by collaborators in the University of Manchester.

### 3.3.10 Atomic Force Microscopy

Atomic force microscopy measurements were made using a Digital Instruments Nanoscope IIIA from Veeco Instruments operating in tapping mode. A vibrating tip is located at the end of a cantilever and this vibrates, tapping the surface of the sample. When the tip comes in contact with an object, the amplitude of this vibration decreases. The AFM senses this and adjusts the amplitude for the next oscillation to retain the initial amplitude. As the tip approaches the surface, it experiences an attractive van der Waals force. As the tip touches the sample there is a strong repulsive force due to ionic repulsion<sup>37</sup>. A laser detects the movement of the cantilever and this information is passed to photodiodes whose signal is collected by a differential amplifier. In this way, an image can be generated by rastering the tip across the sample. Tapping mode minimises frictional forces which would otherwise be present using contact mode AFM<sup>38</sup>. The images in this thesis were obtained under the tapping mode with the tip oscillating at a resonant frequency of 320 kHz. The tip has a diameter of <8nm.

To prepare the samples for AFM, a Si piece was washed in acetone. It was soaked in a diluted sample overnight. Afterwards it was placed in deionised water for 15 mins before gently drying.

### 3.3.11 X-ray Diffraction

Diffraction occurs when waves interact with a regular surface. An X-ray hits a sample and the scattering intensity is analysed. There are various variations of this technique including single crystal X-ray diffraction which is used to find the structure of crystals, powder diffraction which is used to find the crystallographic structure and thin

film diffraction. X-ray diffraction can be used to measure the extent of polymer alignment/crystallinity in a sample as crystalline areas in the sample act as a diffraction grating. This is important as polymer crystallinity influences the mechanical properties of a composite. X-ray diffraction was carried out in the University of Cambridge. Measurements were made on bundles of a few hundred fibres so as to increase the scattering. The patterns were obtained in transmission and were collected for 8 hours. The results were processed using Image J image analysis software. After background removal, orientation plots were obtained by radial integration of the amorphous peak, and plotted against azimuthal angle.

### 3.3.12 Transmission Electron Microscopy (TEM)

Transmission electron microscopy was carried out using a Jeol 2100 TEM operated at 200 kV. Samples were prepared for TEM by dropping small amounts of graphene dispersions onto holey carbon grids. Using this characterisation method, a beam of electrons interacts with a sample. A lanthium hexaboride source was used which has an extended life and good stability. Those electrons that are unobstructed by the flakes or the holey carbon grid hit the fluorescent screen on the other side. Bright field imaging is the most commonly used imaging technique and this mode was used for imaging these samples. In this mode the sample is kept just under the eucentric height. This gives just enough diffraction contrast to analyse the graphene flakes used in this work. The darker areas of an image correspond to areas where fewer electrons could pass through<sup>39</sup> and these areas correspond to a larger number of graphene layers. Approximately 100 flakes were analysed to obtain information on flake size and also on the number of layers present in each flake.

## 3.4 References

- 1 Mark, J. E. *Polymer data handbook*. (Oxford University Press, 1999).
- 2 Hwang, K.-S., Lin, C.-A. & Lin, C.-H. Preparation of high-strength and high-modulus poly(vinyl alcohol) fibers by crosslinking wet spinning/multistep drawing method. *Journal of Applied Polymer Science* **52**, 1181-1189 (1994).
- 3 Perepelkin, K. High-strength, high-modulus fibres made from linear polymers: principles of fabrication, structure, properties, and use. *Fibre Chemistry* **42**, 129-142 (2010).
- 4 Cha, W.-I., Hyon, S.-H. & Ikada, Y. Gel spinning of poly(vinyl alcohol) from dimethyl sulfoxide/water mixture. *Journal of Polymer Science Part B: Polymer Physics* **32**, 297-304 (1994).

- 5 Chang, J.-H., Kim, S. J., Joo, Y. L. & Im, S. Poly(ethylene terephthalate) nanocomposites by in situ interlayer polymerization: the thermo-mechanical properties and morphology of the hybrid fibers. *Polymer* **45**, 919-926 (2004).
- 6 Ochi, T., Okubo, S. & Fukui, K. Development of recycled PET fiber and its application as concrete-reinforcing fiber. *Cement and Concrete Composites* **29**, 448-455 (2007).
- 7 Yeh, W. Y., Young, R. J. Deformation processes in poly(ethylene terephthalate) fibers. Vol. 37 (Taylor & Francis, 1998).
- 8 Hamer, J. W. & Woodhams, R. T. The fracture toughness of polypropylene containing poly(ethylene terephthalate) fibers. *Polymer Engineering & Science* **21**, 603-611 (1981).
- 9 Liu, J. *et al.* Fullerene Pipes. *Science* **280**, 1253-1256 (1998).
- 10 O'Connell, M. J. *et al.* Band Gap Fluorescence from Individual Single-Walled Carbon Nanotubes. *Science* **297**, 593-596 (2002).
- 11 Bachilo, S. M. *et al.* Structure-Assigned Optical Spectra of Single-Walled Carbon Nanotubes. *Science* **298**, 2361-2366 (2002).
- 12 Grossiord, N., van der Schoot, P., Meuldijk, J. & Koning, C. E. Determination of the Surface Coverage of Exfoliated Carbon Nanotubes by Surfactant Molecules in Aqueous Solution. *Langmuir* **23**, 3646-3653 (2007).
- 13 Vigolo, B. *et al.* Macroscopic fibers and ribbons of oriented carbon nanotubes. *Science* **290**, 1331-1334 (2000).
- 14 Sun, Z. *et al.* Quantitative Evaluation of Surfactant-stabilized Single-walled Carbon Nanotubes: Dispersion Quality and Its Correlation with Zeta Potential. *The Journal of Physical Chemistry C* **112**, 10692-10699 (2008).
- 15 Giordani, S. *et al.* Debundling of Single-Walled Nanotubes by Dilution: Observation of Large Populations of Individual Nanotubes in Amide Solvent Dispersions. *The Journal of Physical Chemistry B* **110**, 15708-15718 (2006).
- 16 Bergin, S. D. *et al.* Towards Solutions of Single-Walled Carbon Nanotubes in Common Solvents. *Advanced Materials* **20**, 1876-1881 (2008).
- 17 Hernandez, Y. *et al.* High-yield production of graphene by liquid-phase exfoliation of graphite. *Nat Nano* **3**, 563-568 (2008).
- 18 Ausman, K. D., Piner, R., Lourie, O., Ruoff, R. S. & Korobov, M. Organic Solvent Dispersions of Single-Walled Carbon Nanotubes: Toward Solutions of Pristine Nanotubes. *The Journal of Physical Chemistry B* **104**, 8911-8915 (2000).
- 19 Lotya, M., King, P. J., Khan, U., De, S. & Coleman, J. N. High-Concentration, Surfactant-Stabilized Graphene Dispersions. *ACS Nano* **4**, 3155-3162 (2010).
- 20 Coleman, J. N., Khan, U., Blau, W. J. & Gun'ko, Y. K. Small but strong: A review of the mechanical properties of carbon nanotube-polymer composites. *Carbon* **44**, 1624-1652 (2006).
- 21 Anand, K. A. *et al.* PET-SWNT Nanocomposite Fibers through Melt Spinning. *International Journal of Polymeric Materials* **59**, 438-449 (2010).
- 22 Kim, J. Y., Park, H. S. & Kim, S. H. Multiwall-carbon-nanotube-reinforced poly(ethylene terephthalate) nanocomposites by melt compounding. *Journal of Applied Polymer Science* **103**, 1450-1457 (2007).
- 23 Li, Z., Luo, G., Wei, F. & Huang, Y. Microstructure of carbon nanotubes/PET conductive composites fibers and their properties. *Composites Science and Technology* **66**, 1022-1029 (2006).
- 24 Mun, S. J., Jung, Y. M., Kim, J.-C. & Chang, J.-H. Poly(ethylene terephthalate) nanocomposite fibers with functionalized multiwalled carbon nanotubes via in-situ polymerization. *Journal of Applied Polymer Science* **109**, 638-646 (2008).
- 25 Khan, U., O'Neill, A., Lotya, M., De, S. & Coleman, J. N. High-Concentration Solvent Exfoliation of Graphene. *Small* **6**, 864-871 (2010).

- 26 Callister, W. D. *Materials Science and Engineering An Introduction*. (2007).
- 27 Vernon-Parry, K. D. Scanning electron microscopy: an introduction. *III-Vs Review* **13**, 40-44 (2000).
- 28 Saleh, B. *Intorduction to Subsurface Imaging*. (Cambridge University Press, 2011).
- 29 Gupta, A. K., Russin, T. J., Gutieł rrez, H. R. & Eklund, P. C. Probing Graphene Edges via Raman Scattering. *ACS Nano* **3**, 45-52 (2008).
- 30 Dresselhaus, M. S., Dresselhaus, G. & Hofmann, M. Raman spectroscopy as a probe of graphene and carbon nanotubes. *Philosophical Transactions of the Royal Society A: Mathematical, Physical and Engineering Sciences* **366**, 231-236 (2008).
- 31 Ferrari, A. C. *et al.* Raman Spectrum of Graphene and Graphene Layers. *Physical Review Letters* **97**, 187401 (2006).
- 32 Brown, S. D. M., Jorio, A., Dresselhaus, M. S. & Dresselhaus, G. Observations of the D-band feature in the Raman spectra of carbon nanotubes. *Physical Review B* **64**, 073403 (2001).
- 33 Dresselhaus, M. S., Dresselhaus, G. & Jorio, A. Unusual Properties and Structure of Carbon Nanotubes. *Annual Review of Materials Research* **34**, 247-278 (2004).
- 34 Dresselhaus, M. S., Dresselhaus, G., Saito, R. & Jorio, A. Raman spectroscopy of carbon nanotubes. *Physics Reports* **409**, 47-99 (2005).
- 35 Dresselhaus, M. S., Dresselhaus, G., Jorio, A., Souza Filho, A. G. & Saito, R. Raman spectroscopy on isolated single wall carbon nanotubes. *Carbon* **40**, 2043-2061 (2002).
- 36 Cooper, C. A., Young, R. J. & Halsall, M. Investigation into the deformation of carbon nanotubes and their composites through the use of Raman spectroscopy. *Composites Part a-Applied Science and Manufacturing* **32**, 401-411 (2001).
- 37 Garc, iacute, a, R. & San Paulo, A. Attractive and repulsive tip-sample interaction regimes in tapping-mode atomic force microscopy. *Physical Review B* **60**, 4961 (1999).
- 38 Hansma, P. K. *et al.* Tapping mode atomic force microscopy in liquids. *Applied Physics Letters* **64**, 1738-1740 (1994).
- 39 Reimer, L. & Kohl, H. *Transmission Electron Microscopy: Physics of Image Formation*. (Springer, 2008).

# Chapter 4

## **The Effect of Nanotube Content and Orientation on the Mechanical Properties of Polymer–Nanotube Composite Fibres: Separating Intrinsic Reinforcement from Orientational Effects**

Note: The content of this chapter has been published in *Advanced Functional Materials*, 21, 364-371 (2010). Some of this work was carried out in collaboration with The University of Manchester and Cambridge University. Raman Spectroscopy was carried out in The University of Manchester and the XRD measurements were carried out in Cambridge University. Some mechanical measurements on fibres were also carried out using a tensile tester in Cambridge University to confirm our measurements.

### **4.1 Introduction**

Carbon nanotubes have long been considered the ideal filler for reinforced polymer-based composites because of their superlative mechanical properties<sup>1</sup>. Much work has been done, with some very promising results, particularly in the area of nanotube reinforced fibres<sup>2-10</sup>. It is generally expected that very strong fibres could be produced from polymer-nanotube composites. The strategy for producing very stiff, strong composite fibres is simple: Add nanotubes at as high a loading level as possible and if the rate of increase of stiffness or strength with nanotube content is high enough, very stiff, strong fibres should result. In addition, due to processing or confinement effects, it would be expected that the nanotubes would be partially aligned, thus further improving the mechanical properties. However, this simple recipe has been studied in surprisingly little detail. Very little is known about the real, achievable rate of increase in

fibre stiffness or strength. What is known generally comes from analysis of composite fibres at a single volume fraction<sup>11</sup>, leaving scope for a number of forms of error. In addition, nothing is known about the maximum attainable nanotube content. Only two studies have reported measurements of the mechanical properties of polymer-nanotube composite fibres as a function of nanotube content<sup>12,13</sup>. However, these studies showed very different rates of increase of stiffness with nanotube content, leaving this issue unresolved. In addition, only a relatively low range of nanotube loadings were studied and consequently the maximum achievable loading level remains unknown. This is a serious problem as without knowing the maximum loading level, it is impossible to estimate the maximum achievable stiffness and strength.

In addition, the effect of nanotube orientation on fibre stiffness and strength is not as well understood as it appears. Many papers have shown that filler alignment is achieved on drawing and that this leads to improvements in the mechanical properties obtained<sup>5,13-16</sup>. However, the quantitative analysis has been incomplete. Krenchel realised that the essence of the filler orientation distribution could be distilled down to one parameter, Krenchel's orientation efficiency factor,  $\eta_o$ <sup>16</sup>. Krenchel extended Cox's original model<sup>17</sup> to show that the modulus and strength of composites containing rod-like fillers scales linearly with  $\eta_o$ <sup>16,18</sup>. However it has never been demonstrated experimentally that this scaling holds for a range of orientations (i.e. a range of  $\eta_o$  values) for any composite.

Thus, a systematic study is needed to investigate these deficiencies and this is what this chapter addresses. The effect of nanotube loading on strength and stiffness must be ascertained. The aim would be to measure the rate of increase of both strength and modulus with nanotube content and establish the maximum loading level. In addition, it is important to prepare composites with a range of nanotube orientation distributions and both measure and correlate the mechanical properties with  $\eta_o$ . However to do this, it will be important to choose a suitable model system. Poly(vinyl) alcohol (PVA) is used as a model matrix. This polymer has been used by many groups to produce nanotube-reinforced PVA films<sup>19-25</sup> and fibres<sup>9,10,14,26-37</sup>. Some of the fibres, in particular, have displayed excellent mechanical properties. In general, these fibres are produced by coagulation spinning, a process which involves the injection of surfactant-dispersed nanotubes into a flowing stream of aqueous PVA solution. The PVA adsorbs onto the nanotube, destabilising the dispersion and causing it to collapse into a waterlogged fibre. These fibres can then be dried for testing. Coagulation spinning is useful as its complex parameter space should allow the tuning of fibre properties such as diameter and

nanotube content. In addition the wet fibres are very malleable and can be easily manipulated. This will make control of the orientation distribution by drawing straightforward.

## 4.2 Background

As discussed above, coagulation spun PVA-nanotube fibres show superlative mechanical properties. Dalton et al. prepared PVA-nanotube fibres with Young's moduli,  $Y$ , close to 80 GPa<sup>28</sup>. Extremely strong PVA-nanotube fibres have been reported by Minus et al. with ultimate tensile strengths,  $\sigma_B$ , as high as 2.6 GPa<sup>9</sup>. Perhaps most impressively, PVA-nanotube fibres have displayed exceptional toughness values, up to 870 J/g<sup>31</sup>. While the as-produced composite fibres are water soluble, it has been shown that PVA fibres can be crosslinked in-situ, resulting in high performance water insoluble fibres<sup>38</sup>. Thus, it should be possible, not only to quantitatively examine Krenchel's equation, but to demonstrate the production of relatively stiff, strong fibres.

In this chapter the issues outlined above are addressed. A simple method to control the nanotube volume fraction,  $V_f$ , in coagulation spun fibres is presented. In addition, a practical method to use thermogravimetry to measure the resultant volume fraction is demonstrated. Composite fibres with a range of volume fractions are prepared and the scaling of mechanical properties with  $V_f$  is measured. In addition, fibres of a given volume fraction were drawn and  $dY/dV_f$  and  $d\sigma_B/dV_f$  were monitored to see how they scale with drawing. Critically, Raman spectroscopy was used to monitor both the nanotube orientation parameter and the nanotube effective modulus.

## 4.3 Experimental Procedure

Purified SWNTs (HiPCO, Unidym), poly(vinyl) alcohol (J. T Baker,  $M_w = 77,000-79,000 \text{ g mol}^{-1}$ , 99-99.8% hydrolysed) and the surfactant sodium cholate (Aldrich) were all used as supplied. A surfactant solution was prepared by dissolving sodium cholate in deionised water at 1 wt% (~10mg/mL) and stirring overnight. SWNTs were dispersed in this solution at 0.35 wt% (~3.5mg/mL) using a sonic tip processor (GEX600, 48 W, 24 kHz, flat head probe) operated in pulsed mode (1 sec on/1 sec off) for 7.5 hrs. The resulting nanotube dispersion was mildly centrifuged at 5500 rpm for 90 min (Hettich EBA12) to give a stock solution.

The absorption spectra (Cary 6000i UV-vis-IR spectrometer) measured before and after centrifugation were compared to calculate SWNT concentration in the stock. The stock dispersion was diluted with surfactant solution (1 wt%) to give a range of

nanotube concentrations from 0.07 to 0.316 wt%. A 5 wt% (50 mg/mL) solution of poly(vinyl) alcohol in deionised water was prepared as the coagulant by stirring and then refluxed at approx 110 °C until it became transparent (3-5 hours).

To prepare the fibres the surfactant-dispersed, single-walled nanotubes (SWNTs) were injected (0.214 ml/min) into the centre of a cylindrical pipe (inner diameter 5 mm) in which the poly(vinyl) alcohol solution flowed (81 ml/min). Contact with the PVA solution caused collapse of the nanotube dispersion into a continuous nanotube-PVA fibre which then travelled down the pipe to be collected on a mandrel in a water bath. The fibre length was limited only by the supply of the nanotube dispersion. The fibres collected from the mandrel contained very large quantities of water: they will be referred to as wet-state precursor fibres. They were cut into sections and removed from the bath for drying, initially at ambient conditions and then under vacuum for 48 hours. The diameter of the fibres after drying was typically 5-10  $\mu\text{m}$ . Note that for the first set of experiments the fibres were not drawn in any way. Subsequently, the wet-state precursor fibres were drawn by attaching them to two rollers on a custom built rack. The rollers could be controllably rotated resulting in the drawing of the fibres to well defined draw ratios, DR ( $\text{DR}=(l-l_0)/l_0$ ). After drawing, the fibres were dried as described above.

Thermogravimetric analysis (Perkin Elmer Pyris 1) was used to calculate the nanotube mass fraction of a subset of fibres. Scanning electron microscopy (SEM) was performed using a Hitachi S-4300 field emission scanning electron microscope. Mechanical testing was performed with a Zwick tensile tester Z100 using a 100 N load cell with a strain rate of 1 mm/min. The gauge length was kept constant at 10 mm. The sensitivity of this instrument in this force range was verified by testing Kevlar fibres of similar diameter and known strengths. For each sample, mechanical tests were made on ten fibres, and the mean and standard deviation of the relevant mechanical parameters calculated. A Renishaw 2000 system equipped with a 633 nm He-Ne laser was used to record Raman spectra of the fibres. The laser spot size was 2  $\mu\text{m}$  in diameter, and the power was 1 mW when the laser was focused on the fibre. A custom-made tensile rig was used for stretching the paper card on which the fibre was mounted. The strain was recorded using a micrometer which was attached to the rig. The strain was increased stepwise and Raman spectra were taken at each strain level.

## 4.4 Results and Discussion

### 4.4.1 As Prepared Fibres

Poly(vinyl) alcohol-SWNT fibres were prepared by coagulation spinning. Detailed analysis of the suspension showed it to contain individual nanotubes and small bundles (mean diameter,  $\langle d \rangle = 1.8$  nm and mean length  $\langle l \rangle = 315$  nm<sup>39</sup> (figure 4.1).

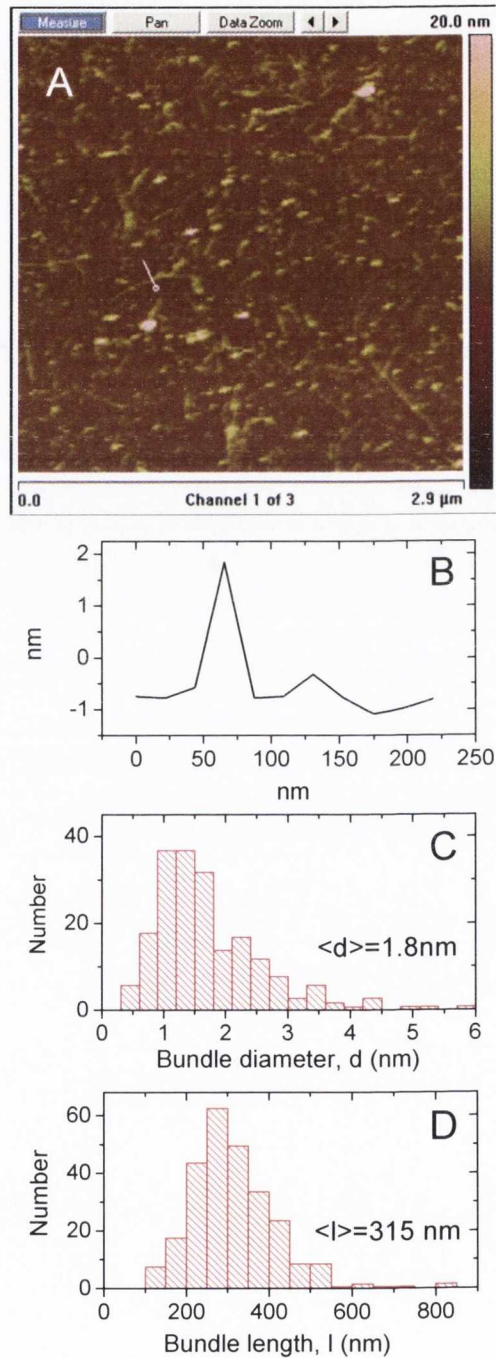


**Figure 4.1:** A) AFM image of nanotube bundles deposited from the spinning dispersion onto Si/SiO<sub>2</sub>. Deposition and AFM characterisation were performed as described in ref<sup>40</sup>. B) Height profile along the bundle marked by the white line. C) and D) Histograms of bundle diameter and height respectively.

Fibres were prepared using a range of nanotube dispersions with differing concentrations (0.07-0.32 wt%). As all other spinning parameters remained the same it is expected that the resultant fibres will differ only in the nanotube mass fraction. To test this, thermogravimetric analysis was performed on four fibres prepared from dispersions with nanotube concentrations ranging from 0.07-0.32 wt%. In addition TGA was performed on the nanotube and PVA powders for comparison. Example TGA curves for PVA, SWNTs and a composite fibre (0.14 wt% nanotubes) are shown in figure 4.2. In addition the derivative TGA curves are shown in blue.

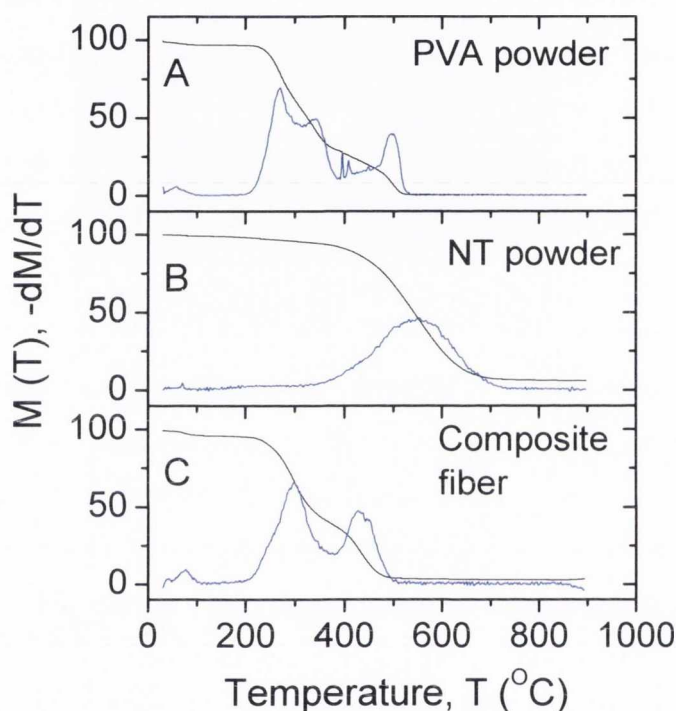


**Figure 4.2: TGA and derivative-TGA curves of A) PVA and B) nanotube powder and C) a composite fibre (0.14wt%= 0.1073vol%).**

It can often be difficult to differentiate the oxidation of polymer and nanotubes in a composite system. This is partly due to the relative proximity of their oxidation temperatures but also due to the fact that the nanotube oxidation can narrow and shift in temperature in the composite versus the nanotube only sample. To circumvent this problem an indirect method can be used to calculate the nanotube mass fraction. The PVA powder DTGA curve consists of two main oxidation events, above and below 400 °C. Conversely, the nanotube only sample hardly burns at  $T < 400$  °C. By integration it can be found that 73% of the PVA powder burns below  $T = 400$  °C. In each composite sample, two features were observed above and below 400 °C similar to those in the PVA powder sample. It is assumed that in all cases, the ratio of polymer mass oxidised above and

below 400 °C remains the same as in the pure polymer. Thus, by separately integrating the composite curves from T=30 °C to T=400 °C and T=400 °C to T=900 °C and applying the ratio of polymer mass oxidised above and below 400 °C, one can calculate the mass of nanotubes burned above 400 °C. Thus the mass fraction of nanotubes in each sample can be calculated. An estimated uncertainty of ~20% is associated with this method. This data is shown in figure 4.3 as a function of the concentration of the nanotube dispersion used in the fibre formation. This curve shows that the nanotube mass fraction in the final fibre is very close to 100 times the nanotube concentration in the dispersion. This allows one to transform the nanotube concentration data to mass fraction for all fibres. The volume fraction can be calculated from the mass fraction taking density values of  $\rho_{NT}=1800 \text{ kg/m}^3$  (this value includes residual catalyst<sup>41</sup>) and  $\rho_{PVA}=1300 \text{ kg/m}^3$ . This results in fibres with volume fraction ranging from 5.3 to 24vol%.

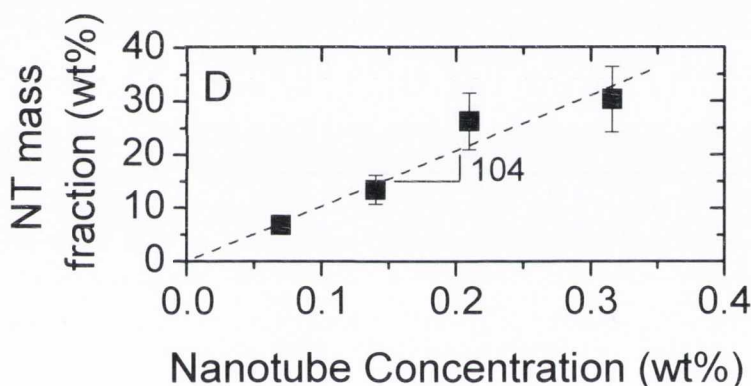


**Figure 4.3: Mass fraction as a function of nanotube concentration in the spinning dispersion.**

This analysis shows the nanotube mass fraction to scale linearly with the concentration of the spinning dispersion.

These fibres (figure 4.4 A-C) are straight with reasonably uniform diameter and circular cross sections. As can be seen from figures 4.3 B&C, when broken, large number of well-dispersed nanotubes are observed protruding from the fracture surface.

The stress-strain curves were measured for a set of fibres with a range of volume fractions. Representative stress-strain curves are shown in figure 4.4D.

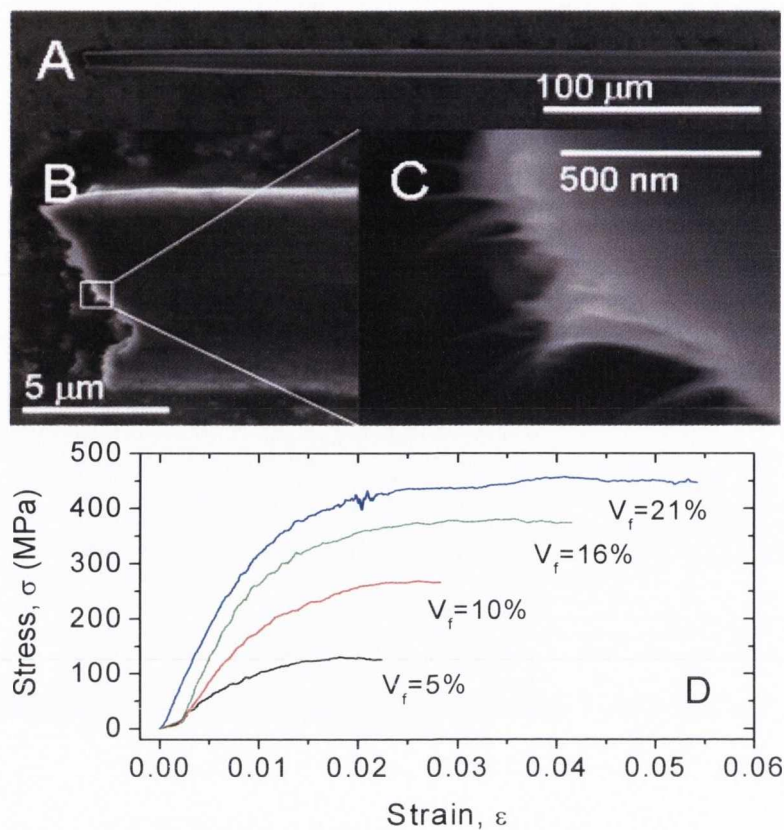


**Figure 4.4: A), B) & C) SEM images of a typical fibre broken under tensile strain. D) Representative stress strain curves for selected fibres of varying SWNT volume fraction. NB the curves have been smoothed using a 9 point moving average.**

It is immediately apparent that the ultimate tensile strength,  $\sigma_B$ , scales with nanotube volume fraction. In addition, it is noted that these fibres are much less ductile than previously reported coagulation spun PVA-SWNT fibres<sup>28,31</sup>. This is attributed to the fact that these fibres were extensively dried before testing (all reported results are for dry fibres). In fact, it was found that exposure of dried fibres to ambient conditions resulted in considerable water uptake and an increase in fibre ductility (and decrease in modulus and strength), see figure 4.5.

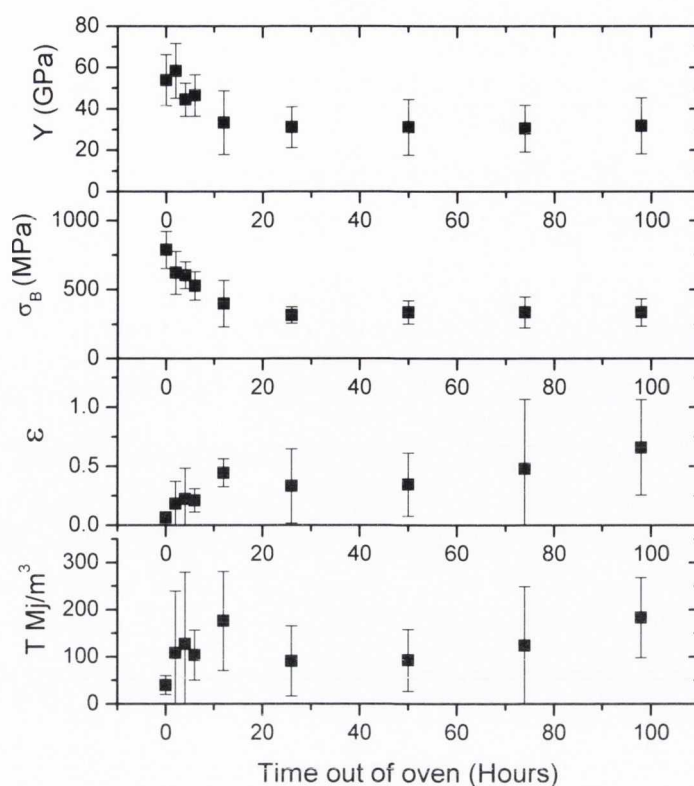


**Figure 4.5: Change in fibre mechanical properties as a function of time after removal from oven. Absorption of water results in the reduction of strength and modulus and the increase in ductility.**

It can be seen that water absorption greatly affects the mechanical properties of the fibres. The Young's modulus decreases from 53.8 GPa to 33.2 GPa after being out of the oven for 12 hours. In the same amount of time, the strength decreased from 787 MPa to 399 MPa. This is accompanied by an increase in the strain at break and in the toughness. To ensure all measurements were consistent, fibres were mechanically tested as soon as they were removed from the oven.

In addition, these fibres display lower tensile strength compared to some previously reported PVA-SWNT coagulation spun fibres<sup>28,31</sup>. This is likely to be related to the polymer matrix that is being used in this study. It is well known that different types of PVA (i.e. different molecular weight, polydispersity, degree of hydrolysis etc), sold by different suppliers, result in fibres with radically different strengths.

The Young's modulus,  $Y$ , ultimate tensile strength,  $\sigma_B$ , the strain at break,  $\epsilon_B$ , and the toughness,  $T$ , were measured as a function of nanotube volume fraction as shown in figure 4.6. This is the first time the volume fraction dependence of the mechanical properties of coagulation-spun, polymer-nanotube fibres has been measured.

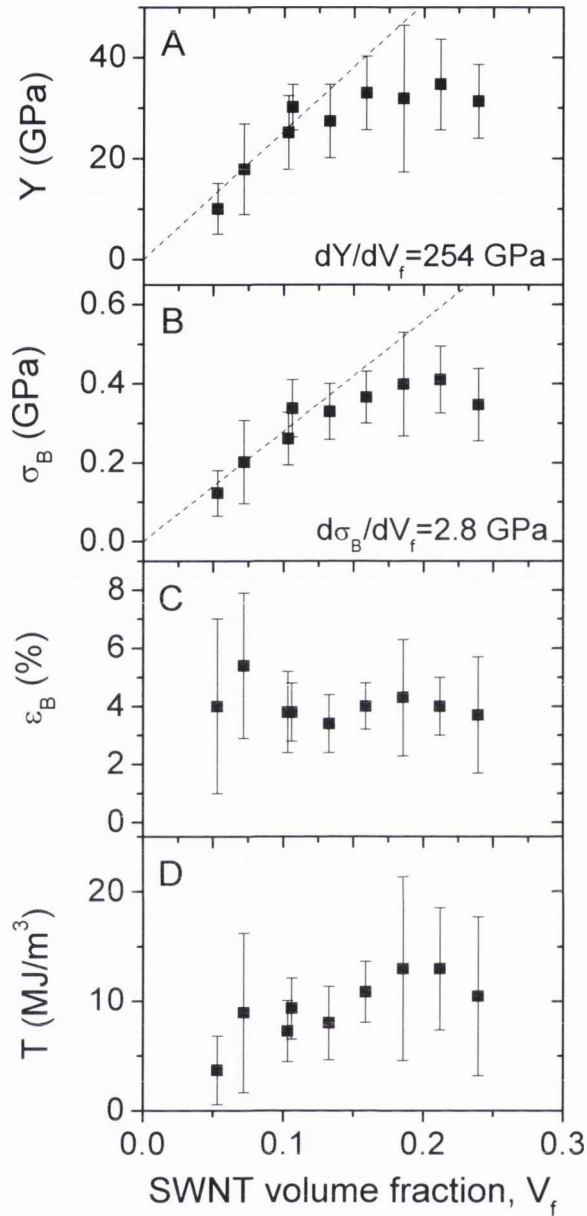


**Figure 4.6: Mechanical properties derived from the stress strain curves plotted as a function of nanotube volume fraction. A) Young's modulus, B) Ultimate tensile strength, C) Strain at break, D) Toughness.**

The modulus increases linearly with volume fraction as expected for volume fractions up to  $\sim 10\text{vol}\%$  before beginning to saturate, possibly due to aggregation effects. Indeed, recent modelling has shown that for nanotubes flowing in a liquid, the tendency to aggregate increases with nanotube concentration<sup>42</sup>. Such aggregated structures tend to be less aligned by the flow, resulting in reduced mechanical properties in the final fibre. Saturation occurs by  $\sim 10\text{ vol}\%$ , with this figure representing the maximum effective nanotube content. It can be estimated that the average spacing between nanotubes at this

volume fraction is  $\sim 6$  nm. Thus, it is hard to imagine any further increase in nanotube content without large-scale aggregation.

For rod-like fillers, the linearity of  $Y$  with  $V_f$  is predicted by the rule of mixtures<sup>16,18</sup>:

$$Y = (\eta_0 \eta_{lY} Y_{NT} - Y_P) V_f + Y_P \approx \eta_0 \eta_{lY} Y_{NT} V_f \quad 4.1$$

where  $\eta_{lY}$  and  $\eta_0$  are the nanotube length and orientation efficiency factors and  $Y_{NT}$  and  $Y_P$  are the nanotube and polymer moduli respectively. Note that  $\eta_{lY}$  applied specifically to fibre modulus (a different length efficiency factor applies to fibre strength). The slope of the linear region has been measured to be  $dY/dV_f = 254$  GPa.

Wang et al.<sup>25</sup> have calculated  $dY/dV_f$  (equivalent to their parameter,  $E_{eff}$ ) for a number of polymer-nanotube composite fibres reported in the literature. These values vary from 4 GPa for MWNT-polyamide fibres<sup>13</sup> to 1269 GPa for SWNT-pitch fibres<sup>2</sup>. It is important to point out that in all cases, Wang had no option but to calculate  $dY/dV_f$  from one or at most two volume fractions. This work is the first to comprehensively measure mechanical properties as a function of volume fraction allowing accurate measurement of  $dY/dV_f$  in the linear region.

For perfectly aligned fibres ( $\eta_0=1$ ) prepared with long nanotubes ( $\eta_{lY}=1$ ),  $dY/dV_f = Y_{NT}$ , which has a maximum value of  $\sim 1000$  GPa. This is consistent with the maximum value reported by Wang. Values of  $dY/dV_f < 1000$  GPa are manifestations of short tube effects, poor alignment, poor stress-transfer or combinations of all three<sup>1</sup>. Incidentally, the value of  $dY/dV_f = 254$  GPa is reasonably high; only five of the 20 papers analysed by Wang et al. show higher values.

Data for fibre strength as a function of volume fraction are shown in figure 4.6B. The trend is similar to the modulus data with a linear region followed by saturation. Here the slope of the linear region has been measured to be  $d\sigma_B/dV_f = 2.8$  GPa. The fibre strength is given theoretically by<sup>18</sup>:

$$\sigma_B = (\eta_0 \eta_{l\sigma} \sigma_{NT} - \sigma_P) V_f + \sigma_P \approx \eta_0 \eta_{l\sigma} \sigma_{NT} V_f \quad 4.2$$

where  $\sigma_{NT}$  and  $\sigma_P$  are the nanotube and polymer strengths respectively. (Note that  $\eta_{l\sigma}$  is a length efficiency factor applicable to fibre strength). As with modulus, the maximum value for  $d\sigma_B/dV_f$  for an aligned, long-nanotube fibre is  $\sigma_{NT}$ , which is expected to have a maximum value of  $\sim 50$ - $150$  GPa. The highest reported value of  $d\sigma_B/dV_f$  is 116 GPa for a PVA-SWNT fibre<sup>9</sup>. Most values are much lower, perhaps because the strength of both nanotubes and fibres are expected to be more sensitive to imperfections than modulus.

It is noted that the low  $V_f$  data for both modulus and strength pass through the origin, validating the approximations given in equations 4.1 & 4.2. This is an important result as

it suggests that the polymer matrix in these coagulation spun fibres is not particularly stiff or strong. This in turn suggests that large scale crystallinity or chain alignment is not occurring in these fibres.

Care must be taken when using equations 4.1 and 4.2 to analyse mechanical data for polymer-nanotube composites. In some cases, particularly when using PVA as a matrix, crystalline polymer can be nucleated by the presence of the nanotubes<sup>1,9,13,20,23,32,43,44</sup>. Under such circumstances, these equations must be replaced by expressions which account for the contribution of nanotube-nucleated crystals to the mechanical properties<sup>1,23</sup>. Thus, unless one can rule out extra contributions to the mechanical properties, one cannot use equations 4.1 and 4.2 to analyse the  $d\sigma_B/dV_f$  and  $dY/dV_f$  data. Later in this work, Raman spectroscopy will be used to show that nanotube-induced polymer crystallinity does not contribute to the mechanical properties of the as-prepared fibres.

In addition, it is noted that the strain at break is relatively invariant with volume fraction, remaining close to 4%. However, the toughness increases with increasing volume fraction, saturating at close to 12 MJ/m<sup>3</sup>. Note that these values are much lower than previously reported values<sup>28,31</sup>, mainly due to the low ductility of these fibres.

#### 4.4.2 Fibre Drawing

As mentioned above, the mechanical properties of composite fibres are limited by the nanotube length, the strength of the polymer-nanotube interface and the degree of nanotube alignment. The nanotube length is constrained to a large degree by the requirement that the nanotubes are well dispersed in the polymer matrix<sup>1</sup>. The reason for this is that nanotube exfoliation and so dispersion is generally achieved by sonication which is also known to shorten the nanotubes by scission<sup>45,46</sup>. Thus, the cost of well dispersed nanotubes is a reduction in length. This means nanotubes which have been exfoliated in the liquid phase tend to have lengths of  $<1\mu\text{m}$ <sup>39,46</sup>. In addition, for a given polymer-nanotube combination, it is not easy to adjust the interfacial strength. However, the nanotube alignment can be modified, for example by drawing the fibre. This makes drawing a critically important technique in fibre research. Drawing will improve the strength and modulus, but more importantly allows control of the nanotube orientation distribution.

Drawing experiments were carried out on fibres with a fixed nanotube volume fraction of 7.1 vol%. This was chosen as a reasonably high volume fraction, yet definitively in the linear regime. The wet-state precursor fibres were stretched to draw

ratios from 7.5% to 63%. Any attempt to draw fibres to higher draw ratios resulted in breakage of all fibres. Any attempt to draw fibres after they had been dried resulted in almost immediate failure. The mechanical properties of a range of drawn fibres were measured and are reported in figure 4.7.

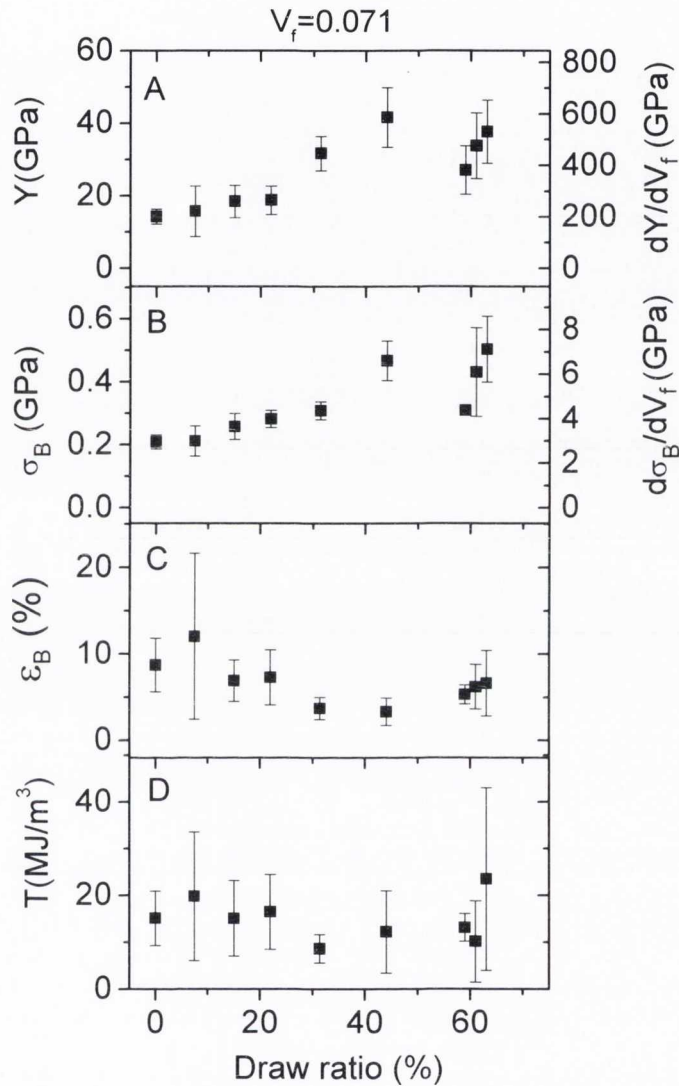


**Figure 4.7: Mechanical properties for fibres produced by drawing the wet-state precursor fibre, plotted as a function of draw ratio. All fibres have volume fraction of 7.1%. A) Young's modulus, B) Ultimate tensile strength, C) Strain at break, D) Toughness. In A) and B) the right axes show the estimated  $dY/dV_f$  and  $d\sigma_B/dV_f$ .**

It is clear from this data that both modulus (figure 4.7A) and strength (figure 4.7B) increase steadily with drawing from their undrawn values (14 and 0.2 GPa respectively), saturating at values of 40 and 0.5 GPa respectively for draw ratios of >40%. From this data  $dY/dV_f$  and  $d\sigma_B/dV_f$  can be estimated by dividing  $Y$  and  $\sigma_B$  by the volume fraction (7.1vol%). (NB, this approximation only works because the  $Y$  and  $\sigma_B$

data in figure 4.6 go through the origin.) This is shown on the right axes. Here the fibres have  $dY/dV_f \sim 600$  GPa and  $d\sigma_B/dV_f \sim 7$  GPa for DR >40%.

Interestingly, the strain at break of these fibres doesn't decrease significantly on drawing; generally increases in strength and modulus on drawing are obtained at the expense of ductility. In addition, the toughness remains relatively constant at  $\sim 15$  MJ/m<sup>3</sup>. Drawing of polymer-nanotube fibres results in a reduction in diameter commensurate with the conservation of fibre volume. This diameter reduction is accompanied by an increase in the degree of orientation of the nanotubes. It is possible to directly measure the effect of drawing on nanotube orientation using Raman spectroscopy. This makes use of the fact that the observed Raman intensity depends on the angle between the nanotube axis and the electric field vector of the excitation beam<sup>47</sup>. By measuring the Raman signals with the incident beam polarised parallel and perpendicular to the fibre, in both VV and VH arrangements, it is possible to calculate<sup>48</sup> the Herman's orientation parameter, S, where:

$$S = [3\langle \cos^2\theta \rangle - 1] / 2 \quad 4.3$$

and  $\theta$  is the angle between a given nanotube and the fibre axis. A typical Raman spectra is shown in figure 4.8.

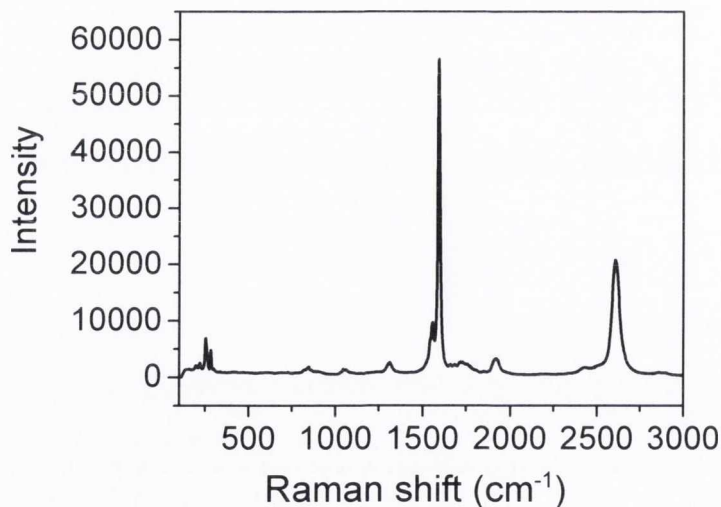


**Figure 4.8: Raman spectrum of a PVA-SWNT composite fibre.**

Raman spectra were collected on fibres orientated at different angles ( $\phi$ ) with respect to the laser polarization obtained with VV configuration. Typical spectra for both drawn and undrawn fibres are shown in figure 4.9A&B. The normalised G band intensity

for one fibre is shown in figure 4.9C. This data could be fitted with the following function (after Liu et al.):

$$I_{Fibre}^{VV}(\varphi) \propto \left( \cos^4 \varphi - \frac{6}{7} \cos^2 \varphi + \frac{3}{35} \right) \langle P_4(\cos \beta) \rangle + \left( \frac{6}{7} \cos^2 \varphi - \frac{2}{7} \right) \langle P_2(\cos \beta) \rangle + \frac{1}{5} \quad 4.4$$

where  $\beta$  is a variable describing the angle between a given nanotube and the fibre axis.

The parameter  $\langle P_2(\cos \beta) \rangle$  is identical to  $S$  and was found from the fit.

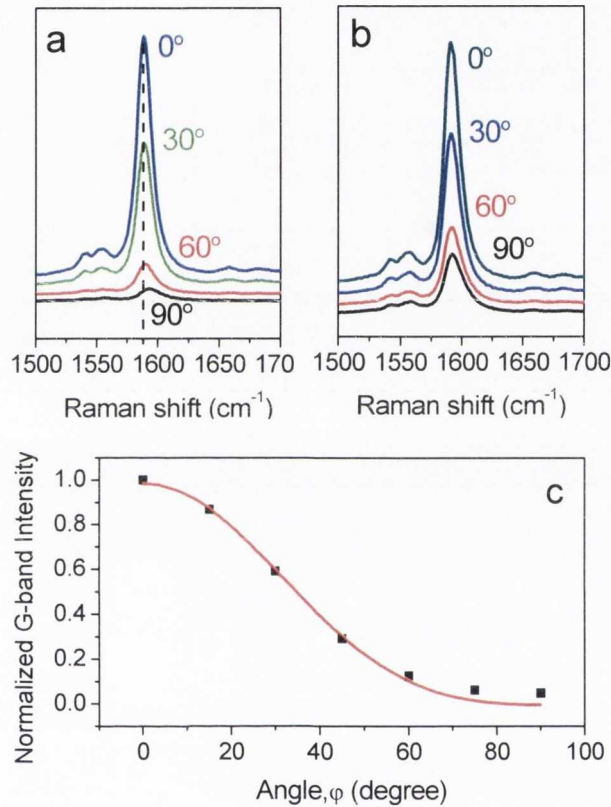


**Figure 4.9: Nanotube G-band for PVA-SWNT coagulation spun fibres at different angle with respect to the laser polarization obtained with VV configuration: a) fibre with a draw ratio of 63% and b) undrawn fibre. C) Experimental data fitted using Equation 4.4.**

Theoretically, this orientation parameter varies from  $S=-0.5$  for rods aligned in plane to  $S=0$  for random orientation to  $S=1$  for perfect axial alignment. Data showing  $S$  as a function of draw ratio for the fibres described above can be seen in figure 4.10.

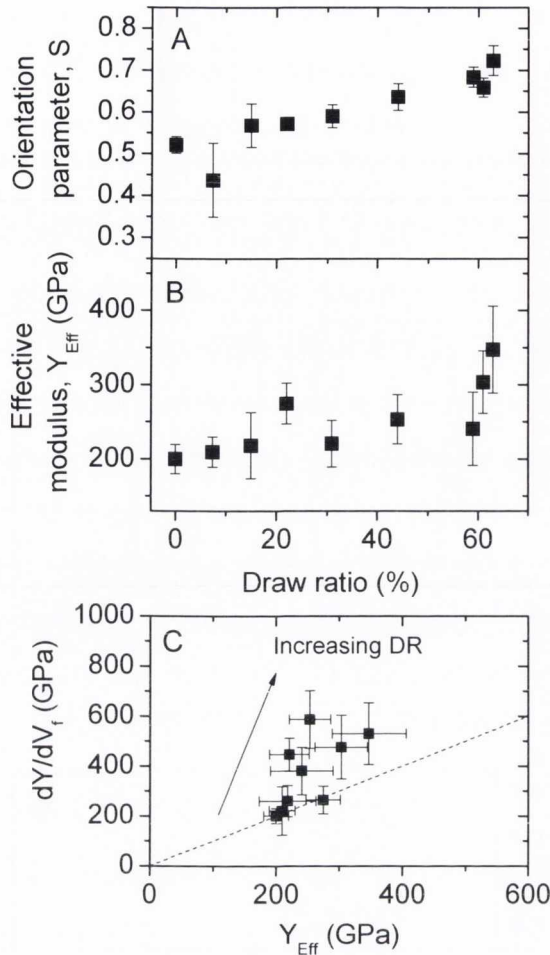


**Figure 4.10: Nanotube orientation parameter and effective modulus as measured by Raman spectroscopy. A) Orientation parameter and B) Effective nanotube modulus, both as a function of draw ratio. C) Effective nanotube modulus as a function of mechanically measured  $dY/dV_f$ . The dashed line shows  $dY/dV_f=Y_{\text{eff}}$ .**

It was observed that  $S$  increased from  $\sim 0.5$  for the undrawn fibre to  $\sim 0.7$  for the DR=63% fibre. Assuming Gaussian orientation distribution functions, these values are equivalent to distributions with half widths of  $\gamma/2=32^\circ$  and  $\gamma/2=21^\circ$  respectively. This data can be compared with the results of Badaire et al. and Pichot et al. on X-ray scattering studies performed on similar PVA-nanotube fibres<sup>14,33</sup>. In each case the undrawn fibres had nanotube distributions with  $\gamma/2\sim 24-28^\circ$ , while after drawing to 60-70% the distributions had narrowed significantly, resulting in  $\gamma/2\sim 15-17^\circ$ . Both of these studies reported narrower distributions than observed in this study even though their fibres were of significantly larger diameter ( $\sim 30\ \mu\text{m}$ ) than the fibres described here (5-10  $\mu\text{m}$ ). This may partially be explained by the shortness of the nanotubes used in this study

( $l \sim 325$  nm). In addition, the maximum achieved draw ratio does not result in extremely aligned nanotubes. This suggests that further improvement is possible.

#### 4.4.3 Measurement of Nanotube Effective Modulus

It is also possible to use Raman spectroscopy to probe the stress transferred from polymer to nanotube<sup>49</sup>. The basis of this measurement is that, as the fibre is strained, the nanotube G' Raman band tends to shift linearly to a lower wavenumber (at low strain) with the strain on the nanotube. The rate of change of G' peak position with strain is related to the nanotube effective modulus. (For example a shift rate of  $-13\text{cm}^{-1}/\%$  implies that the nanotube effective modulus is 260GPa. This is calculated by using the calibration of  $-5\text{cm}^{-1}/\text{GPa}$ ). The nanotube effective modulus is defined by:

$$Y_{Eff} = \eta_0 \eta_l Y_{NT} \quad 4.5$$

In the ideal case,  $Y_{Eff}$  should be identical to  $dY/dV_f$ .  $Y_{Eff}$  was measured as a function of draw ratio for the fibres described above. The resultant data is shown in figure 4.10B and varies from 200 GPa for the undrawn fibre to 350 GPa for the DR= 63% fibre. Data for  $dY/dV_f$  and  $Y_{Eff}$  is compared in figure 4.10C. It is clear from this data that two regimes exist. For undrawn fibres and for  $DR \leq 22\%$ ,  $dY/dV_f = Y_{Eff}$ . However, for higher draw ratios,  $dY/dV_f > Y_{Eff}$ .

Only in the simplest case should  $dY/dV_f = Y_{Eff}$ . Any contribution to the reinforcement over and above that of the nanotubes (e.g. nanotube nucleated crystallinity) will result in an increase in  $dY/dV_f$  over that predicted by equation 4.1. However,  $Y_{Eff}$  measured on the same sample will remain unchanged as it is a measure of the actual stress on the nanotube. Thus, comparison of the  $dY/dV_f$  and  $Y_{Eff}$  data tells us two things. First, because  $dY/dV_f = Y_{Eff}$  for  $DR \leq 22\%$ , it can be inferred that the nanotubes provide the only contribution to the reinforcement at low draw ratios. This is actually rather surprising. Poly(vinyl) alcohol crystals are often nucleated by the presence of the nanotubes<sup>9,20,22-24,32,36,44</sup>. As the crystalline polymer tends to be stronger and stiffer than amorphous polymer, this usually results in an extra component of reinforcement and so measured values of  $dY/dV_f$  which are larger than expected<sup>23,24</sup>. It is not clear why nanotube-nucleated crystallinity does not occur for the as-prepared fibres studied here. However, that  $dY/dV_f > Y_{Eff}$  for  $DR > 22\%$  suggests that crystal nucleation occurs on extended drawing. This phenomenon may be similar to strain induced crystallisation which occurs for many polymeric systems.

#### 4.4.4 Measurement of Polymer Orientation in PVA-NT Fibres by X-Ray Diffraction

In order to test for polymer alignment/crystallinity as a result of drawing, X ray diffraction was performed on bundles of both as-spun and drawn (DR=43%) fibres by collaborators in Cambridge University. X-ray measurements were made on bundles of a few hundred fibres so as to increase the scattering intensity. The patterns obtained were relatively weak and dominated by the background. Nevertheless, they show evidence of a broad crystal diffraction ring at a value of 2-theta of approximately 20 degrees and likely to correspond to the 101 reflection from the poly(vinyl) alcohol. An azimuthal profile of the pattern for a 2-theta interval of 19 – 22 degrees (figure 4.11) shows higher intensity perpendicular to the fibre axis and indicates that there is a small degree of polymer orientation parallel to the fibre axis. There is little difference between the undrawn sample and that drawn by 43% of its original length in terms of their XRD patterns. It appears likely that the presence of water during the 43% draw plasticised the non-crystalline material so that the load at 43% was insufficient to significantly deform the crystalline entities and thus activate the crystal orientation mechanism.

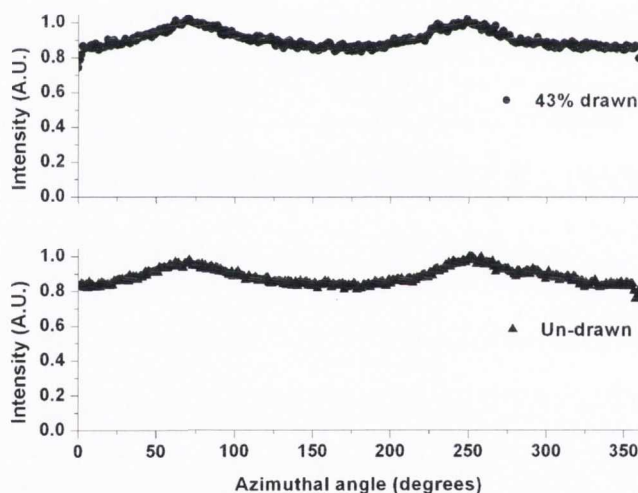


**Figure 4.11: Azimuthal profiles at 2-theta values of 19 - 22° from XRD measurements on un-drawn and drawn PVA-NT fibres.**

The profiles do not show a significant improvement in polymer orientation as a consequence of this level of drawing (43%). The relatively high background is due to other scattering sources and the low volume of the samples. No evidence was found for any strain induced crystallinity, ruling out this as an explanation for the unexplained  $dY/dV_f$  at higher strain. Further work is necessary to explain the fact that  $dY/dV_f > Y_{Eff}$  for  $DR > 22\%$ .

#### 4.4.5 Correlation of Fibre Modulus with $\eta_0$

In order to test the relationship between fibre modulus with  $\eta_0$  predicted by equation 4.1,  $dY/dV_f$  and  $\eta_0$  need to be correlated. However, it can already be seen that  $dY/dV_f$  includes additional components of reinforcement for high draw ratios. Thus, it is more appropriate to use  $Y_{Eff}$ , as it effectively plays the same role as  $dY/dV_f$ , but importantly only describe the reinforcement due to nanotubes. However, this is hardly ever done as  $\eta_0$  is rarely known for a given fibre. As described above, data has been acquired for both  $Y_{Eff}$  and  $S$  as a function of draw ratio (figure 4.10 A&B). This data would allow one to analyse the relationship between  $Y_{Eff}$  and  $\eta_0$  if the relationship between  $S$  and  $\eta_0$  was known.

By calculating both  $S$  and  $\eta_0$  for a number of different theoretical nanotube distributions, a semi-empirical relationship between  $\eta_0$  and  $S$  can be found. Both  $\eta_0$  and  $S$  can be calculated for any array of rods once their distribution in space is known. In a fibre, it is generally assumed that their distribution function is symmetric about the fibre axis. This means the distribution is a function only of the angle between rod axis and fibre axis,  $\theta$ . With this in mind, the definition of Krenchel's orientation factor,  $\eta_0$  is

$$\eta_0 = \frac{\int_0^{\pi/2} f(\theta) \cos^4 \theta d\theta}{\int_0^{\pi/2} f(\theta) d\theta} \quad 4.6$$

The Herman's orientation parameter is defined as

$$S = \frac{3\langle \cos^2 \theta \rangle - 1}{2} \quad 4.7$$

where

$$\langle \cos^2 \theta \rangle = \frac{\int_0^{\pi/2} f(\theta) \cos^2 \theta d\theta}{\int_0^{\pi/2} f(\theta) d\theta} \quad 4.8$$

As described above, both  $\eta_0$  and  $S$  can be calculated once  $f(\theta)$  is known. It is often assumed that the distribution of rods as a function of  $\theta$  can be described by a Gaussian distribution. However, one must also account for the fact that there is a higher probability of finding a rod at  $\theta=\pi/2$  rather than at  $\theta=0$  simply due to geometric reasons. This is simply a manifestation of the fact that the solid angle traced out between  $\theta$  and  $d\theta$  is given by  $d\Omega = 2\pi \sin \theta d\theta$ .

This means the distribution function can be rewritten as

$$f(\theta) = \sin \theta e^{-[1.6(\theta-\theta_0)/\gamma]^2} \quad 4.9$$

where  $\gamma$  is the FWHM of the distribution. In addition  $\theta_0=0$  for distributions preferentially aligned along the fibre axis while  $\theta_0=\pi/2$  for distributions preferentially aligned perpendicular to the fibre axis.

$\eta_0$  and  $S$  were calculated numerically for a range of distribution widths for distributions defined by  $\theta_0=0$  ( $0.25 \text{ rad} \leq \gamma \leq 10 \text{ rad}$ ) and  $\theta_0=\pi/2$  ( $0.1 \text{ rad} \leq \gamma \leq 5 \text{ rad}$ ). The results are shown in figure 4.12 for  $\eta_0$  and  $S$  as a function of  $\gamma$  and for  $\eta_0$  as a function of  $S$ .

In order to obtain an analytical function relating  $\eta_0$  to  $S$ , the data in figure 4.12 was fitted to a number of trial functions. It was found that

$$\eta_0 = 0.19 + 0.52S + 0.26S^2 \quad 4.10$$

fit the data well ( $R^2=0.9996$ ). This expression gives  $\eta_0$  to an accuracy of 0.01 or better.

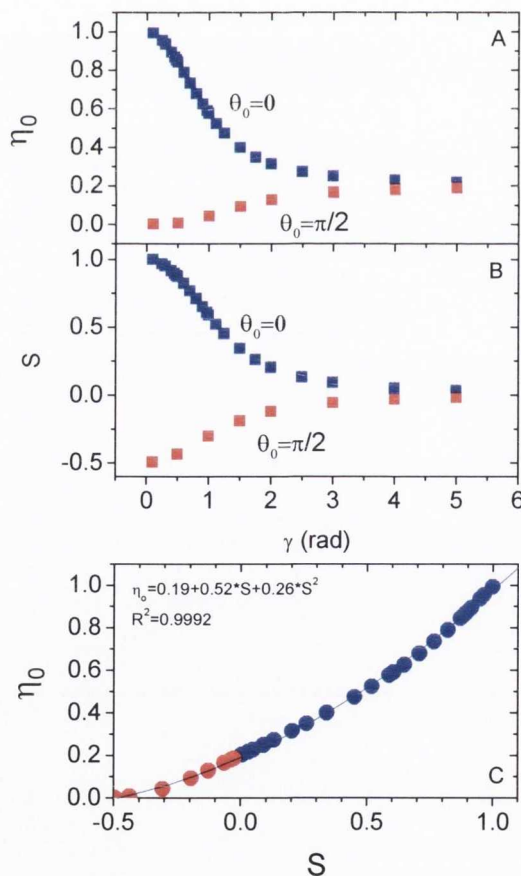


**Figure 4.12:** Calculated values for  $\eta_0$  and  $S$ . In all cases,  $\eta_0$  and  $S$  were calculated using Gaussian distributions with FWHM,  $\gamma$ , and centered at either  $\theta_0 = 0$  or  $\pi/2$ .

It is now possible to calculate  $\eta_o$  from  $S$  for the data shown in figure 4.10. Shown in figure 4.13A is a plot of the measured values of  $Y_{eff}$  versus  $\eta_o$ .

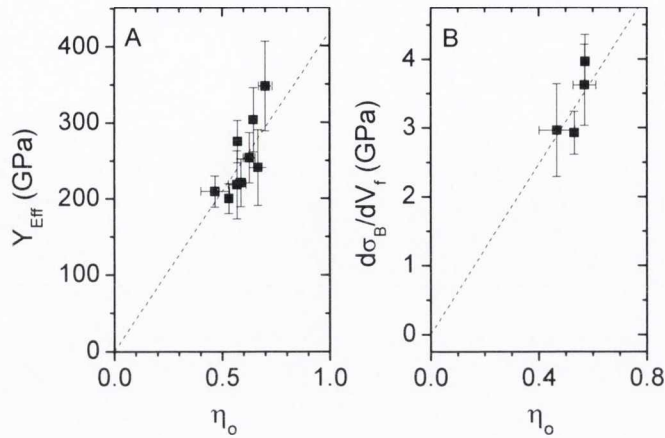


**Figure 4.13: A) Effective nanotube modulus as a function of orientation parameter. B)  $d\sigma_B/dV_f$  (estimated from  $\sigma_B/V_f$ ) of the drawn samples as a function of  $\eta_o$  (calculated from  $S$  using equation 4.10). Note only those fibres with  $DR \leq 22\%$  are plotted i.e. those with no induced crystallinity.**

The data scales reasonably linearly (equation 4.5) confirming that  $Y_{eff}$  and hence the fibre modulus scales linearly with  $\eta_o$ .

Another advantage of this method is that it can be used to gauge the true effectiveness of the reinforcement. To do this the nanotube modulus needs to be calculated from the data in figure 4.13A using equation 4.5 and compared it to the ideal value of  $Y_{NT}=1000$  GPa. Fitting the data gives  $\eta_{ly}Y_{NT} = 420 \pm 20$  GPa.  $\eta_{ly}$  can be estimated using shear lag theory<sup>50</sup>:

$$\eta_{ly} = 1 - \frac{\tanh(nl/d)}{nl/d} \quad 4.11$$

where

$$n = \left[ \frac{-2Y_p}{Y_{NT}(1 + \nu_p) \ln(V_f)} \right]^{1/2}$$

where  $l$  is the mean nanotube length,  $d$  is the mean nanotube diameter,  $Y_p$  is the polymer modulus and  $\nu_p$  is the polymer Poisson ratio.  $\eta_{ly}$  can be calculated for  $V_f=7.1\%$ , using  $l=325$  nm,  $d=2$  nm,  $Y_p=1$  GPa,  $\nu_p=0.5$  and values of  $Y_{NT}$  between 200 GPa and 1000 GPa.  $\eta_{ly}$  varies very weakly with  $Y_{NT}$  and is close to 0.85 for the conditions appropriate to these composites. This gives a value for the nanotube modulus of  $Y_{NT}=480 \pm 40$  GPa or about half the expected value. The discrepancy can be explained by the fact that the dispersed

phase consists not of individual nanotubes but of bundles which are expected to be less stiff<sup>51</sup>. In addition, the interface may be less than perfect which will result in a lower apparent nanotube modulus.

#### 4.4.6 Fibre Strength

The values of  $d\sigma_B/dV_f$  achieved, even for the drawn fibres are relatively low; <7 GPa compared to a potential value of 50-150 GPa. To understand this, the fracture mechanism needs to be considered. Shown in figure 4.4C is an SEM image of a fracture surface which clearly shows nanotubes protruding. This means that the failure mechanism is nanotube pullout which implies that the nanotubes used here ( $l=325$  nm) are shorter than the critical length,  $l_c$ <sup>50,52</sup>. This is the nanotube length, above which the stress transferred from the polymer is enough to fracture the nanotubes:

$$l_c = \frac{\sigma_{NT}d}{2\tau} \quad 4.12$$

where  $d$  is the nanotube (or bundle) diameter and  $\tau$  is the polymer-nanotube interfacial strength or the polymer shear yield strength, whichever is lower<sup>52</sup>. While it can be said that  $l_c > 325$  nm, without knowing  $\tau$ , it cannot be estimated with greater accuracy.

When the nanotube length is less than the critical length, the strength is effectively the stress required to break the matrix-nanotube interfaces and to fracture the polymer in cross section. Inserting the relevant length efficiency factor,  $\eta_{l\sigma}$ , equation 4.2 can then be written as:<sup>18</sup>

$$\sigma_B = \left( \eta_0 \frac{l}{d} \tau - \sigma_p \right) V_f + \sigma_p \approx \eta_0 \frac{l}{d} \tau V_f \quad 4.13$$

As discussed above, no polymer crystallinity is induced for draw ratios up to 22%. Thus, the strength of the drawn fibres (DR ≤ 22%) can be analysed using equation 4.13, where  $\eta_0$  can be calculated from  $S$  using equation 4.10. The data is plotted as  $d\sigma_B/dV_f$  versus  $\eta_0$  in figure 4.13B. Although the data is limited, good linearity is observed, confirming that  $\sigma_B$  scales with  $\eta_0$  as expected<sup>18</sup>. From the fit, and taking the values of  $l$  and  $d$  given above,  $\tau$  can be calculated as  $\tau = 40 \pm 4$  MPa. This is very close to the known shear yield strength of PVA (41 MPa)<sup>53</sup>. This suggests that interfacial failure occurs in the polymer just outside the polymer-nanotube interface<sup>54</sup>. It is likely that this occurs because the polymer is weaker than the polymer-nanotube interface<sup>23</sup>. This in turn suggests that the actual polymer-nanotube interfacial strength is greater than 40 MPa, significantly higher than recent estimates<sup>55</sup>. Thus, in one sense, the fibre strength is limited by the properties of the polymer. However, in reality the strength is low because the failure mechanism is

pullout rather than nanotube fracture. This is the case because the nanotubes are shorter than the critical length. Once  $\tau$  is known, it is possible to estimate  $l_c$  using equation 4.12. Taking a conservative value of  $\sigma_{NT}=50$  GPa, a lower limit of the critical length can be estimated to be  $l_c=1250$  nm. It is possible to disperse nanotubes at lengths of at least  $5 \mu\text{m}$  in aqueous surfactant solutions<sup>56</sup>. By increasing  $l$  from 325 to 1250 nm, an increase in  $d\sigma_B/dV_f$  by a factor of 4 is expected with slower rate of increase for  $l>l_c$ . Thus, it should be feasible to develop composite fibres from hyper-critical length nanotubes, significantly increasing fibre strength.

## 4.5 Conclusions

A method has been developed to control and measure the nanotube volume fraction in poly(vinyl) alcohol-nanotube fibres. This allows one to study the effect of nanotube volume fraction on the mechanical properties, facilitating analysis using models such as the rule of mixtures. Both the fibre modulus,  $Y$ , and strength,  $\sigma_B$ , scale linearly with nanotube volume fraction up to  $V_f \sim 10\%$ , after which saturation occurs.  $dY/dV_f=254$  GPa and  $d\sigma_B/dV_f=2.8$  GPa were measured in the linear region. By drawing fibres with  $V_f < 10\%$ , these values can be increased to  $dY/dV_f=600$  GPa and  $d\sigma_B/dV_f=7$  GPa. Raman measurements show the Herman's orientation parameter,  $S$ , to increase with drawing, indicating that significant nanotube alignment occurs. Raman spectroscopy also shows that the nanotube effective modulus,  $Y_{Eff}$ , increases with drawing, due to the increased alignment. As expected for simple two-phase composites, the undrawn samples display  $dY/dV_f=Y_{Eff}$ . However, for draw ratios above 22%,  $dY/dV_f > Y_{Eff}$ , suggesting that drawing induces polymer crystallinity. An empirical relationship between Krenchel's nanotube orientation efficiency factor,  $\eta_o$ , and  $S$  has been calculated. This allows one to fit the  $Y_{Eff}$  versus  $S$  data, confirming that the fibre modulus scales linearly with  $\eta_o$ . In addition, the Young's modulus of the nanotubes used in this work can be estimated to be  $Y_{NT}=480$  GPa. That this value is about half of the expected value of 1 TPa, suggests that these composites are limited either by an imperfect polymer-nanotube interface or that the nanotubes are less stiff than expected. Finally, it is shown that the fibre strength also scales linearly with  $\eta_o$ . The effective interfacial shear strength and critical length can now be calculated to be 40 MPa and 1250 nm respectively.

In summary, both the volume fraction and orientation dependence contained in Krenchel's equation has been experimentally demonstrated and quantified. This should contribute to the future production of stiff, strong polymer-nanotube composite fibres.

It is shown that both  $Y$  and  $\sigma_B$  scale linearly with  $\eta_0$  as expected. These measurements allow one to estimate the actual modulus of the nanotubes used in these fibres to be  $\sim 500$  GPa and the effective interfacial strength to be 40 MPa.

## 4.6 References

- 1 Coleman, J. N., Khan, U., Blau, W. J. & Gun'ko, Y. K. Small but strong: A review of the mechanical properties of carbon nanotube-polymer composites. *Carbon* **44**, 1624-1652 (2006).
- 2 Andrews, R. *et al.* Nanotube composite carbon fibers. *Applied Physics Letters* **75**, 1329-1331 (1999).
- 3 Chae, H. G., Sreekumar, T. V., Uchida, T. & Kumar, S. A comparison of reinforcement efficiency of various types of carbon nanotubes in polyacrylonitrile fiber. *Polymer* **46**, 10925-10935 (2005).
- 4 Dalton, A. B. *et al.* Super-tough carbon-nanotube fibres. *Nature* **423**, 703-703 (2003).
- 5 Gao, J. *et al.* Continuous Spinning of a Single-Walled Carbon Nanotube Nylon Composite Fiber. *Journal of the American Chemical Society* **127**, 3847-3854 (2005).
- 6 Kearns, J. C. & Shambaugh, R. L. Polypropylene fibers reinforced with carbon nanotubes. *Journal of Applied Polymer Science* **86**, 2079-2084 (2002).
- 7 Koziol, K. *et al.* High-Performance Carbon Nanotube Fiber. *Science* **318**, 1892-1895 (2007).
- 8 Miaudet, P. *et al.* Hot-Drawing of Single and Multiwall Carbon Nanotube Fibers for High Toughness and Alignment. *Nano Letters* **5**, 2212-2215 (2005).
- 9 Minus, M. L., Chae, H. G. & Kumar, S. Interfacial Crystallization in Gel-Spun Poly(vinyl alcohol)/Single-Wall Carbon Nanotube Composite Fibers. *Macromolecular Chemistry and Physics* **210**, 1799-1808 (2009).
- 10 Vigolo, B. *et al.* Macroscopic fibers and ribbons of oriented carbon nanotubes. *Science* **290**, 1331-1334 (2000).
- 11 Wang *et al.* The extraordinary reinforcing efficiency of single-walled carbon nanotubes in oriented poly(vinyl alcohol) tapes. Vol. 18 (Institute of Physics, 2007).
- 12 Liu, T. & Kumar, S. Effect of Orientation on the Modulus of SWNT Films and Fibers. *Nano Letters* **3**, 647-650 (2003).
- 13 Sandler, J. K. W. *et al.* A comparative study of melt spun polyamide-12 fibres reinforced with carbon nanotubes and nanofibres. *Polymer* **45**, 2001-2015 (2004).
- 14 Badaire, S. *et al.* Correlation of properties with preferred orientation in coagulated and stretch-aligned single-wall carbon nanotubes. *Journal of Applied Physics* **96**, 7509-7513 (2004).
- 15 Pichot, V. *et al.* Structural and mechanical properties of single-wall carbon nanotube fibers. *Physical Review B* **74**, 245416 (2006).
- 16 Krenchal, H. Fibre Reinforcement;: Theoretical and practical investigations of the elasticity and strength of fibre-reinforced materials. *Akademisk forlag* (1964).
- 17 Cox, H. L. The elasticity and strength of paper and other fibrous materials. *British Journal of Applied Physics* **3**, 72-79 (1952).
- 18 Rosenthal, J. A model for determining fiber reinforcement efficiencies and fiber orientation in polymer composites. *Polymer Composites* **13**, 462-466 (1992).

- 19 Shaffer, M. S. P. & Windle, A. H. Fabrication and Characterization of Carbon Nanotube/Poly(vinyl alcohol) Composites. *Advanced Materials* **11**, 937-941 (1999).
- 20 Cadek, M., Coleman, J. N., Barron, V., Hedicke, K. & Blau, W. J. Morphological and mechanical properties of carbon-nanotube-reinforced semicrystalline and amorphous polymer composites. *Applied Physics Letters* **81**, 5123-5125 (2002).
- 21 Zhang, X. F. *et al.* Poly(vinyl alcohol)/SWNT composite film. *Nano Letters* **3**, 1285-1288 (2003).
- 22 Cadek, M. *et al.* Reinforcement of polymers with carbon nanotubes: The role of nanotube surface area. *Nano Letters* **4**, 353-356 (2004).
- 23 Coleman, J. N. *et al.* High-performance nanotube-reinforced plastics: Understanding the mechanism of strength increase. *Advanced Functional Materials* **14**, 791-798 (2004).
- 24 Coleman, J. N. *et al.* Reinforcement of polymers with carbon nanotubes. The role of an ordered polymer interfacial region. Experiment and modeling. *Polymer* **47**, 8556-8561 (2006).
- 25 Wang, Z., Ciselli, P. & Peijs, T. The extraordinary reinforcing efficiency of single-walled carbon nanotubes in oriented poly(vinyl alcohol) tapes. *Nanotechnology* **18**, 455709 (2007).
- 26 Poulin, P., Vigolo, B. & Launois, P. Films and fibers of oriented single wall nanotubes. *Carbon* **40**, 1741-1749 (2002).
- 27 Vigolo, B., Poulin, P., Lucas, M., Launois, P. & Bernier, P. Improved structure and properties of single-wall carbon nanotube spun fibers. *Applied Physics Letters* **81**, 1210-1212 (2002).
- 28 Dalton, A. B. *et al.* Super-tough carbon-nanotube fibres - These extraordinary composite fibres can be woven into electronic textiles. *Nature* **423**, 703-703 (2003).
- 29 Munoz, E. *et al.* Multifunctional carbon nanotube composite fibers. *Advanced Engineering Materials* **6**, 801-804 (2004).
- 30 Zhang, X. F. *et al.* Gel spinning of PVA/SWNT composite fiber. *Polymer* **45**, 8801-8807 (2004).
- 31 Miaudet, P. *et al.* Hot-drawing of single and multiwall carbon nanotube fibers for high toughness and alignment. *Nano Letters* **5**, 2212-2215 (2005).
- 32 Minus, M. L., Chae, H. G. & Kumar, S. Single wall carbon nanotube templated oriented crystallization of poly(vinyl alcohol). *Polymer* **47**, 3705-3710 (2006).
- 33 Pichot, V. *et al.* Structural and mechanical properties of single-wall carbon nanotube fibers. *Physical Review B* **74** (2006).
- 34 Miaudet, P. *et al.* Thermo-electrical properties of PVA-nanotube composite fibers. *Polymer* **48**, 4068-4074 (2007).
- 35 Razal, J. M. *et al.* Arbitrarily shaped fiber assemblies from spun carbon nanotube gel fibers. *Advanced Functional Materials* **17**, 2918-2924 (2007).
- 36 Almecija, D., Blond, D., Sader, J. E., Coleman, J. N. & Boland, J. J. Mechanical properties of individual electrospun polymer-nanotube composite nanofibers. *Carbon* **47**, 2253-2258 (2009).
- 37 Kannan, P., Eichhorn, S. J. & Young, R. J. Deformation of isolated single-wall carbon nanotubes in electrospun polymer nanofibres. *Nanotechnology* **18** (2007).
- 38 Tang, C., Saquing, C. D., Harding, J. R. & Khan, S. A. In Situ Cross-Linking of Electrospun Poly(vinyl alcohol) Nanofibers. *Macromolecules* **43**, 630-637 (2009).
- 39 Bergin, S. D. *et al.* Large populations of individual nanotubes in surfactant-based dispersions without the need for ultracentrifugation. *Journal of Physical Chemistry C* **112**, 972-977 (2008).

- 40 Bergin, S. D. *et al.* Large Populations of Individual Nanotubes in Surfactant-Based Dispersions without the Need for Ultracentrifugation. *The Journal of Physical Chemistry C* **112**, 972-977 (2008).
- 41 Bergin, S. D. *et al.* Towards solutions of single-walled carbon nanotubes in common solvents. *Advanced Materials* **20**, 1876 (2008).
- 42 Ma, W. K. A., Chinesta, F., Ammar, A. & Mackley, M. R. Rheological modeling of carbon nanotube aggregate suspensions. *Journal of Rheology* **52**, 1311-1330 (2008).
- 43 Coleman, J. *et al.* High Performance Nanotube-Reinforced Plastics: Understanding the Mechanism of Strength Increase. *Advanced Functional Materials* **14**, 791-798 (2004).
- 44 Zhang, S., Minus, M. L., Zhu, L. B., Wong, C. P. & Kumar, S. Polymer transcrystallinity induced by carbon nanotubes. *Polymer* **49**, 1356-1364 (2008).
- 45 Hennrich, F. *et al.* The mechanism of cavitation-induced scission of single-walled carbon nanotubes. *Journal of Physical Chemistry B* **111**, 1932-1937 (2007).
- 46 Lucas, A. *et al.* Kinetics of Nanotube and Microfiber Scission under Sonication. *Journal of Physical Chemistry C* **113**, 20599-20605 (2009).
- 47 Duesberg, G. S., Loa, I., Burghard, M., Syassen, K. & Roth, S. Polarized Raman Spectroscopy on Isolated Single-Wall Carbon Nanotubes. *Physical Review Letters* **85**, 5436 (2000).
- 48 Liu, T. & Kumar, S. Quantitative characterization of SWNT orientation by polarized Raman spectroscopy. *Chemical Physics Letters* **378**, 257-262 (2003).
- 49 Cooper, C. A., Young, R. J. & Halsall, M. Investigation into the deformation of carbon nanotubes and their composites through the use of Raman spectroscopy. *Composites Part a-Applied Science and Manufacturing* **32**, 401-411 (2001).
- 50 Hull, D. & Clyne, T. W. *An Introduction to Composite Materials*. Second edn, (Cambridge University Press, 1996).
- 51 Salvetat, J.-P. *et al.* Elastic and Shear Moduli of Single-Walled Carbon Nanotube Ropes. *Physical Review Letters* **82**, 944-947 (1999).
- 52 Callister, W. D. *Materials Science and Engineering an Introduction*. Seventh edn, (Wiley, 2007).
- 53 Yaltee, R. B. & Young, R. J. *Composites, Part A* **29**, 1353 (1998).
- 54 Ding, W. *et al.* Direct observation of polymer sheathing in carbon nanotube-polycarbonate composites. *Nano Letters* **3**, 1593-1597 (2003).
- 55 Duncan, R. K., Chen, X. Y. G., Bult, J. B., Brinson, L. C. & Schadler, L. S. Measurement of the critical aspect ratio and interfacial shear strength in MWNT/polymer composites. *Composites Science and Technology* **70**, 599-605 (2011).
- 56 Doherty, E. M. *et al.* The spatial uniformity and electromechanical stability of transparent, conductive films of single walled nanotubes. *Carbon* **47**, 2466-2473 (2009).

# Chapter 5

## Strong Dependence of Mechanical Properties on Fibre Diameter for Polymer–Nanotube Composite Fibres: Differentiating Defect from Orientation Effects

Note: The content of this chapter has been published in ACS Nano, 4, 11 (2010). Some of this work was carried out in collaboration with The University of Manchester and Cambridge University. Raman Spectroscopy was carried out in The University of Manchester and the XRD measurements were carried out in Cambridge University. Some mechanical measurements on fibres were also carried out using a tensile tester in Cambridge University to confirm our measurements.

### 5.1 Introduction

Alongside graphene, carbon nanotubes are among the stiffest and strongest materials known to man. For well-graphitised single-walled nanotubes (SWNTs), the Young's modulus has consistently been reported as close to 1 TPa while the tensile strength is thought to be in the range 50-150 GPa<sup>1-7</sup>. Because of these superlative mechanical properties and due to their 1-dimensional nature, SWNTs are considered to be the ultimate filler for reinforced composite fibres<sup>8-23</sup>. The simplest possible model to describe the mechanical properties of composite fibres is the rule of mixtures which predicts that the fibre modulus,  $Y$ , and strength,  $\sigma_B$ , are given by<sup>2,24-26</sup>:

$$Y = (\eta_o \eta_{LY} Y_{NT} - Y_P) V_f + Y_P \approx \eta_o \eta_{LY} Y_{NT} V_f \quad 5.1$$

$$\sigma_B = (\eta_o \eta_{L\sigma} \sigma_{NT} - \sigma_P) V_f + \sigma_P \approx \eta_o \eta_{L\sigma} \sigma_{NT} V_f \quad 5.2$$

Here the subscripts NT and P refer to nanotube and polymer respectively. In addition  $\eta_o$  and  $\eta_L$  are factors which vary between 0 and 1 and correct for the effects of nanotube

orientation and length respectively<sup>19,24</sup>. (Note,  $\eta_L$  takes different forms for modulus and strength;  $\eta_{LY}$  and  $\eta_{L\sigma}$ . In addition,  $\eta_{L\sigma}$  has two forms depending on whether the nanotube length is greater or less than the critical length)<sup>25</sup>. The approximations are accurate for appreciable volume fractions and when the polymer modulus and strength are significantly lower than those of the nanotubes. The latter condition is not generally true for high performance polymers such as PBO<sup>15</sup>. However, for coagulation spun fibres such as those studied here, the polymer chains are likely to be weakly aligned resulting in relatively low values of  $Y_P$  and  $\sigma_P$ .

In chapter 4, it was shown that this approximation holds very well for PVA-SWNT coagulation spun fibres with diameters of 5-10  $\mu\text{m}$ <sup>27</sup>. This means that the maximum possible rate of increase of stiffness or strength with nanotube volume fraction is just the nanotube stiffness or strength:  $dY/dV_f \approx Y_{NT}$  or  $d\sigma_B/dV_f \approx \sigma_{NT}$  (i.e. when  $\eta_o=1$ ,  $\eta_L=1$ ). Thus, it should be possible to prepare polymer-nanotube composites with  $dY/dV_f \approx 1 \text{ TPa}$  and  $d\sigma_B/dV_f \approx 100 \text{ GPa}$ . If appreciable volume fractions can be achieved, excellent fibres are to be expected.

However, such exceptional properties are not generally obtained. While a number of papers have described fibres with  $dY/dV_f > 400 \text{ GPa}$  (see table in ref<sup>28</sup>, maximum 1270 GPa<sup>9</sup>) only two papers have described fibres with  $d\sigma_B/dV_f > 40 \text{ GPa}$  (56<sup>29</sup> and  $\sim 116$ <sup>30</sup> GPa). In fact, much of the reinforcement observed in the latter paper can be attributed to the effect of nanotube-nucleated crystallinity<sup>2,31</sup>. It is important to point out that very strong composite fibres have been produced; strengths of up to 4.2 GPa have been observed. However, such fibres have only been produced by reinforcing already strong polymers at high loading levels, resulting in relatively low values of  $d\sigma_B/dV_f$ . Thus, the question remains: Why is it straightforward to prepare composites with  $dY/dV_f$  approaching 1 TPa but very difficult to prepare fibres with  $d\sigma_B/dV_f$  approaching 100 GPa?

It is generally thought that fibre strength is limited by nanotube length and the strength of the polymer nanotube interface<sup>24,32</sup> (or polymer shear strength in some cases<sup>33,34</sup>). While these are always limiting factors, two other parameters are critically important and perhaps slightly overlooked; the effect of nanotube orientation and the presence of defects. Fibres with greater nanotube alignment have higher  $\eta_0$  and so higher  $Y$  and  $\sigma_B$ . A number of papers have shown that drawing improves nanotube alignment and so the mechanical properties<sup>2,27,35</sup>. However, detailed studies comparing  $Y$  and  $\sigma_B$  to

parameters which describe the nanotube orientation distribution have been lacking. A systematic study comparing  $Y$  and  $\sigma_B$  to  $\eta_0$ , for example, has yet to be published<sup>33</sup>. More generally, materials failure is very often related to the presence of defects. However, only a very small number of studies have been carried out to investigate the role of defects in polymer-nanotube fibre fracture mechanics<sup>16</sup>. These factors have never been considered together and their relative importance is not known.

In this work composite fibres are prepared from poly(vinyl) alcohol (PVA) and SWNTs by coagulation spinning.  $Y$  and  $\sigma_B$  were measured for a range of fibre diameters from  $\sim 1$  to  $\sim 15$   $\mu\text{m}$ . When normalised to nanotube volume fraction, power law scaling is observed for both modulus and strength with diameter. By performing Weibull analysis on fracture stress data, it can be shown that the presence of surface defects can explain approximately one third of the diameter dependence of the fibre strength. By measuring the relationship between nanotube orientation and fibre diameter it can be shown that orientation effects can explain the other two thirds of the diameter dependence of the fibre strength and all of the diameter dependence of the fibre modulus.

## 5.2 Experimental Procedure

The procedure for the production and analysis of coagulation spun PVA-nanotube fibres was described in chapter 4.

## 5.3 Results and Discussion

### 5.3.1 Fibre Formation

Poly(vinyl) alcohol-SWNT fibres were prepared by coagulation spinning<sup>12,18,22,23,36-41</sup>. This involves the injection of a surfactant-stabilised nanotube suspension into the centre of a glass pipe through which an aqueous poly(vinyl) alcohol (PVA) solution was flowing<sup>37</sup>.

Detailed analysis of the suspension showed it to contain individual nanotubes and small bundles (mean diameter,  $\langle d \rangle = 1.8$  nm and mean length  $\langle l \rangle = 315$  nm (figure 4.1).

Exposure of the dispersed SWNTs to the polymer solution results in destabilisation of the suspension, which leads to the formation of a fibre. These fibres were collected on a mandrel in a rotating water bath. On removal from the bath, the fibres contained large quantities of water. In some cases, the fibres were drawn in this wet state to a range of draw ratios,  $DR$  ( $DR = (L - L_0) / L_0$ ). All fibres were dried initially at

ambient conditions, and then under vacuum for 48 hours. In all cases, the dried fibre diameter,  $D$ , was measured at typically 20 positions along the length using a profilometer (Dektak 6M Stylus Profiler). For all fibres, the nanotube mass fraction was measured by thermogravimetric analysis<sup>33</sup>. This was then converted to volume fraction,  $V_f$ , using  $\rho_{SWNT}=1800 \text{ kg/m}^3$  (this value includes the effects of iron catalyst) and  $\rho_{PVA}=1300 \text{ kg/m}^3$ . While the parameter space associated with this procedure is large, once the apparatus is built the only spinning parameters which can easily be varied are the concentration of the nanotube suspension,  $C_{NT}$ , and the PVA and SWNT flow rates,  $\dot{V}_{PVA}$  and  $\dot{V}_{SWNT}$ . Initially fibres were prepared with various diameters and nanotube volume fractions by spinning with various combinations of  $C_{NT}$ ,  $\dot{V}_{PVA}$  and  $\dot{V}_{SWNT}$ . However, it became apparent that the final fibre diameter scaled linearly with  $\dot{V}_{SWNT} / \dot{V}_{PVA}$  (figure 5.1).

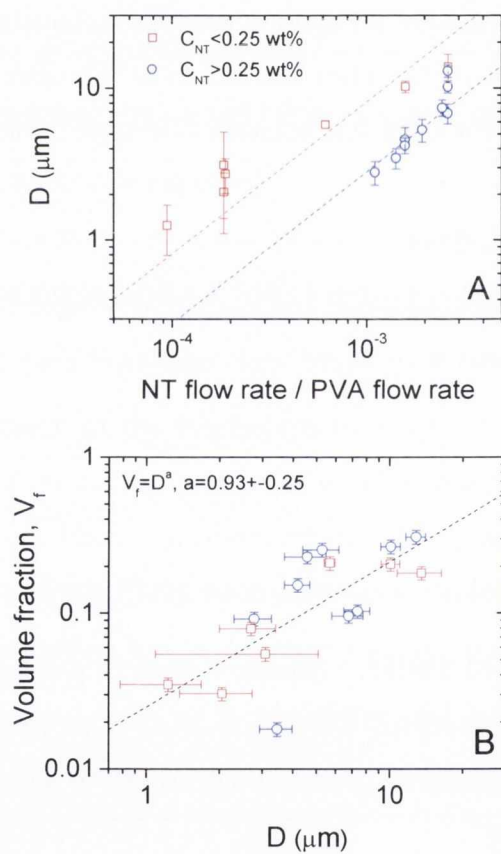


**Figure 5.1: A) Dependence of fibre diameter on flow rate ratios. Note that the behaviour is different depending on whether the nanotube concentration in the spinning dispersion is above or below 0.25 wt%. B) Dependence of nanotube volume fraction on fibre diameter.**

In addition, it was found that  $V_f$  scaled approximately linearly with  $D$  as shown in figure 5.1B ( $V_f \propto D^a$ ,  $a=0.93 \pm 0.25$ ), a correlation that is probably due to the details of

the spinning process. This allowed some control of the final fibre properties. A range of different fibres were prepared with varying  $D$  ( $\sim 1$  to  $\sim 15$   $\mu\text{m}$ ) and  $V_f$  (2% - 26%). Three of these fibres were drawn to a range of draw ratios (up to 63%). In all cases the dried fibres were very uniform along their length as shown in figure 5.2A. In addition, the cross-sections were close to circular (figure 5.2B inset). On tensile fracture, large quantities of nanotube bundles were observed protruding from the broken ends (figure 5.2B).

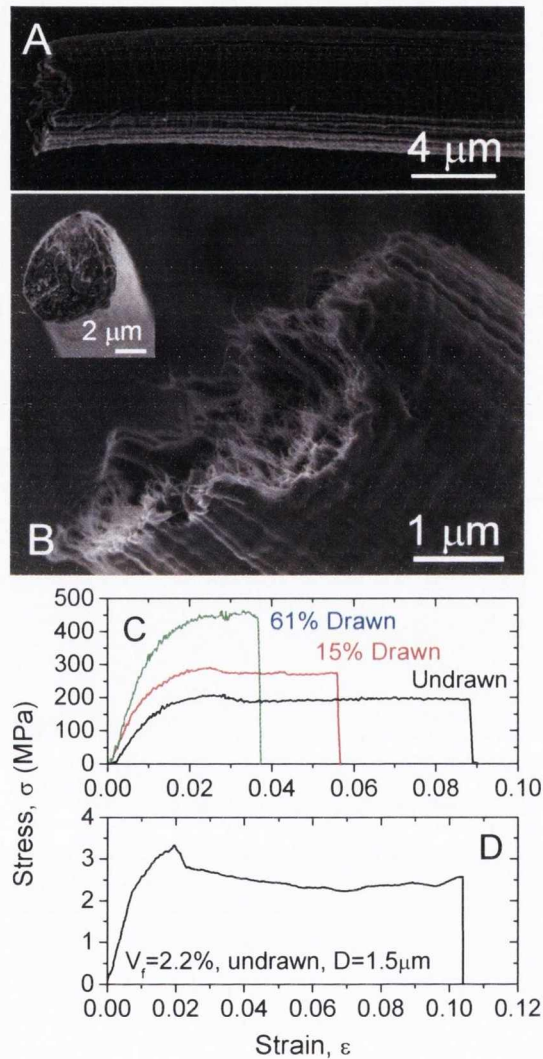


**Figure 5.2:** A) & B) SEM images of coagulation spun polymer-nanotube composite fibres. ( $V_f=26.5\%$ , drawn DR=15%). C) Stress strain curves for fibre with  $V_f=26.5\%$ , drawn to 0, 15, 61%, ( $D=10.2, 8.6, 6.3$   $\mu\text{m}$  respectively). D) Stress strain curve for the strongest fibre studied.

### 5.3.2 Mechanical Properties

Stress-strain curves were measured for fibres using Zwick Z100 and Textechno Favimat tensile testers. Shown in figure 5.2C are stress-strain curves for a  $V_f=26.5\%$

fibre, drawn to 0, 15, 61%, ( $D=10.2, 8.6, 6.3 \mu\text{m}$  respectively). It is clear from this figure that the ultimate tensile strength,  $\sigma_B$ , and modulus,  $Y$ , increase on drawing. However, in this case the strain at break,  $\varepsilon_B$ , tends to fall off with drawing. For all fibres measured,  $\sigma_B$ ,  $Y$  and  $\varepsilon_B$  were recorded (as well as  $D$  and  $V_f$ ). In chapter 4, it has been discussed that for PVA-SWNT fibres, both  $\sigma_B$  and  $Y$  scale in direct proportion with  $V_f$  in agreement with equations 5.1 & 5.2<sup>33</sup>. However, the dependence of  $\sigma_B$ ,  $Y$  and  $\varepsilon_B$  on fibre diameter has not been widely reported for polymer-nanotube fibres<sup>43</sup>. Shown in figure 5.3A-C are  $Y$ ,  $\sigma_B$  and  $\varepsilon_B$  respectively, plotted as a function of fibre diameter,  $D$ .

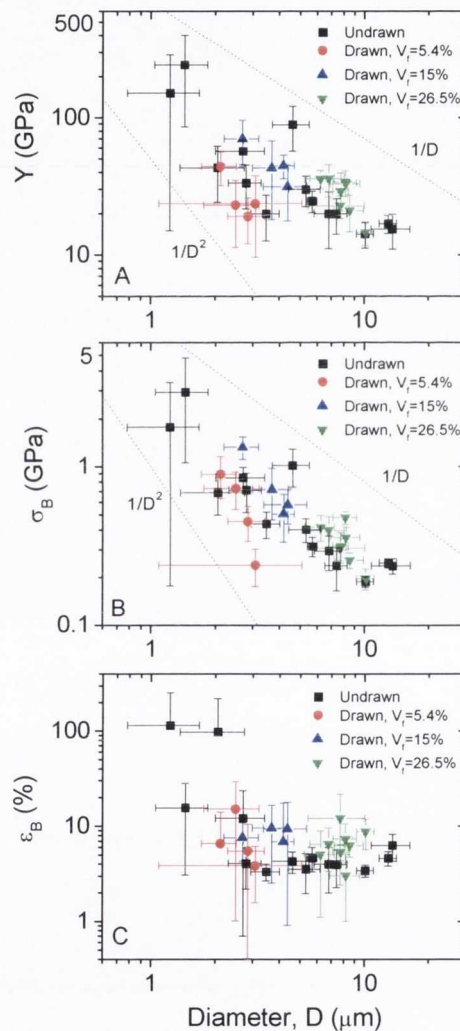


**Figure 5.3: Mechanical properties of composite fibres as a function of fibre diameter. A) Young’s modulus, B) ultimate tensile strength and C) strain at break.**

The data set marked undrawn consists of a range of different fibres with different diameters and a range of nanotube volume fractions between 2% and 31%. The data sets marked “drawn” consist of fibres of a given volume fraction, drawn to different draw

ratios (and so different diameters). In A) and B), the dotted lines represent  $D^{-1}$  and  $D^{-2}$  behaviour and have been included for reference.

In each case, the data is separated into undrawn fibres and drawn fibres (three different  $V_f$ ). From this data, it is clear that both  $Y$  and  $\sigma_B$  scale strongly with  $D$ . The mean modulus scales from  $\sim 15 \pm 4$  GPa for large  $D$  fibres ( $\sim 13 \mu\text{m}$ ) to  $244 \pm 160$  GPa for very low  $D$  fibres ( $D = 1.4 \mu\text{m}$ ). The stiffest coagulation spun polymer-nanotube composite fibre had  $Y \sim 80$  GPa<sup>12</sup> while low diameter electrospun fibres<sup>44</sup> have been reported with moduli up to 85 GPa. Similarly, the mean strength scales from  $190 \pm 15$  MPa for large  $D$  fibres ( $\sim 10 \mu\text{m}$ ) to  $2.9 \pm 1.9$  GPa for very low  $D$  fibres ( $D = 1.4 \mu\text{m}$ ,  $V_f = 2.2\%$ ). These high mean strengths are consistent with similar fibres reported by Dalton et al<sup>12</sup> (1.8 GPa), Miaudet et al<sup>18</sup> (1.6 GPa) and Minus et al<sup>19</sup> (2.6 GPa). The strongest individual (rather than average over  $\sim 10$  individuals) fibre observed in this study had  $\sigma_B = 3.5 \pm 1.7$  GPa ( $D = 1.4 \pm 0.7 \mu\text{m}$ ,  $V_f = 2.2\%$ , figure 5.2D). This exceeds the strongest reported coagulation spun PVA-SWNT fibre, which displayed  $\sigma_B = 2.6$  GPa<sup>19</sup>.

The trend is less clear for the strain at break. However,  $\epsilon_B$  appears to decrease with decreasing  $D$  before increasing again at diameters below  $\sim 5 \mu\text{m}$ . (Note that the errors quoted above for the low  $D$  fibres are largely due to the spread in diameter measurements. Given that failure is more likely in low  $D$  regions of the fibre, the negative parts of the error bars are probably over estimated.)

The data shown in figure 5.3 is quite scattered simply because all the reported fibres had different nanotube volume fractions. As both  $Y$  and  $\sigma_B$  scale linearly with  $V_f$ , this will mask the true diameter dependence. In addition, as  $V_f$  scales with  $D$  (see above), fibres with higher  $D$ , tend to have higher  $V_f$  and are thus stiffer and stronger. This results in the undrawn data appearing to have a different slope in figure 5.3 A&B compared to the drawn data. The effects of varying volume fraction can be removed by noting that the modulus and strength can be approximated as scaling in direct proportion to the volume fraction (equations 5.1 & 5.2). This means one can correct for varying  $V_f$  by dividing both  $Y$  and  $\sigma_B$  by  $V_f$ . The added advantage of this procedure is that  $Y/V_f$  and  $\sigma_B/V_f$  can be thought of as measures of the degree of the reinforcement achieved (i.e. approximately equivalent to  $dY/dV_f$  and  $d\sigma_B/dV_f$ )<sup>2</sup>. However, the approximation in equations 5.1 & 5.2 is only correct if the composite is much stronger / stiffer than the polymer alone. While this is generally the case, it may break down for high performance fibres with highly aligned polymer chains. In that case, the mechanical contribution of the matrix is much more important than that of the nanotubes<sup>45</sup>. While it has been shown in chapter 4 that the

approximation holds for fibres with  $D \sim 5\text{-}10 \mu\text{m}$ ,<sup>33</sup> some of the lower diameter fibres studied in this work may display some chain alignment and so higher than expected stiffness and strength. This could mean that  $Y/V_f > dY/dV_f$  and  $\sigma_B/V_f > d\sigma_B/dV_f$  for the very low  $D$  fibres.

As described in the introduction, the upper limits achievable are  $Y/V_f \approx Y_{NT} = 1$  TPa and  $\sigma_B/V_f \approx \sigma_{NT} \approx 100$  GPa. In some publications  $Y/V_f$  and  $\sigma_B/V_f$  are referred to as  $Y_{Eff}$  and  $\sigma_{Eff}$  respectively. Shown in figure 5.4 are  $Y/V_f$  and  $\sigma_B/V_f$  plotted as a function of  $D$ . It is clear that the scatter is much reduced in each case.

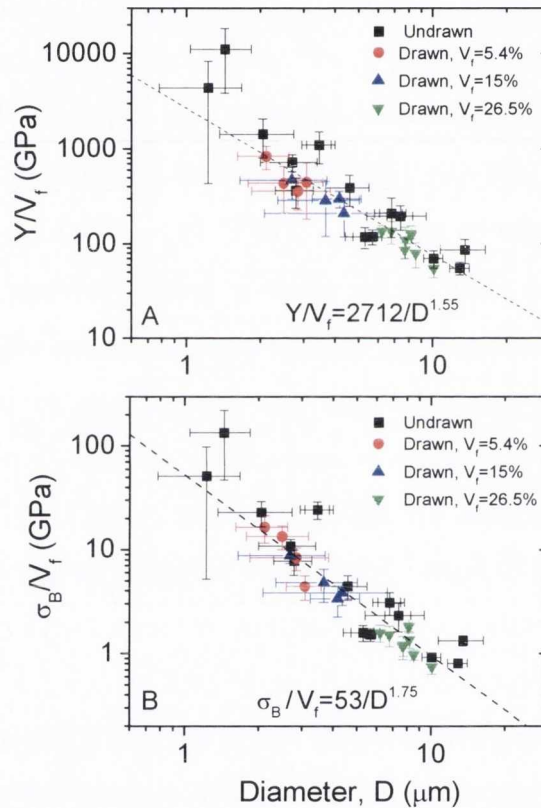


**Figure 5.4:** The same data as in figure 5.3 A) and B). However, in this case the modulus and strength have been divided by the fibre volume fraction. The resultant parameter is expected to be very close to the rate of increase of mechanical properties with volume fraction,  $dY/dV_f$  and  $d\sigma_B/dV_f$  (better agreement for larger diameter fibres).

The mean modulus data varies from  $Y/V_f = 55 \pm 8$  GPa ( $D = 13 \mu\text{m}$ ) to  $Y/V_f = 11 \pm 7$  TPa ( $D = 1.4$ ). Similarly, the mean strength data varies from  $\sigma_B/V_f = 800 \pm 55$  MPa ( $D = 13 \mu\text{m}$ ) to  $\sigma_B/V_f = 134 \pm 65$  GPa ( $D = 1.4$ ). The highest observed values of  $Y/V_f$  (11 TPa) are significantly higher than the expected maximum. This has been observed before<sup>19,34,44</sup>

and may indicate the presence of nanotube-templated crystallinity. In addition the maximum value of  $\sigma_B/V_f$  (134 GPa) is extremely high compared to the majority of values reported in the literature. However, it is also possible that such low diameter fibres tend to have well aligned polymer chains, resulting in  $Y/V_f > dY/dV_f$  and  $\sigma_B/V_f > d\sigma_B/dV_f$  as described above. Further studies will be required to test this possibility.

The data shown in figure 5.4 appears to be well described by power laws of the form  $Y/V_f \propto D^{-u}$  and  $\sigma_B/V_f \propto D^{-v}$ . By fitting the data values of  $u=1.55\pm 0.2$  and  $v=1.75\pm 0.2$  can be obtained. Remarkably, the data for both undrawn and drawn fibres lie on the same curve. This is interesting as it suggests that the fibre diameter is the controlling factor, not the mechanism (drawing or spinning) which determined the diameter. Given that  $V_f \propto D^{0.93\pm 0.25}$ , this means for a given  $V_f$ ,  $Y \propto D^{-0.62\pm 0.45}$  and  $\sigma_B \propto D^{-0.82\pm 0.45}$ .

It is important to try to understand the nature of the diameter dependence. It is easiest to discuss the fibre strength first. The tensile strength of most fibres tends to scale with fibre diameter<sup>30,46-50</sup>. The simplest model proposed to explain this behaviour is Smook's<sup>51</sup> modification of Griffith's model for stress enhancement due to surface flaws<sup>52</sup>. However, this model does not match the observed diameter dependence (figure 5.5).

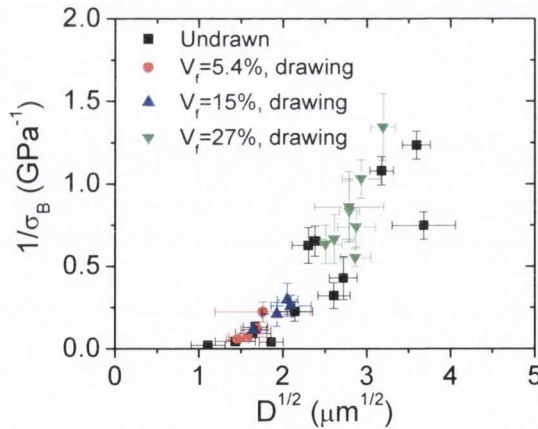


**Figure 5.5: Griffith analysis. The simplest model proposed to explain this behaviour is Smook's<sup>51</sup> modification of Griffith's model for stress enhancement due to surface flaws.<sup>52</sup>**

Smook proposed that fibre strength scales with  $D$  as,

$$\frac{1}{\sigma_B} = \frac{1}{\sigma_0} + a \left[ \frac{D - D_0}{G_{lc} Y} \right]^{1/2} \quad 5.3$$

where  $\sigma_0$  is the strength of a flawless fibre,  $D_0$  is the diameter of a flawless fibre (usually taken as zero),  $G_{Ic}$  is the energy needed for the creation of a crack of critical dimensions,  $Y$  is the Young's modulus and  $a$  is a constant. To test this model  $1/\sigma_B$  versus  $D^{1/2}$  were plotted as shown in figure 5.5. This model does not describe this data well at all: The curve is non-linear and the intercept is negative. Thus Smook's model of surface flaws alone cannot explain the observed diameter dependence.

### 5.3.3 Fibre Strength: Defects

Perhaps more common are statistical models based on defect induced fracture. The Weibull model<sup>53</sup> assumes that defects are homogeneously distributed throughout the material and failure at the most serious flaw leads to total failure of the material<sup>46,48,54</sup>. Within this framework the probability of failure of a sample under a stress,  $\sigma$ , is given by:

$$P(\sigma) = 1 - \exp \left[ -n \left( \frac{\sigma}{\sigma_0} \right)^b \right] \quad 5.4$$

where  $n$  is the number of flaws present (Weibull originally considered fracture of a chain of  $n$  links with fracture occurring at the weakest link<sup>53</sup>),  $\sigma_0$  is the scale factor and  $b$  is the Weibull modulus. Generally,  $P(\sigma)$  is approximated by ranking a set of breaking stresses (strengths) measured for a given fibre type in ascending order (in this work, for each fibre type, 10 fibre sections were typically tested, each of gauge length  $L=10$  mm). Then the probability of failure is taken as the  $i^{\text{th}}$  stress in a group of  $N$  measurements as  $P(\sigma) = i/(N+1)$ . Equation 5.4 can be rewritten as

$$\ln[-\ln(1-P(\sigma))] = \ln(n/\sigma_0^b) + b \ln \sigma \quad 5.5$$

Thus, plotting  $\ln[-\ln(1-P(\sigma))]$  versus  $\ln \sigma$  allows one to find  $b$ . This is important because it can be shown that the mean strength,  $\sigma_B$ , is given by  $\sigma_B = \sigma_0 n^{-1/b} \Gamma(1+1/b)$ , where  $\Gamma$  is the gamma function<sup>46</sup>. For any real sample the flaws may be on the surface or distributed in the bulk. This means that  $n$  is proportional to either the sample surface area or volume respectively. Thus the mean fibre strength is given by

$$\sigma_B = \sigma_0 \left( \frac{N}{A} \pi D L_0 \right)^{-1/b} \Gamma(1+1/b)$$

or

5.6

$$\sigma_B = \sigma_0 \left( \frac{N}{V} \frac{\pi}{4} D^2 L_0 \right)^{-1/b} \Gamma(1+1/b)$$

depending on the location of the dominant flaw (i.e. surface or bulk), where  $N/A$  and  $N/V$  are the surface and bulk flaw densities and  $L_0$  is the gauge length. This is important as it shows that  $\sigma_B \propto D^{-\alpha/b}$ , where  $\alpha$  is 1 or 2, depending on the flaw type.  $b$  can be found for these fibres by measuring the breaking stress a number of times for each fibre type and analysing the data using equation 5.5. This analysis has been done for all fibres studied. An example of this is shown in figure 5.6A for a  $V_f=5.4\%$  fibre drawn to different draw ratios.

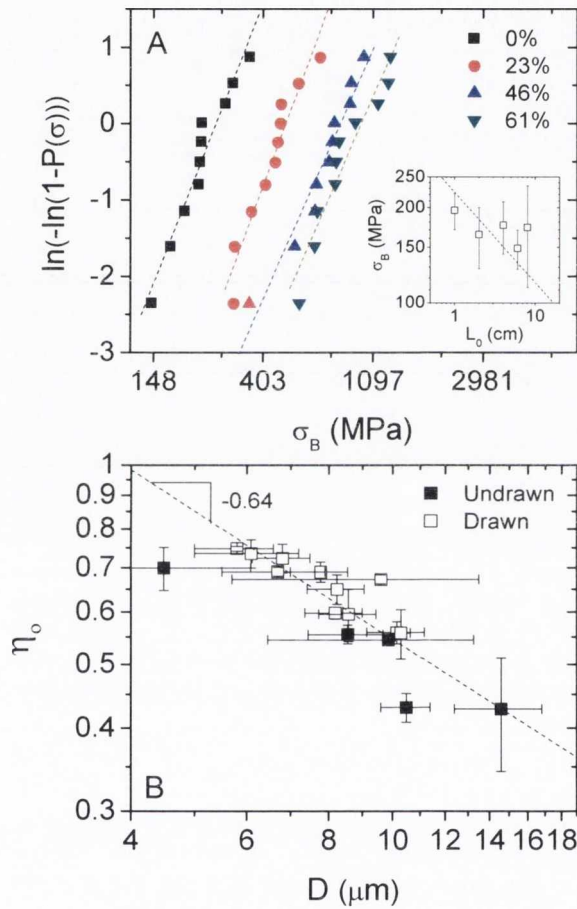


**Figure 5.6:** A) Weibull analysis of the distribution of fibre breaking stresses for a given fibre type. Here  $P(\sigma)$  is approximately the probability that the fibre will fracture at a given stress,  $\sigma$ . In this figure, the Weibull analysis has been carried out for fibres of volume fraction  $V_f=5.4\%$ , drawn to different degrees. The inset shows the strength plotted as a function of gauge length,  $L$ , for undrawn fibres. In this case,  $D=11.5 \mu\text{m}$  and  $V_f=11\%$ . The dashed line has slope  $-1/b=-1/3.5$ . B) Krenchel's orientation parameter plotted as a function of fibre diameter for both drawn and undrawn fibres.

In all cases a very good fit was obtained giving values of  $b$  close to 3.5 in all cases. No dependence of  $b$  on  $V_f$  was observed. Overall it was found that  $b=3.5\pm 0.5$ , averaging over all samples (figure 5.7).

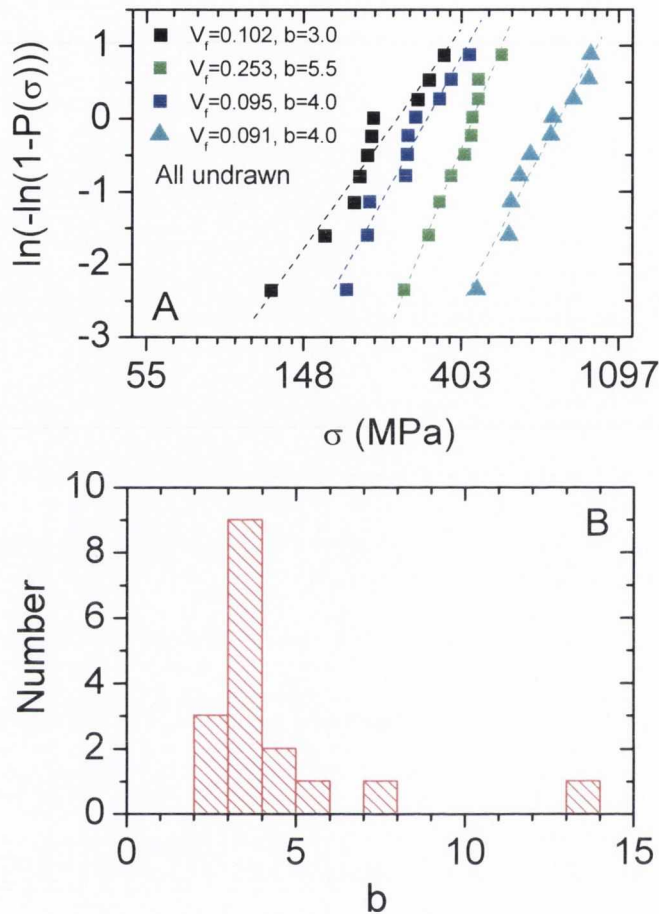


**Figure 5.7: A) Weibull analysis for fibres of varying volume fraction. The calculated  $b$  value is indicated. B) Histogram of the calculated  $b$  values for all fibres studied.**

This value is very close to the value of  $b=3.4$  reported by Liu et al for electrospun polymer-nanotube fibres<sup>16</sup>. These values are relatively small compared to the values of  $b\sim 27$  reported for polyethylene fibres<sup>46</sup>, illustrating that the failure stress distribution is relatively broad in these PVA-SWNT composite fibres.

Weibull analysis can be tested by noting that according to equation 5.6,  $\sigma_B \propto L_0^{-1/b}$ , where  $L_0$  is the gauge length of the fibre under study. Mechanical tests were performed on fibres with identical diameter and volume fraction ( $D=11.5 \mu\text{m}$ ,  $V_f=11\%$ ) at range of gauge lengths from 1 to 10 cm. The fibre strength is plotted versus gauge length in the inset of figure 5.6A showing a slight decrease in strength with increasing gauge length. The dashed line illustrates the type of dependence expected if the Weibull

analysis is appropriate and taking  $b=3.5$  ( $\sigma_B \propto L_0^{-1/3.5}$ ). While the agreement is not perfect, the data is certainly consistent with the Weibull analysis within the error bounds.

Having measured  $b$ , one can compare the dependence of fibre strength on diameter predicted by the Weibull analysis with the data in figure 5.4B. To do this, the  $D$  dependence of  $\sigma_B/V_f$  is needed. Remembering that  $V_f$  scales with  $D$  ( $V_f \propto D^a$ ,  $a=0.93\pm 0.25$ ), this means  $\sigma_B/V_f \propto D^{-\alpha/b-a}$ . From the values of  $b$  and  $a$  obtained,  $\alpha/b+a$  can be calculated to be  $1.2\pm 0.5$  for  $\alpha=1$  and  $1.5\pm 0.5$  for  $\alpha=2$ . Both of these values are compatible the measurements  $\sigma_B$  here as a function of  $D$  ( $\sigma_B/V_f \propto D^{-(1.75\pm 0.2)}$ ), with the volumetric flaw scenario ( $\alpha=2$ ) a much closer match. However, this is unlikely to be the final answer. This is because the model described above works best for homogenous fibres, made from a single component such as polyethylene<sup>46,55</sup> or SiC<sup>56</sup>.

### 5.3.4 Fibre Strength: Nanotube Orientation

However, the fibres under study in this work are polymer-nanotube composite fibres. In such structures, the strength is strongly correlated with the nanotube orientation distribution. This is represented in equation 5.2 by  $\eta_o$ , Krenchel's orientation parameter<sup>57</sup>. This parameter can vary from  $\eta_o=0$  for the nanotubes aligned in-plane perpendicular to the applied stress to  $\eta_o=0.2$  for randomly aligned nanotubes to  $\eta_o=1$  for nanotubes perfectly aligned in the direction of the applied stress. For fibres with diameters of order tens of microns or lower, the nanotubes tend to become partially aligned during fibre spinning<sup>39,40</sup>. Such alignment is expected to increase as  $D$  decreases. Thus, it is expected that  $\eta_o$  and so  $\sigma_B$  will vary with  $D$  due to orientation effects. This is in addition to any flaw-related diameter dependence.

Wagner has proposed that equation 5.4 can be modified slightly to account for orientation effects by introducing a diameter dependence to the Weibull scale parameter,  $\sigma_0 \propto D^{-\gamma}$ <sup>48</sup>. This means a new component of diameter dependence is added to the fibre strength so equation 5.6 can be rewritten, including the dependence of  $V_f$  on  $D$ :

$$\sigma_B/V_f \propto D^{-\alpha/b-a} D^{-\gamma} \quad 5.7$$

where  $\alpha/b+a$  is  $1.2\pm 0.5$  for  $\alpha=1$  and  $1.5\pm 0.5$  for  $\alpha=2$ . Here, the  $D^{-\alpha/b}$  part represents the effect of flaws while the  $D^{-\gamma}$  part represents the effects of nanotube orientation (the  $D^{-a}$  part represents the diameter dependence of the volume fraction). By comparing equations 5.2 and 5.7, one can associate  $D^{-\gamma}$  with the diameter dependence of  $\eta_o$ :

$$\eta_o(D) \propto D^{-\gamma} \quad 5.8$$

For the effects of defects and nanotube orientation to fully explain the observed diameter dependence, it will be necessary to show that equation 5.7 accurately describes the data presented in figure 5.4B. For this to occur, the experimentally measured exponents must balance i.e:

$$v = \frac{\alpha}{b} + a + \gamma \quad 5.9$$

where  $v$  is the experimentally measured exponent:  $\sigma_B/V_f \propto D^{-v}$  ( $v=1.75 \pm 0.2$ ). This requires  $\gamma=0.25 \pm 0.7$  for bulk defects ( $\alpha=2$ ) or  $\gamma=0.55 \pm 0.7$  for surface defects ( $\alpha=1$ ). It should be emphasised that  $v$ ,  $b$  and  $a$  were measured independently by measuring the tensile strength as a function of diameter, from the Weibull analysis and from the scaling of volume fraction with fibre diameter respectively. To test this defect/orientation hypothesis, it will be necessary to measure the diameter dependence of  $\eta_o$  in these fibres.

As discussed in chapter 4, it is possible to obtain information on the nanotube alignment using Raman spectroscopy<sup>58</sup>. This makes use of the fact that the observed Raman intensity depends on the angle between the nanotube axis and the electric field vector of the excitation beam<sup>59</sup>. As described in chapter 4, by measuring the Raman signals with the incident beam polarised parallel and perpendicular to the fibre, it is possible to calculate<sup>60</sup> the Herman's orientation parameter,  $S$ , where:

$$S = [3\langle \cos^2\theta \rangle - 1]/2 \quad 5.10$$

and  $\theta$  is the angle between a given nanotube and the fibre axis

This orientation parameter varies from  $S=-0.5$  for rods aligned in plane to  $S=0$  for random orientation to  $S=1$  for perfect axial alignment.  $S$  has been measured for a number of undrawn fibres of varying diameters between 4.5 and 14.6  $\mu\text{m}$ , giving values from 0.72 to 0.38 respectively. In addition  $S$  was measured for one fibre type, drawn to different draw ratios. The diameter was measured for all draw ratios. Here  $S$  scaled from 0.39 to 0.77 as drawing reduced the diameter from 10.5  $\mu\text{m}$  to 5.8  $\mu\text{m}$ . In order to obtain  $\eta_o$  for these fibres,  $S$  and  $\eta_o$  were both calculated for Gaussian distributions of fibres with a range of angular widths as was seen in section 4.4.5 and figure 4.12.

As was seen in chapter 4, by fitting this data an empirical relationship between  $S$  and  $\eta_o$  can be found:

$$\eta_o = 0.19 + 0.52S + 0.26S^2 \quad 5.11$$

This expression gives  $\eta_0$  to an accuracy of 0.01 or better. Thus, for this subset of fibres, data is available for  $\eta_0$  as a function of D. This data is plotted in figure 5.6B. Here it can be seen that  $\eta_0$  increases from 0.43 to 0.75 as D is decreased from 15  $\mu\text{m}$  to 5.8  $\mu\text{m}$ . Notably both the as-spun and drawn data follow the same curve showing that the orientation distribution is controlled by D. The data follows a clear power law as predicted by equation 5.8, with exponent  $\gamma=0.64\pm 0.1$ . This agrees extremely well with the requirement outlined above that  $\gamma=0.55\pm 0.7$  for surface defects ( $\alpha=1$ ).

All exponents are summarised in table 5.1.

Exponent	Parameter controlled	value
$a$	Volume fraction, $V_f \propto D^a$	$a=0.93\pm 0.25$
$u$	Fibre modulus (measured), $Y/V_f \propto D^{-u}$	$u=1.55\pm 0.2$
$v$	Fibre strength (measured), $\sigma_B/V_f \propto D^{-v}$	$v=1.75\pm 0.2$
$\alpha/b$	Strength (defects), $\sigma_B \propto D^{-\alpha/b}$	$\alpha/b=0.29\pm 0.04$ , ( $\alpha=1$ , surface defects)
$\gamma$	Strength (orientation), $\sigma_B \propto D^{-\gamma}$	$\gamma=0.64\pm 0.1$

**Table 5.1 Summary of exponents**

It is worth noting that such behaviour can also be seen in the data of other researchers. Both Badaire et al.<sup>39</sup> and Pichot et al.<sup>40</sup> prepared PVA-SWNT coagulation spun fibres which they characterised by X-ray scattering. They reported the FWHM of the nanotube distribution as a function of draw ratio.  $\eta_0$  has been calculated for their fibres and has been plotted versus D (figure 5.8).

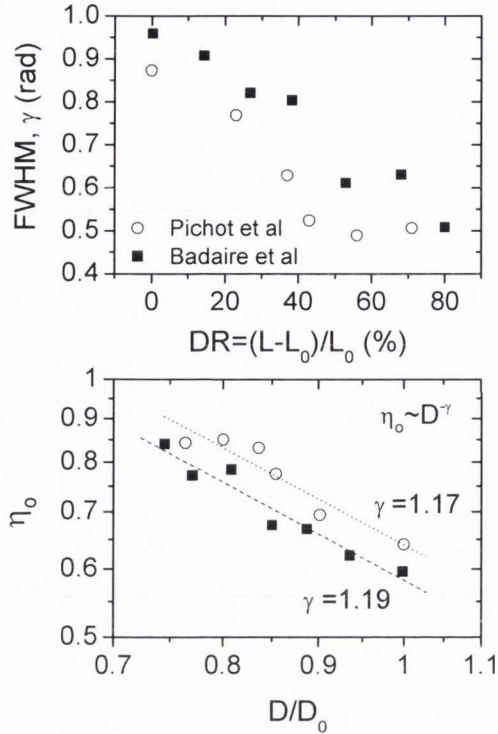


**Figure 5.8: A) Width of Gaussian nanotube distribution as a function of DR as measured by X-ray diffraction by Badaire et al. and Pichot et al. Values of  $\eta_0$  calculated from  $\gamma$  (see figure 4.12) plotted as a function of  $D/D_0$ , calculated from  $D/D_0 = (DR+1)^{-1/2}$ .**

This data shows the sort of power law behaviour predicted by equation 5.8, although notably with exponents significantly different to the one in this study ( $\gamma = 1.19$  and 1.17 respectively). This shows that the details of the nanotube distribution are set by the spinning parameters and apparatus.

### 5.3.5 Young's Modulus

The Young's modulus of fibres does not tend to be as susceptible to defects as the strength is. However, the modulus will depend on nanotube orientation as described by equation 5.1. As described above, it is now possible to separate the effects of defects from those due to the nanotube orientation. The orientation dependence is described by the exponent  $\gamma$ , thus it is expected that the modulus will scale with  $D$  as  $Y/V_f \propto D^{-a-\gamma}$ , where  $a$  accounts for the dependence of  $V_f$  on  $D$ .  $a$  and  $\gamma$  have already been measured to be  $a = 0.93 \pm 0.25$  and  $\gamma = 0.64 \pm 0.1$ , giving  $a + \gamma = 1.57 \pm 0.35$ . However the diameter

dependence of the modulus has already been measured:  $Y/V_f \propto D^{-u}$  where  $u=1.55\pm 0.2$ . The agreement between observed and predicted modulus exponents is almost perfect. The Young's modulus data shown in figure 5.4A can be used, coupled with the relationship between  $\eta_o$  and  $D$ , to check that the measured moduli (and hence the measured stresses in general) are in the correct range. By plotting  $Y/V_f$  versus  $\eta_o$ , equation 5.1 can be used to estimate  $Y_{NT}$  (see figure 5.9).

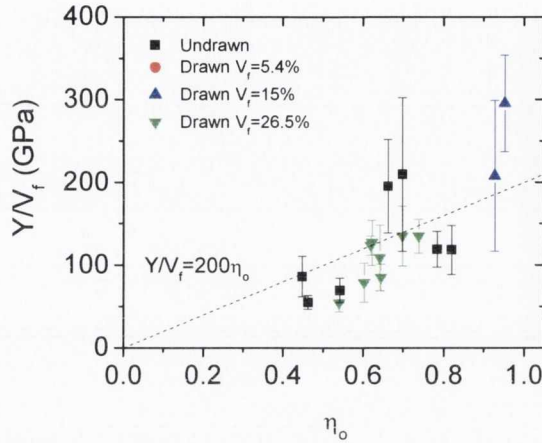


**Figure 5.9: Graph of  $Y/V_f$  v  $\eta_o$  for the large diameter fibres shown in figure 5.4A.  $\eta_o$  is estimated from  $D$  using the fit in figure 5.6B:  $\eta_o \approx 2.39D^{-0.64}$ .**

Note that, as is clear from figure 5.6B, this fit is only valid for  $D > 4 \mu\text{m}$ . Krenchel's modified rule of mixtures says:

$$Y = (\eta_o \eta_{LY} Y_{NT} - Y_P) V_f + Y_P \approx \eta_o \eta_{LY} Y_{NT} V_f \quad 5.12$$

This means:

$$Y/V_f \approx \eta_o \eta_{LY} Y_{NT} \approx dY/dV_f \quad 5.13$$

The data in figure 5.9 is reasonably linear as expected. For the nanotubes used here, it has been previously estimated in chapter 4 that  $\eta_{LY} \sim 0.85$ . This means  $Y_{NT}$  can be estimated as  $Y_{NT} \sim 235 \pm 25$  GPa. This is in line with what would be expected (a value somewhat less than 100 GPa) and reasonably close to the previous estimate of  $480 \pm 40$  GPa<sup>33</sup>.

### 5.3.6 Relative Contribution of Defects and Orientation

It is worth briefly considering the relative contributions of defect and nanotube orientation to fibre strength. For a given  $V_f$ , the actual fibre strength depends on  $D$  as  $\sigma_B \propto D^{-\alpha/b-\gamma}$ . As it has been seen, the data indicates that  $\alpha=1$  suggesting that surface defects initiate failure. This allows one to write the diameter dependence numerically as

$\sigma_B \propto D^{-0.29} D^{-0.64}$ , where the first term describes the defect contribution while the second term describes the orientation contribution. This clearly shows that nanotube orientation is more important than the presence of surface flaws in the fibres studied here. The balance may be different for other types of fibre or indeed coagulation spun fibres produced using different spinning parameters.

This diameter dependence should not hold over the entire diameter range. While the defect contribution should hold over a wide diameter range, the orientation dependence should only apply over the limited range of diameters where  $0.2 < \eta_o < 1$ . Outside this range, the nanotubes will either be randomly orientated or completely aligned. By extrapolating the  $\eta_o(D) \propto D^{-\gamma}$  curve, it can be found that this  $\eta_o$  range is equivalent to  $4\mu\text{m} < D < 50\mu\text{m}$ . Thus, it is expected that coagulation spun fibres with  $D > 50\mu\text{m}$  should have completely randomly aligned nanotubes and commensurately poor mechanical properties. In addition, the orientation component of  $\sigma_B$  should have saturated for  $D < 4\mu\text{m}$ , leaving a weaker defect controlled diameter dependence. This change is not apparent in figure 5.4B, possibly due to polymer chain alignment effects discussed above.

## 5.4 Conclusions

In conclusion, the mechanical properties of polymer-nanotube fibres have been characterised as a function of fibre diameter. A strong dependence of fibre modulus and strength on diameter has been observed. This  $D$  dependence is a combination of the effects of nanotube orientation and surface defects. The balance of these effects has been determined and it has been shown that orientation effects are dominant for fibre diameters between 4 and 50  $\mu\text{m}$ . For low diameter fibres where the nanotubes are well aligned, fibres have been prepared with moduli approaching 250 GPa and strength of 2.9 GPa.

While the defect contribution to the diameter dependence is relatively small ( $D^{-0.29}$ ), this could probably be reduced dramatically by improving the spinning process. Better processing should reduce the surface defect density and so increase  $b$  dramatically. The orientation contribution to the diameter dependence is larger ( $D^{-0.64}$ ). However, it should be possible to change  $\gamma$  by changing the processing conditions (Pichot et al. and Badaire et al. reported data consisted with  $\gamma=1.17$  and  $\gamma=1.19$  respectively). A reduction of  $\gamma$ , possibly by optimisation of needle and pipe diameters and flow rates, would reduce

the orientation contribution to the diameter dependence. Such improvements could result in extremely high stiffness and strength for higher diameter fibres.

### 5.5 Appendix. Table of Fibre Properties

Fibre name	Starting conc (wt%)	DR (%)	$\dot{V}_{NT}$ (ml/min)	$\dot{V}_{PVA}$ (ml/min)	NT mass fraction	$\sigma_B$ (MPa)	Y (GPa)	$\epsilon_B$	D ( $\mu\text{m}$ )
Sample 1	0.349	0	0.05	270	0.073	237	23.6	0.038	3.09
Sample 1	0.349	23	0.05	270	0.073	448	19	0.054	2.85
Sample 1	0.349	46	0.05	270	0.073	723	23	0.15	2.49
Sample 1	0.349	61	0.05	270	0.073	883	44	0.065	2.12
Sample 2	0.075	0	0.214	135	0.1968	503.7	44.6	0.068	4.2
Sample 2	0.075	23	0.214	135	0.1968	577.2	31.4	0.093	4.38
Sample 2	0.075	46	0.214	135	0.1968	718.6	43	0.095	3.7
Sample 2	0.075	69	0.214	135	0.1968	1422.8	66.9	0.075	2.7
Sample 3	0.095	0	0.2	81	0.136	239	20	0.0398	7.4
Sample 4	0.095	0	0.214	110	0.319	404	30	0.0357	5.3
Sample 5	0.1007	0	0.214	81	0.127	296	20	0.04	6.8
Sample 6	0.095	0	0.214	81	0.3328	197.424	14.5	0.087	10.16
Sample 6	0.095	7.4	0.214	81	0.3328	308.7	22.7	0.12	7.74
Sample 6	0.095	15	0.214	81	0.3328	257.7	21	0.062	8.58
Sample 6	0.095	22	0.214	81	0.3328	480.5	33.8	0.073	8.18
Sample 6	0.095	44	0.214	81	0.3328	359.88	32.9	0.03	8.24
Sample 6	0.095	59	0.214	81	0.3328	318.14	29	0.053	7.78
Sample 6	0.095	61	0.214	81	0.3328	418.6	35.9	0.05	6.25
Sample 6	0.095	63	0.214	81	0.3328	398.98	36	0.064	6.81
Sample 7	0.095	0	0.214	150	0.02468	439	19.96	0.0335	3.47
Sample 8	0.095	0	0.15	135	0.122	715	33.4	0.0407	2.79
Sample 9	0.2485	0	0.214	135	0.2905	1017	89.2	0.043	4.6
Sample 10	0.294	0	0.1	530	0.1052	850	56.9	0.122	2.7
Sample 11	0.336	0	0.05	270	0.041	690	43.2	0.982	2.05
Sample 12	0.313	0	0.05	530	0.047	1780	152	1.15	1.23
Sample 13	0.301	0	0.214	81	0.2303	238.25	15.4	0.063	13.54
Sample 14	0.2485	0	0.214	81	0.3786	248	16.9	0.0464	12.9
Sample 15	0.2835	0	0.214	135	0.261	188.82	14.2	0.0344	10.09
Sample 16	0.2835	0	0.05	81	0.2652	317.1	24.7	0.0468	5.68
Sample 17	0.336	0	0.05	351	0.03	2920	384	0.115	1.45
Sample 17 (I)	0.336	0	0.05	351	0.03	3480	272	0.108	1.45

**Table 5.2: Summary of the fibres studied mechanically in this work. All data are averages over 5-10 pieces of fibre, with the exception of sample 17 (marked I). This is the data for the piece of fibre with the highest individual strength.**

## 5.6 References

- 1 Belytschko, T., Xiao, S. P., Schatz, G. C. & Ruoff, R. S. Atomistic simulations of nanotube fracture. *Physical Review B* **65**, 235430 (2002).
- 2 Coleman, J. N., Khan, U., Blau, W. J. & Gun'ko, Y. K. Small but strong: A review of the mechanical properties of carbon nanotube-polymer composites. *Carbon* **44**, 1624-1652 (2006).
- 3 Li, C. & Chou, T.-W. A structural mechanics approach for the analysis of carbon nanotubes. *International Journal of Solids and Structures* **40**, 2487-2499 (2003).
- 4 Lu, J. P. Elastic properties of single and multilayered nanotubes. *Journal of Physics and Chemistry of Solids* **58**, 1649-1652 (1997).
- 5 Lu, J. P. Elastic Properties of Carbon Nanotubes and Nanoropes. *Physical Review Letters* **79**, 1297 (1997).
- 6 Yakobson, B. I., Campbell, M. P., Brabec, C. J. & Bernholc, J. High strain rate fracture and C-chain unraveling in carbon nanotubes. *Computational Materials Science* **8**, 341-348 (1997).
- 7 Yu, M.-F., Files, B. S., Arepalli, S. & Ruoff, R. S. Tensile Loading of Ropes of Single Wall Carbon Nanotubes and their Mechanical Properties. *Physical Review Letters* **84**, 5552 (2000).
- 8 Kannan, P., Young, R. J. & Eichhorn, S. J. Debundling, Isolation, and Identification of Carbon Nanotubes in Electrospun Nanofibers. *Small* **4**, 930-933 (2008).
- 9 Andrews, R. *et al.* Nanotube composite carbon fibers. *Applied Physics Letters* **75**, 1329-1331 (1999).
- 10 Chae, H. G., Sreekumar, T. V., Uchida, T. & Kumar, S. A comparison of reinforcement efficiency of various types of carbon nanotubes in poly acrylonitrile fiber. *Polymer* **46**, 10925-10935 (2005).
- 11 Chen, X. Y., Beyerlein, I. J. & Brinson, L. C. Curved-fiber pull-out model for nanocomposites. *Mechanics of Materials* **41**, 279-292 (2009).
- 12 Dalton, A. B. *et al.* Super-tough carbon-nanotube fibres. *Nature* **423**, 703-703 (2003).
- 13 Gao, J. B. *et al.* Continuous spinning of a single-walled carbon nanotube-nylon composite fiber. *Journal of the American Chemical Society* **127**, 3847-3854 (2005).
- 14 Haggenueller, R., Fischer, J. E. & Winey, K. I. Single wall carbon nanotube/polyethylene nanocomposites. *Macromolecules* **39**, 2964-2971 (2006).
- 15 Kumar, S. *et al.* Synthesis, structure, and properties of PBO/SWNT composites. *Macromolecules* **35**, 9039-9043 (2002).
- 16 Liu, L. Q., Tasis, D., Prato, M. & Wagner, H. D. Tensile mechanics of electrospun multiwalled nanotube/poly(methyl methacrylate) nanofibers. *Advanced Materials* **19**, 1228, (2007).
- 17 Ma, W. K. A., Chinesta, F., Ammar, A. & Mackley, M. R. Rheological modeling of carbon nanotube aggregate suspensions. *Journal of Rheology* **52**, 1311-1330 (2008).
- 18 Miaudet, P. *et al.* Hot-drawing of single and multiwall carbon nanotube fibers for high toughness and alignment. *Nano Letters* **5**, 2212-2215 (2005).
- 19 Minus, M. L., Chae, H. G. & Kumar, S. Interfacial Crystallization in Gel-Spun Poly(vinyl alcohol)/Single-Wall Carbon Nanotube Composite Fibers. *Macromolecular Chemistry and Physics* **210**, 1799-1808 (2009).
- 20 Mu, M. & Winey, K. I. Improved load transfer in nanotube/polymer composites with increased polymer molecular weight. *Journal of Physical Chemistry C* **111**, 17923-17927 (2007).

- 21 Sandler, J. K. W. *et al.* A comparative study of melt spun polyamide-12 fibres reinforced with carbon nanotubes and nanofibres. *Polymer* **45**, 2001-2015 (2004).
- 22 Vigolo, B. *et al.* Macroscopic fibers and ribbons of oriented carbon nanotubes. *Science* **290**, 1331-1334 (2000).
- 23 Vigolo, B., Poulin, P., Lucas, M., Launois, P. & Bernier, P. Improved structure and properties of single-wall carbon nanotube spun fibers. *Applied Physics Letters* **81**, 1210-1212 (2002).
- 24 Hull, D. & Clyne, T. W. *An introduction to composite materials*. (Cambridge University Press, 1996).
- 25 Rosenthal, J. A model for determining fiber reinforcement efficiencies and fiber orientation in polymer composites. *Polymer Composites* **13**, 462-466 (1992).
- 26 Wang, Z., Ciselli, P. & Peijs, T. The extraordinary reinforcing efficiency of single-walled carbon nanotubes in oriented poly(vinyl alcohol) tapes. *Nanotechnology* **18**, 45570 (2007).
- 27 Blighe, F. M. *et al.* The Effect of Nanotube Content and Orientation on the Mechanical Properties of Polymer-Nanotube Composite Fibers. *Advanced Functional Materials* **21**, 364-371 (2010)
- 28 Wang *et al.* The extraordinary reinforcing efficiency of single-walled carbon nanotubes in oriented poly(vinyl alcohol) tapes. Vol. 18 (Institute of Physics, 2007).
- 29 Kearns, J. C. & Shambaugh, R. L. Polypropylene fibers reinforced with carbon nanotubes. *J. Appl. Polym. Sci.* **86** (2002).
- 30 Chae, H. G., Choi, Y. H., Minus, M. L. & Kumar, S. Carbon nanotube reinforced small diameter polyacrylonitrile based carbon fiber. *Composites Science and Technology* **69**, 406-413 (2009).
- 31 Wang, Z., Ciselli, P. & Peijs, T. The Extraordinary Reinforcing Efficiency of Single-Walled Carbon Nanotubes in Oriented Poly(vinyl alcohol) Tapes. *Nanotechnology* **18** (2007)
- 32 Coleman, J. N. *et al.* Reinforcement of polymers with carbon nanotubes. The role of an ordered polymer interfacial region. Experiment and modeling. *Polymer* **47**, 8556-8561 (2006).
- 33 Blighe, F. M. *et al.* The effect of nanotube content and drawing on the mechanical properties of coagulation-spun polymer-nanotube composite fibres. *Advanced Functional Materials* **21**, 364-371 (2010)
- 34 Coleman, J. N. *et al.* High-performance nanotube-reinforced plastics: Understanding the mechanism of strength increase. *Advanced Functional Materials* **14**, 791-798 (2004).
- 35 Bergin, S. D. *et al.* Towards Solutions of Single-Walled Carbon Nanotubes in Common Solvents. *Advanced Materials* **20**, 1876-1881 (2008).
- 36 Munoz, E. *et al.* Multifunctional carbon nanotube composite fibers. *Advanced Engineering Materials* **6**, 801-804 (2004).
- 37 Razal, J. M. *et al.* Arbitrarily shaped fiber assemblies from spun carbon nanotube gel fibers. *Advanced Functional Materials* **17**, 2918-2924 (2007).
- 38 Poulin, P., Vigolo, B. & Launois, P. Films and fibers of oriented single wall nanotubes. *Carbon* **40**, 1741-1749 (2002).
- 39 Badaire, S. *et al.* Correlation of properties with preferred orientation in coagulated and stretch-aligned single-wall carbon nanotubes. *Journal of Applied Physics* **96**, 7509-7513 (2004).
- 40 Pichot, V. *et al.* Structural and mechanical properties of single-wall carbon nanotube fibers. *Physical Review B* **74** (2006).
- 41 Miaudet, P. *et al.* Thermo-electrical properties of PVA-nanotube composite fibers. *Polymer* **48**, 4068-4074 (2007).

- 42 Bergin, S. D. *et al.* Large populations of individual nanotubes in surfactant-based dispersions without the need for ultracentrifugation. *Journal of Physical Chemistry C* **112**, 972-977 (2008).
- 43 Sui, X. M. & Wagner, H. D. Tough Nanocomposites: The Role of Carbon Nanotube Type. *Nano Letters* **9**, 1423-1426 (2009).
- 44 Almecija, D., Blond, D., Sader, J. E., Coleman, J. N. & Boland, J. J. Mechanical properties of individual electrospun polymer-nanotube composite nanofibers. *Carbon* **47**, 2253-2258 (2009).
- 45 Deng, L., Young, R. J., van der Zwaag, S. & Picken, S. Characterization of the adhesion of single-walled carbon nanotubes in poly(p-phenylene terephthalamide) composite fibres. *Polymer* **51**, 2033-2039 (2010).
- 46 Amornsakchai, T., Cansfield, D. L. M., Jawad, S. A., Pollard, G. & Ward, I. M. The Relation between Filament Diameter and Fracture Strength for Ultra-High-Modulus Polyethylene Fibers. *Journal of Materials Science* **28**, 1689-1698 (1993).
- 47 Ji, Y., Li, B. Q., Ge, S. R., Sokolov, J. C. & Rafailovich, M. H. Structure and nanomechanical characterization of electrospun PS/clay nanocomposite fibers. *Langmuir* **22**, 1321-1328 (2006).
- 48 Wagner, H. D. Dependence of Fracture-Stress Upon Diameter in Strong Polymeric Fibers. *Journal of Macromolecular Science-Physics* **B28**, 339-347 (1989).
- 49 Wagner, H. D. Stochastic Concepts in the Study of Size Effects in the Mechanical Strength of Highly Oriented Polymeric Materials. *Journal of Polymer Science Part B-Polymer Physics* **27**, 115-149 (1989).
- 50 Arinstein, A., Burman, M., Gendelman, O. & Zussman, E. Effect of supramolecular structure on polymer nanofibre elasticity. *Nat. Nanotechnol.* **2**, 59-62 (2007).
- 51 Smook, J., Hamersma, W. & Pennings, A. J. The Fracture Process of Ultrahigh Strength Polyethylene Fibers. *Journal of Materials Science* **19**, 1359-1373 (1984).
- 52 Griffith, A. A. The phenomena of rupture and flow in solids. *Philos. Trans. Roy. Soc.* **A221**, 163 (1921).
- 53 Weibull, W. A Statistical Distribution Function of Wide Applicability. *Journal of Applied Mechanics-Transactions of the Asme* **18**, 293-297 (1951).
- 54 Doremus, R. H. Fracture Statistics - A Comparison of the Normal, Weibull, and Type-I Extreme Value Distributions. *Journal of Applied Physics* **54**, 193-198 (1983).
- 55 Karbhari, V. M. & Wilkins, D. J. Significance of Longitudinal and Transversal Size Effects on the Statistics of Fiber Strength. *Philos. Mag. A-Phys. Condens. Matter Struct. Defect Mech. Prop.* **64**, 1331-1344 (1991).
- 56 Lissart, N. & Lamon, J. Statistical analysis of failure of SiC fibres in the presence of bimodal flaw populations. *Journal of Materials Science* **32**, 6107-6117 (1997).
- 57 Krenchel, H. Fibre reinforcement;: Theoretical and practical investigations of the elasticity and strength of fibre-reinforced materials. (Akademisk forlag 1964).
- 58 Kannan, P., Eichhorn, S. J. & Young, R. J. Deformation of isolated single-wall carbon nanotubes in electrospun polymer nanofibres. *Nanotechnology* **18** (2007).
- 59 Duesberg, G. S., Loa, I., Burghard, M., Syassen, K. & Roth, S. Polarized Raman Spectroscopy on Isolated Single-Wall Carbon Nanotubes. *Physical Review Letters* **85**, 5436 (2000).
- 60 Liu, T. & Kumar, S. Quantitative characterization of SWNT orientation by polarized Raman spectroscopy. *Chemical Physics Letters* **378**, 257-262 (2003).

# Chapter 6

## High strength composite fibres from polyester filled with nanotubes and graphene

### 6.1 Introduction

Synthetic polymeric fibres are a very important part of modern life and are used extensively in applications in areas such as textiles, packaging and medical technology. Their widespread use is largely due to their high strength and low density but also due to their durability, abrasion resistance, and chemical and environment stability. Polyester fibres are probably the most widespread form of synthetic polymeric fibre<sup>1</sup>, while the most common polyester fibres are produced from poly(ethylene terephthalate) (PET)<sup>2</sup>. PET fibres are most widely used in textiles and can be produced with Young's modulus, strength and tensile toughness up to  $\sim 10$  GPa,  $\sim 1$  GPa and  $200 \text{ MJ/m}^3$  respectively<sup>3</sup>. In addition, these fibres are reasonably ductile with strain at break usually varying in the range  $\sim 20$ - $100\%$ . (Note that bulk PET is generally less stiff, less strong and can be more ductile)<sup>4</sup>. The strongest polyester fibre ever reported was produced from poly(ethylene naphthalate) and had modulus, strength and ductility of 26 GPa, 1.3 GPa and 7.6% respectively (assuming a density of  $1.35 \text{ g/cc}$ )<sup>5</sup>. However, while these mechanical properties are impressive, they cannot compare to high performance rigid rod polymeric fibres such as ultra-high molecular weight polyethylene (Dyneema® or Spectra), polyparaphenylene terephthalamide (Kevlar®) and polypyridobisimidazole (PIPD) which can display modulus and strength as high as 330 GPa and 4 GPa respectively<sup>6</sup>. However, one advantage of polyester fibres is that they can be melt-spun, cheaply and in large quantities. Thus, there would be significant advantages to modifying existing polyesters to produce fibres with enhanced mechanical properties.

Over the last decade, a lot of work has been done to reinforce polymeric fibres with nanoscale fillers<sup>7-9</sup>. When stiff, strong, rodlike (or planar) fillers are added to polymers, the mechanical properties can be improved dramatically. As described in chapter 2, the simplest possible model to describe this reinforcement is the rule of mixtures which predicts that the fibre modulus,  $Y$ , and strength,  $\sigma_B$ , depend on the filler volume fraction,  $V_f$ , by<sup>10,11,10,11</sup>

$$Y = (\eta_o \eta_{LY} Y_R - Y_P) V_f + Y_P \quad 6.1$$

$$\sigma_B = (\eta_o \eta_{L\sigma} \sigma_R - \sigma_P) V_f + \sigma_P \quad 6.2$$

Here, the subscripts R and P refer to the reinforcing filler and the polymer respectively. In addition  $\eta_o$  and  $\eta_L$  are factors which vary between 0 and 1 and correct for the effects of nanotube orientation and length respectively<sup>12,13</sup>. These expressions mean that the rate of increase in both fibre modulus and strength with filler content have upper limits given by

$$dY/dV_f \leq Y_R \text{ or } d\sigma_B/dV_f \leq \sigma_R \quad 6.3$$

Due to their intrinsically high stiffness and strength, one of the most exciting filler materials of recent years has been carbon nanotubes. These high aspect ratio carbon cylinders have diameters of ~nm, lengths of ~microns and display superlative mechanical properties with modulus and strength up to 1 TPa and 50-150 GPa respectively<sup>8,14-19</sup>. Significant successes have been achieved by reinforcing polymers with carbon nanotubes<sup>8</sup>. Polymer-carbon nanotube composite fibres have been produced using a range of matrices and spinning methods and in some cases have achieved exceptional mechanical properties, with a number of papers describing composite fibres with strength in excess of 1 GPa<sup>13,20-24</sup>. However, in many cases the key to such impressive results has been the quality of the nanotube dispersion, which is usually achieved through solution processing. This often means that the fibres have been formed from solution using methods such as coagulation spinning<sup>25</sup>. This is unfortunate as many commercial plastic fibres are melt processed; it has proved more difficult to produce excellent composite fibres from the melt than from solution<sup>8</sup>.

Surprisingly few papers have reported the reinforcement of polyester fibres. A small number of papers have described the reinforcement of PET fibres with carbon nanofibres<sup>26</sup> or organoclays<sup>27</sup> with limited improvements in mechanical properties. In addition, some papers have reported the production of nanotube-PET composite fibres<sup>28-30</sup>. Of these, the most impressive results were those of Anand et al. who prepared composite fibres by melt compounding, followed by spinning and drawing<sup>28</sup>. They

obtained fibres with a modulus and strength of 15.9 GPa and 712 MPa, significantly better than the pure polymer.

The fibres described in this chapter aim to build on this work to generate fibres with significantly higher stiffness and strength at reduced cost. It is known that some nanotubes are present as large aggregates when melt mixed into PET<sup>30</sup>. This is probably a result of incomplete exfoliation during mixing. Such aggregates act to concentrate stress and can precipitate failure. This issue could be addressed by first exfoliating the nanotubes in a solvent before mixing into the PET melt. This should lead to a uniform composite with well dispersed nanotubes and minimal aggregates. Another problem with using nanotubes as a filler, is that the nanotubes with high strength (i.e. single walled nanotubes) tend to be extremely expensive (~€500/g). This issue could be resolved by using solvent exfoliated graphene as a filler material. Using these strategies, the production of composite fibres with extremely high stiffness and strength can be demonstrated, using a filler (graphene) exfoliated from a starting material which costs as little as ~€5/kg.

## 6.2 Background

PET-nanotube fibres have been produced by several groups. Li et al. have produced such composites by compounding PET resin with nanotubes followed by extrusion. They carried out electrical measurements on these fibres and found them to have a resistance of  $10^3 \Omega \text{ cm}$  which is 12 orders lower than pure PET. These fibres had a diameter of  $30 \mu\text{m}$  and a strength of  $14.9 \text{ MPa}$ <sup>31</sup>. Kim et al. have also produced PET-nanotube fibres using fibre extrusion<sup>29</sup>. The strength of PET only fibres was  $60 \text{ MPa}$  and this increased to  $68 \text{ MPa}$  upon the addition of  $2\text{wt}\%$  MWNTs. This corresponds to a  $d\sigma/dV_f$  value of  $670 \text{ MPa}$ . The Young's modulus increased from  $1.55 \text{ GPa}$  to  $1.85 \text{ GPa}$  for composites containing  $2\text{wt}\%$  nanotubes. For these fibres,  $dY/dV_f$  was  $25 \text{ GPa}$ . PET-SWNT fibres were also melt spun by Anand et al<sup>32</sup>. Fibres were drawn by 4, 5 and 6 times their original length. For samples drawn by 4 times their original length, a strength of  $195 \text{ MPa}$  for PET only fibres was obtained which increased to  $509 \text{ MPa}$  upon the addition of  $2\text{wt}\%$  SWNTs. This corresponds to a  $d\sigma/dV_f$  value of  $22.1 \text{ GPa}$ . The Young's modulus of the fibres also increased from  $2.21 \text{ GPa}$  up to  $11.69 \text{ GPa}$  at a concentration of  $2\text{wt}\%$  resulting in a  $dY/dV_f$  value of  $667.6 \text{ GPa}$ . Nanotube templated crystallinity was present in these fibres and contributes to reinforcement. For these composites, it was found that by using melt compounding for fibre production, nanotube aggregates as large as  $50\text{-}100 \mu\text{m}$  could be observed giving their fibres an uneven surface. This was due to

poor dispersion due to the melt compounding method. Thus, the nanotube dispersion method used in this chapter aims to disperse the nanotubes more effectively and thus improve on mechanical properties of fibres.

Mun et al. produced PET-functionalised MWNT composite fibres by in situ polymerisation<sup>30</sup>. Fibres were produced by hot pressing, followed by fibre extrusion. Fibres were also drawn to improve mechanical properties. For a draw ratio of 1, PET only fibres had a strength of 46 MPa while composites containing 0.5 wt% functionalised MWNTs had a strength of 64 MPa. This corresponds to a  $d\sigma/dV_f$  value of 5.97 GPa. PET only fibres had a Young's modulus of 2.21 GPa while at a higher draw ratio, composites containing 1.5wt% nanotubes had a modulus of 4.91 GPa. This gives a  $dY/dV_f$  value of 301 GPa.

Other PET composite fibres were reinforced with materials such as nanofibres and organoclays. PET-carbon nanofibre composites were produced by Ma et al. The tensile strength stayed much the same for PET only and composite fibres. PET only fibres were 0.43 GPa in strength while 5 wt% composites were 0.42 GPa. The Young's modulus increased from 10 GPa to 11 GPa upon the addition of 5 wt% carbon nanofibres. While these properties did not improve by much, the compressive strength of the composites was considerably higher than for PET only fibres. This increased from 0.08 GPa to 0.12 GPa<sup>26</sup>.

Chang et al. used hot pressing followed by fibre extrusion for fibre production. PET only fibres had strengths of 46MPa and PET-organoclay fibres had strengths of 71 MPa for drawn fibres at an organoclay concentration of 3wt%<sup>27</sup>.

As described in chapter 2, graphene can also be used for composite reinforcement. There are currently no papers reporting the production of PET-graphene fibres to date and this research aims to produce and mechanically test fibres of this kind. A simple method of PET-nanotube and PET-graphene composite fibre production will be described in this chapter.

### 6.3 Experimental Procedure

Composite melts were produced by adding solvent-dispersed, exfoliated single walled nanotubes or graphene to a PET melt while stirring. After solvent evaporation, a uniform melt was obtained with no visual evidence of aggregates. The procedure is described in detail below.

### 6.3.1 Dispersion of Graphene

Graphite powder (Aldrich product number 332461, batch number 06106DE) was dispersed in N-methyl-2-pyrrolidone (NMP, Aldrich) at an initial concentration of 3mg/ml (1800mgs in 600mls) by bath sonication (Branson1510E-MT) for 144 hours using methods described recently<sup>33,34</sup>. In order to produce a more concentrated dispersion<sup>35</sup>, this was then filtered on a porous nylon membrane (Sterlitech, pore diameter 0.45  $\mu\text{m}$ ). The deposited graphene was then re-dispersed in 15 mls of fresh NMP by bath sonication for a further 24 hrs. This dispersion was then centrifuged at 1000 rpm for 45 mins and the supernatant collected.

### 6.3.2 Dispersion of Nanotubes

SWNTs (HiPCO, Unidym) were dispersed in NMP at an initial concentration of 7mg/ml using a sonic tip processor (GEX600, 120 W, 60 kHz, flat head probe) operated in pulsed mode (9 sec on/9 sec off) for 16 hrs<sup>36-38</sup>. The resulting dispersion was further sonicated in a sonic bath for 4 hours.

### 6.3.3 Estimation of Nanotube and Graphene Concentration

The dispersed concentration was estimated by filtering 2ml of dispersion through a nylon membrane which was then dried in an oven (60 °C) for an hour. The filtrate mass was found by careful weighing, yielding concentrations of 7mgs/ml and 9mgs/ml for nanotube and graphene dispersions respectively.

This method was confirmed by carrying out UV Vis measurements on the dispersion. This was calculated using the Beer-Lambert law, (equation (6.4)) which states that the absorbance of the solution is directly proportional to the solutions concentration:

$$\frac{I}{I_0} = e^{-A} \quad 6.4$$

where  $A = \alpha Cl$ .

$\alpha$  is the extinction coefficient. Its value for a carbon nanotube dispersion is 3264ml  $\text{mg}^{-1}\text{m}^{-1}$  and 3620ml  $\text{mg}^{-1}\text{m}^{-1}$  for a graphene dispersion<sup>38,39</sup>, C is the concentration and l is the length of the cuvette (1 mm).

Once the nanotube mass fraction is known, this can be converted into volume fraction using equation 6.5<sup>40</sup>.

$$V_f = \left[ 1 + \left( \frac{\rho_{NT}}{\rho_{Pol}} \right) \left( \frac{1 - M_f}{M_f} \right) \right]^{-1} \quad 6.5$$

### 6.3.4 Melt Processing of PET fibres

A sheet of PET (Deyn Plastics Ltd.) weighing 1gram, (of measured mechanical properties  $Y=1.3$  GPa,  $\sigma_B=148$  MPa,  $\epsilon_B=150\%$ ) was cut into pieces, placed in a beaker on a hotplate (190 °C) and allowed to melt over the course of approximately 10 mins. Composite melts were produced by adding a dispersion of nanotubes/graphene with well-defined volume and concentration (and so well defined dispersed mass) to the PET melt. The mixture was constantly stirred to give a homogenous liquid. After approximately 10 mins of heating, the NMP had completely evaporated to give a composite melt. The mass fraction of the composite is controlled by the mass of nanotubes/graphene added and the PET mass. Nanotube and graphene filled composite melts were prepared at mass fractions (0.5wt%, 1wt%, 2wt%) and (0.25wt%, 0.5wt% 1wt%, 4wt%) respectively.

Fibres could be formed from either a PET or composite melt by inserting a fine needle to which the melt adhered strongly. The needle was drawn out of the melt at a rate of  $\approx 40$  cm/s to give a fibre. The fibres were then drawn to the maximum possible draw ratio before failure. Interestingly, while the PET fibres could only be drawn to  $\sim 200\%$ , the composite fibres could generally be drawn considerably further: SWNT fibres - (0.5wt%, 400% draw), (1wt%, 250%), (2wt%, 400%) and graphene fibres - (0.25wt%, 370%), (0.5wt%, 350%) (1wt%, 400%), (4wt%, undrawable). This is in contrast to the experience of Anand et al.<sup>28</sup> and Mun et al.<sup>30</sup> who found that the maximum draw ratio either remained constant or was reduced in the presence of nanotubes.<sup>28,30</sup> In addition, the 1 wt% nanotube fibres and 0.5 wt% graphene fibres were drawn to a range of draw ratios (and so a range of final diameters).

Using this procedure, between 4 and 23 fibres were produced for each volume fraction of both nanotubes and graphene. After drawing, the fibre diameters were measured at typically 3 positions along their lengths using a profilometer (Dektak 6M Stylus Profiler). The diameter variance along a fibre was typically small (<10%). The mean diameter varied from 3-19  $\mu\text{m}$  for the nanotube composites and 5-20  $\mu\text{m}$  for the graphene composites. Note that using this procedure there is no control over the fibre diameter before drawing but some control of the diameter after drawing.

Tensile testing was performed on all fibres with a Zwick Z100 tensile at a strain rate of 5mm/min. SEM measurements were performed using a Carl Zeiss Ultra Plus Field Emission Scanning Electron Microscope. The nanotube/graphene mass fraction was converted to volume fraction assuming the densities:  $\rho_{\text{PET}}=1300\text{kg/m}^3$ ,  $\rho_{\text{SWNT}}=1800\text{kg/m}^3$  &  $\rho_{\text{Graphene}}=2100\text{kg/m}^3$ .

## 6.4 Results and Discussion

### 6.4.1 PET-nanotube fibres: Volume fraction dependence

The processing procedure used in this work resulted in large set of PET-nanotube fibres with a range of volume fractions and diameters. SEM images of a selection of these fibres are shown in figure 6.1.

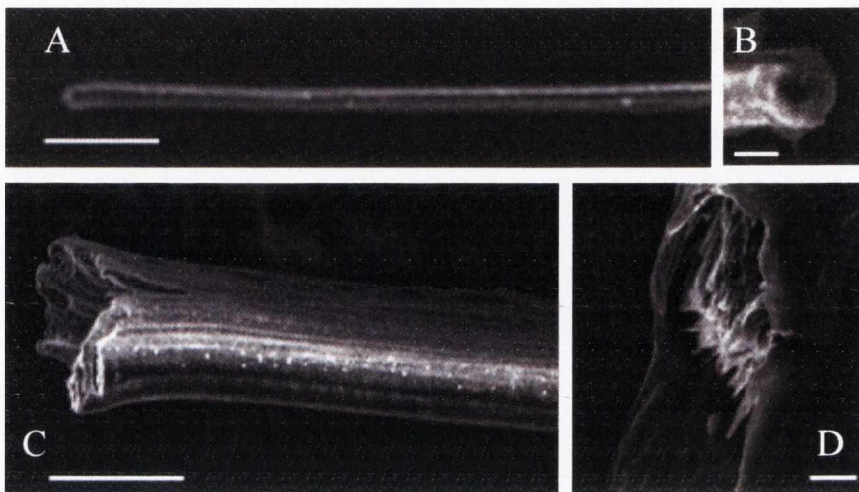


**Figure 6.1: SEM images of melt processed PET-SWNT fibres. The scale bars are A) 20  $\mu\text{m}$ , B) 2  $\mu\text{m}$ , C) 10  $\mu\text{m}$  and D) 1  $\mu\text{m}$ .**

As shown in figure 6.1A the fibre is extremely uniform and the cross-section relatively circular (figure 6.1B). In addition, the side-walls are relatively smooth and well defined (figure 6.1C). No signs of nanotube aggregates were observed in any fibres. Shown in figure 6.1D is a fracture surface of a broken fibre. Close to the centre of the fibre, a number of SWNT bundles can be seen protruding. This suggests that the fracture mechanism is by nanotube pullout. This suggests that the nanotubes used here are shorter than the critical length and ultimately means that the fibre strength will not be limited by the nanotube strength<sup>12</sup>.

Stress-strain measurements were made for all fibres. For composites, the most fundamental question is how the mechanical properties scale with filler content. The measured fibres were divided into subsets including all volume fractions and with similar diameters (maximum deviation from mean diameter was  $\sim 10\%$ ). Note that less than half of the total fibres could be grouped into such subsets. This allowed the study of the effect of nanotube volume fraction on mechanical properties without any contribution from varying fibre diameter. This is critical as the mechanical properties of fibres can vary

strongly with fibre diameter<sup>23,41-46</sup>. Shown in figure 6.2A are stress-strain curves for a PET fibre and composite fibres with 0.36 vol%, 0.72 vol% and 1.4 vol% SWNT.

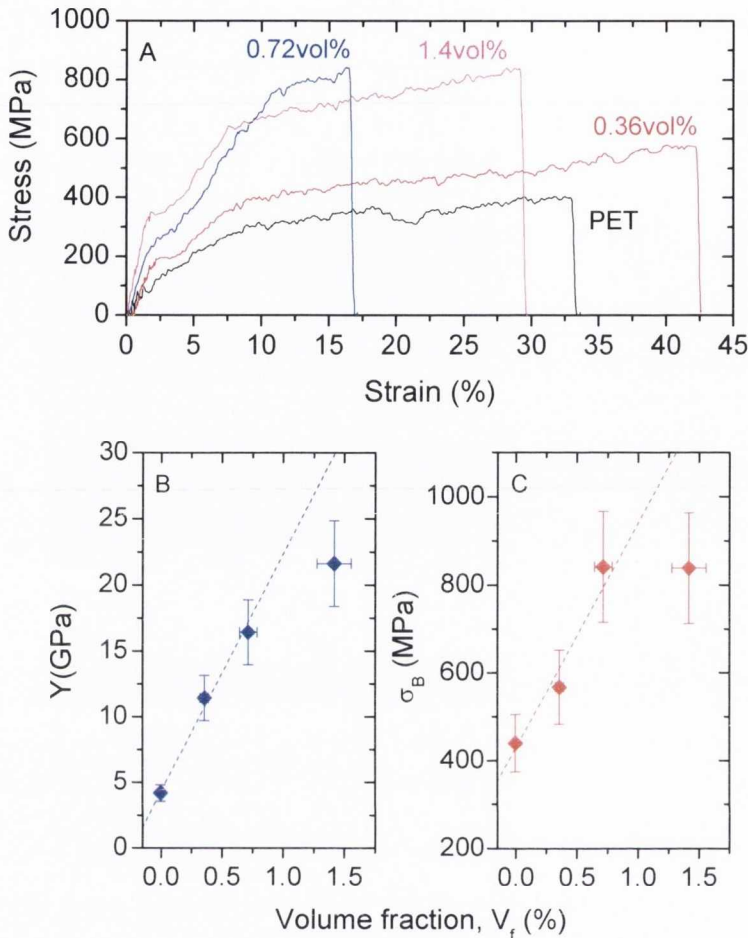


**Figure 6.2: Mechanical properties of PET-SWNT fibres with diameter  $D \approx 5 \mu\text{m}$  as a function of nanotube volume fraction. A) Stress strain curves. B) Young's modulus. The slope of the straight line is  $dY/dV_f = 1805 \pm 150$  GPa. C) Ultimate tensile strength. The slope of the straight line is  $d\sigma_B/dV_f = 51 \pm 12$  GPa.**

In all cases the fibres were very close to  $5 \mu\text{m}$  in diameter. On addition of the nanotubes the modulus and strength increase significantly. The increases in modulus,  $Y$ , and strength,  $\sigma_B$  can be quantified by plotting them as a function of volume fraction,  $V_f$ , in figure 6.2B and C. The modulus increases from 4 GPa for PET to 22 GPa for the 1.5 vol% sample. The initial portion of this curve is linear with slope  $dY/dV_f = 1805 \pm 150$  GPa. This is significantly beyond the upper limit of 1000 GPa set by the intrinsic nanotube modulus and the rule of mixtures<sup>8,11,12,47</sup>, indicating that an additional component of reinforcement is present. This is not unusual, with nanotube-nucleated

crystallinity a common cause<sup>46,47,48,49</sup>. In fact, this is a reasonable explanation as nanotube-induced crystallinity has been observed in PET-nanotube composites<sup>29</sup>.

Similarly, the strength increases from 420 MPa for PET to 820 MPa for the 1.5 vol% sample. Again, the initial portion of this curve is linear with slope  $d\sigma_B/dV_f=51\pm 12$  GPa. While this value is not beyond the upper limit of  $\sim 50$ -100 GPa set by the intrinsic nanotube strength and the rule of mixtures<sup>8,47</sup>, it is extremely high for a nanotube reinforced composite<sup>50</sup>. Because nanotubes are often shorter than the critical length (as is the case here)<sup>12</sup>, composite strength is usually much lower than if it was limited by the nanotube strength<sup>8,47</sup>. Usually, the strength increase is limited by either defects<sup>23</sup> or the shear strength of the polymer-nanotube interface (or the polymer shear strength depending on which is smaller)<sup>45,46,47,48</sup>. The large value of  $d\sigma_B/dV_f$  suggests that defects don't dramatically affect the strength or that the interfacial/polymer shear strengths are relatively large. Alternatively, nanotube nucleated crystallinity may contribute strongly to the reinforcement<sup>48</sup>. Note that both strength and modulus behaved similarly for other fibre diameters as shown in figure 6.3.

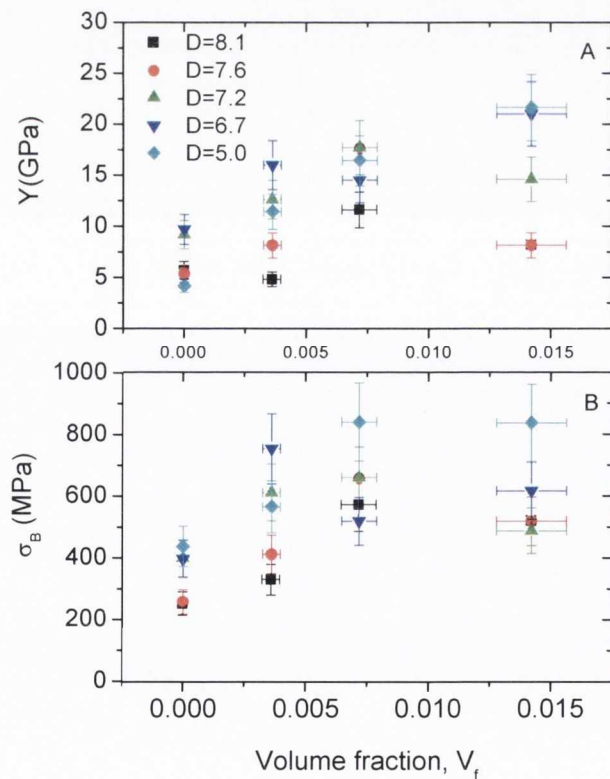


**Figure 6.3: Young's modulus (A) and ultimate tensile strength (B) as a function of nanotube volume fraction for fibres with a range of mean diameters from 5.0 to 8.1  $\mu\text{m}$ .**

The strain at break,  $\epsilon_B$ , was also measured and found to be relatively invariant with nanotube volume fraction, remaining between 20 and 40% for almost all volume fractions for each diameter set. The same behaviour was observed for the tensile toughness,  $T$ , (energy per unit volume required to break the fibre) which was typically between 75 and 175 MJ/m<sup>3</sup> for most samples (see figure 6.4).

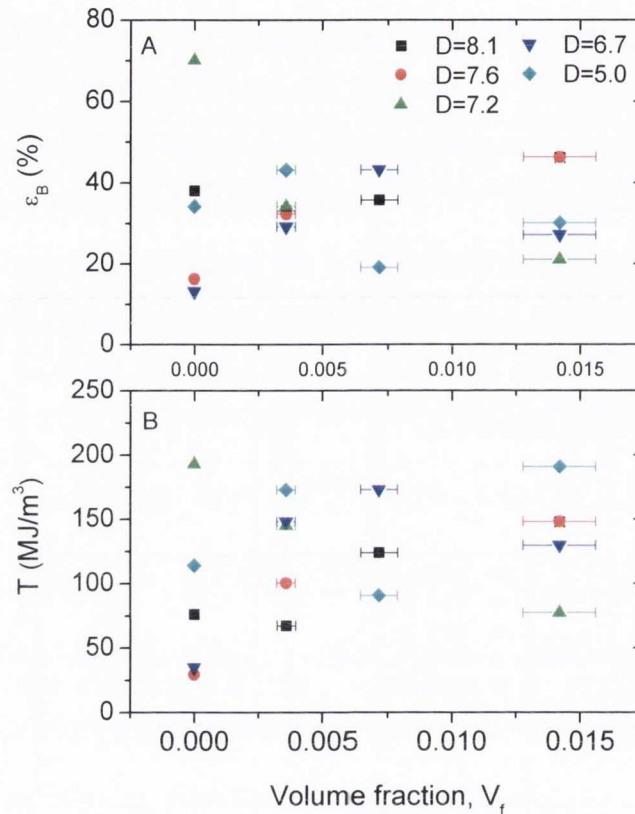


**Figure 6.4: Strain at break (A) and tensile toughness (B) as a function of nanotube volume fraction for fibres with a range of mean diameters from 5.0 to 8.1  $\mu\text{m}$ .**

### 6.4.2 PET-nanotube fibres: Diameter dependence

The entire data set can be summarised by plotting each mechanical parameter ( $Y$ ,  $\sigma_B$ ,  $\epsilon_B$  and  $T$ ) as a function of fibre diameter as shown in figure 6.5.

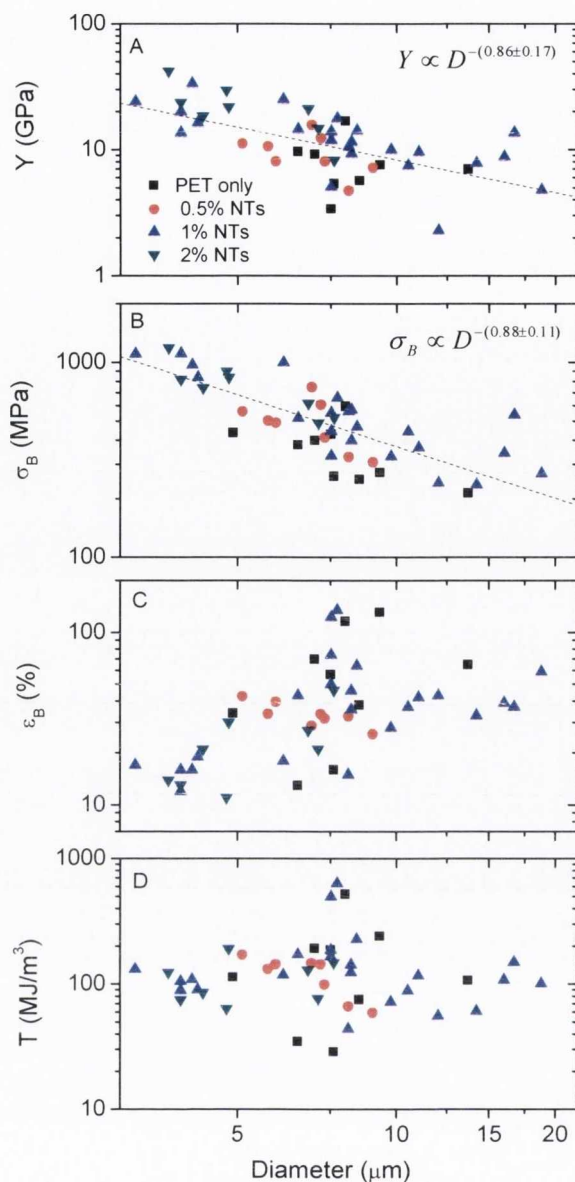


**Figure 6.5: Mechanical properties of PET-SWNT fibres as a function of fibre diameter. For a given fibre the typical spread in the diameter is <10%. A) Young's modulus, B) ultimate tensile strength, C) strain at break and D) tensile toughness. In A) and B) the dashed lines are power law fits to the entire data set. The nanotube contents are given as wt%.**

Both modulus and strength increase with decreasing fibre diameter. The highest modulus and strength observed were 42 GPa and 1.2 GPa, both for a 3.7  $\mu\text{m}$  diameter fibre. In chapter 5, it was shown that both modulus and strength of polymer-nanotube composite fibres scale with fibre diameter as power laws;<sup>23</sup>  $Y \propto D^{-\alpha}$  and  $\sigma_B \propto D^{-(\alpha+\beta)}$ . The diameter dependence of the modulus is controlled only by changes in nanotube orientation with fibre diameter (as described by  $\alpha$ ). However, the diameter dependence of

the strength is controlled by a combination of orientation effects and surface defects (as described by  $\beta$ ). For poly(vinyl) alcohol fibres,  $\alpha \approx 0.6$  while  $\beta \approx 0.3$ .<sup>23</sup>

This behaviour was tested here by fitting the entire modulus and strength versus diameter data sets to power laws. Reasonable agreement is found in both cases with  $\alpha = 0.86 \pm 0.17$  and  $\alpha + \beta = 0.88 \pm 0.11$ , consistent with  $\beta \leq 0.3$ . It can be concluded from this that the observed diameter dependence is entirely consistent with this defect/orientation model. However, it is likely that the orientation dependence here is slightly stronger and the defect dependence slightly weaker than that observed previously.

The strain at break as a function of fibre diameter is shown in figure 6.5C. In general the strain at break tends to increase with increasing D, from  $\sim 10\%$  to  $\sim 70\%$  as D is increased from 4 to 18  $\mu\text{m}$ . Interestingly there appears to be a peak in the strain at break for  $D \approx 8 \mu\text{m}$  where  $\epsilon_B$  reaches 130%. The origin of this remains unclear. Shown in figure 6.5D is the tensile toughness as a function of D. This remains relatively flat at  $\sim 100 \text{ MJ/m}^3$  but shows signs of a peak again around  $D \approx 8 \mu\text{m}$ . The highest value obtained was  $637 \text{ MJ/m}^3$  for composites containing 1 wt% nanotubes. This is relatively large compared to tough materials such as Kevlar and dragline spider silk ( $48 \text{ MJ/m}^3$  and  $214 \text{ MJ/m}^3$ )<sup>51</sup>. However, it is worth noting that this toughness is attained at relatively large ductility i.e.  $>100\%$ .

### 6.4.3 PET-graphene fibres

Polymer-nanotube composite fibres are relatively straightforward to prepare and have been known for over 10 years<sup>52</sup>. In contrast, polymer-graphene fibres have not been reported to date. Like nanotubes, graphene is a promising filler due to the exceptional mechanical properties of monolayer graphene which has been reported at  $Y \approx 1 \text{ TPa}$  and  $\sigma_B \approx 100 \text{ GPa}$ <sup>53</sup>. While a number of papers have reported bulk composites based on chemically modified graphene as a filler<sup>54-61</sup>, in general the level of reinforcement achieved has been significantly below that predicted by the rule of mixtures<sup>11</sup>. This is probably due to a combination of the relatively poor mechanical properties of chemically modified graphene<sup>62</sup> and the fact that reasonably large graphene flakes are required to achieve effective reinforcement<sup>61,62,63,64</sup>. However, it has recently been shown that high quality, defect free graphene with relatively large flake size can be produced by exfoliation of graphite in solvents or surfactants<sup>37,65-73</sup>. In this work, a solvent based dispersion and exfoliation method recently pioneered in our group is used<sup>33-35</sup>. This method results in dispersions of few layer graphene flakes with mean length, width and

thickness (in this case) of 1.1  $\mu\text{m}$ , 0.51  $\mu\text{m}$  and 4.6 layers respectively. This was found by investigating the graphene dispersion using transmission electron microscopy (TEM) by dropping a small quantity of the dispersion onto holey carbon grids. Representative TEM images are shown in figure 6.6.

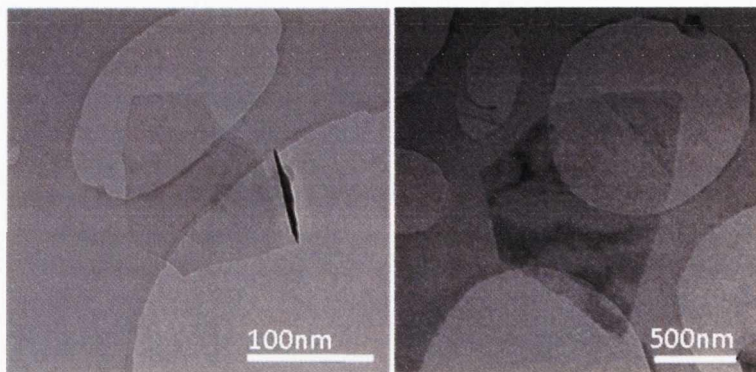


**Figure 6.6: TEM images of exfoliated graphene multilayers deposited from the dispersion used to prepare the PET-graphene composite melts.**

TEM flake size statistics can also be found for the graphene dispersion. The flake thickness,  $n$ , was measured using the edge counting method (see figure 6.7)<sup>34</sup>.

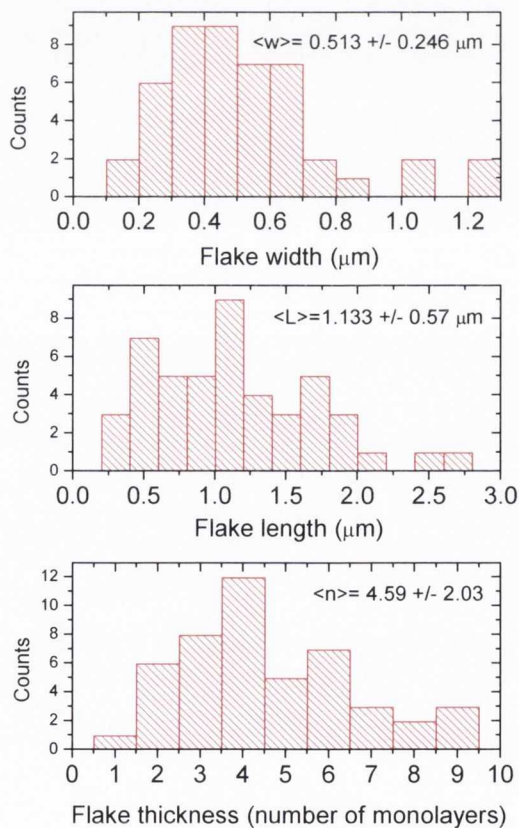


**Figure 6.7: TEM statistics of graphene flakes centrifuged at 1000rpm where  $w$  is the width of the flake,  $L$  is the length and  $n$  is the number of graphene layers.**

Raman spectroscopy shows the flakes to be relatively free of basal plane defects. Raman spectra for the graphene dispersion used for this work are shown in figure 6.8. A reference graphite powder is shown also as a comparison. Here the D band ( $\sim 1300\text{cm}^{-1}$ ) is indicative of the presence of defects. However, note that for small flakes such as those observed here, significant D bands can come simply from the presence of flake edges<sup>34</sup>.

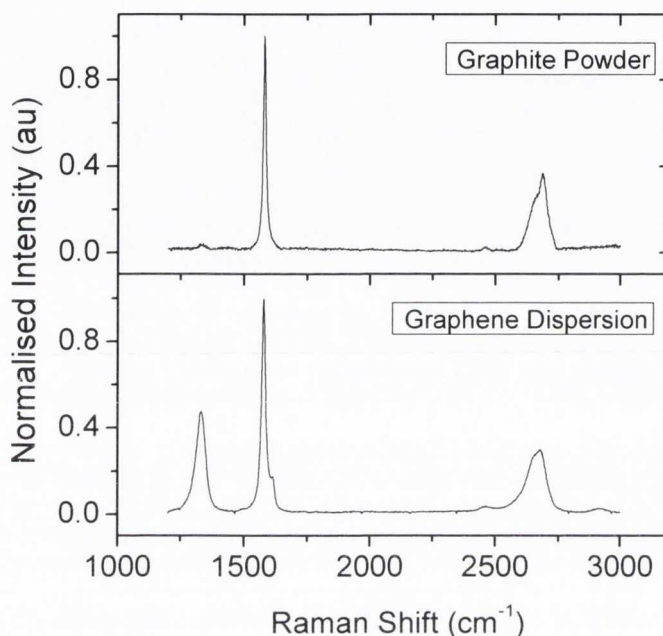


**Figure 6.8 Raman spectra for the graphene dispersion used for this work with spectrum for reference graphite powder shown for comparison.**

As a result, it is expected that they will have mechanical properties approaching that of monolayer graphene. This exfoliation method can be combined with the polymer-nanotube fibre formation method described above to prepare high quality polymer-graphene fibres.

#### **6.4.4 PET-graphene fibres: Volume fraction dependence**

Shown in figure 6.9 are SEM images of PET-graphene fibres.

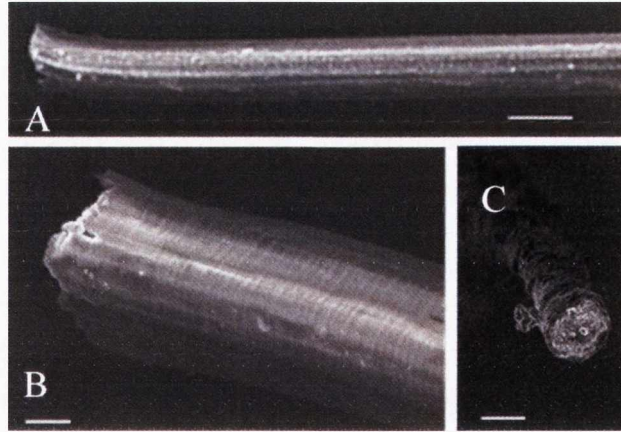


**Figure 6.9: SEM images of melt processed PET-graphene fibres. The scale bars are A) 10  $\mu\text{m}$ , B) 2  $\mu\text{m}$  and C) 2  $\mu\text{m}$ .**

Like the PET-nanotube fibres, the PET-graphene fibres are uniform in diameter, have smooth, well defined walls and a circular cross-section.

Shown in figure 6.10A are stress strain curves for a subset of PET-graphene fibres with  $D \approx 13 \mu\text{m}$ .

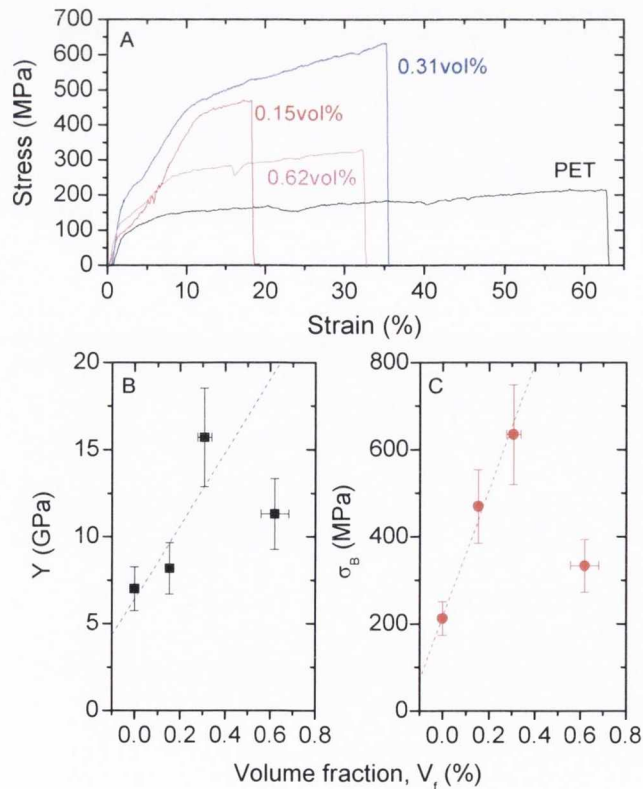


**Figure 6.10: Mechanical properties of PET-graphene fibres with diameter  $D \approx 13 \mu\text{m}$  as a function of graphene volume fraction. A) Stress strain curves. B) Young's modulus. The slope of the straight line is  $dY/dV_f = 2100 \pm 1300$  GPa. C) Ultimate tensile strength. The slope of the straight line is  $d\sigma_B/dV_f = 145 \pm 15$  GPa.**

Here both modulus and strength increase with graphene content while the strain at break tends to fall off. The modulus increases approximately linearly with graphene volume fraction from  $\sim 7$  GPa to  $\sim 15.7$  GPa for the 0.3 vol% sample. The rate of increase is  $dY/dV_f=2100\pm 1300$  GPa. Similarly the strength increases linearly with graphene volume fraction from  $\sim 200$  MPa to  $\sim 636$  MPa for the 0.3 vol% sample with a rate of increase of  $dY/dV_f=145\pm 15$  GPa. Again, these rates are large compared to that expected from the intrinsic properties of graphene and the rule of mixtures<sup>10</sup>, suggesting the presence of graphene nucleated crystallinity. Note that at higher volume fractions, both modulus and strength fall off dramatically, suggesting large scale graphene aggregation. Similar data was found for other fibre diameters (figure 6.11).

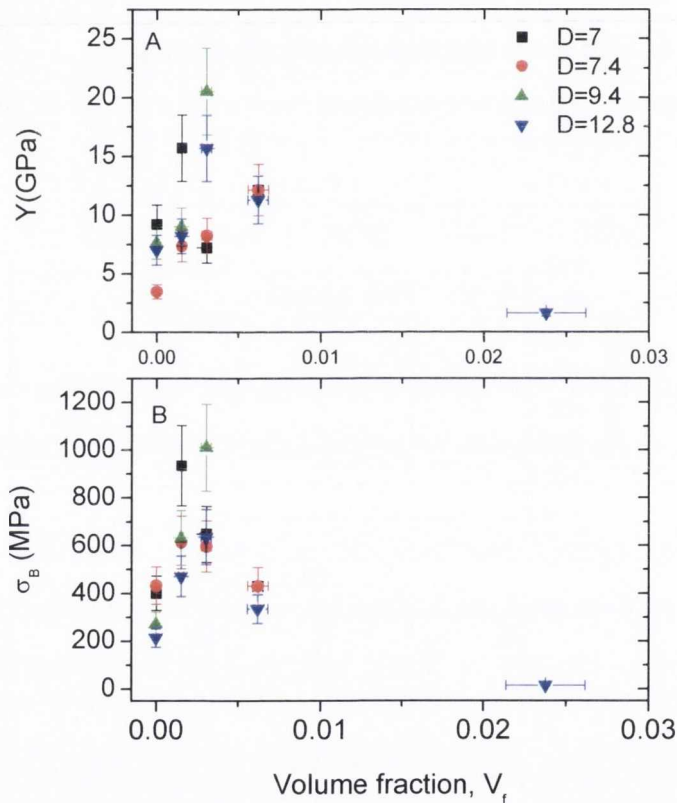


**Figure 6.11: Young's modulus (A) and strength (B) as a function of graphene volume fraction for fibres with a range of mean diameters from 7 to 12.8  $\mu\text{m}$ .**

The strain at break and toughness were also measured as a function of graphene volume fraction (figure 6.12).

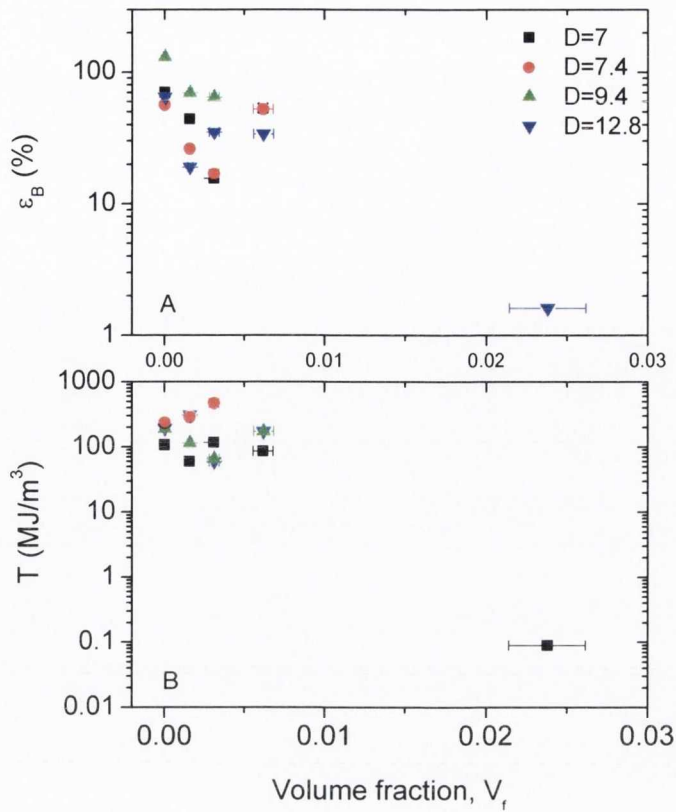


**Figure 6.12: Strain at break (A) and tensile toughness (B) as a function of graphene volume fraction for fibres with a range of mean diameters from 7 to 12.8  $\mu\text{m}$ .**

Significant differences were observed here in comparison to the PET-nanotube fibres. Both ductility and toughness fell dramatically with graphene content. The strain at break fell exponentially with volume fraction from  $\sim 100\%$  to 1-2% on addition of 4wt% graphene. A similar reduction was observed for toughness.

#### 6.4.5 PET-graphene fibres: Diameter dependence

As with the PET-nanotube composites, an overview can be achieved by plotting the mechanical parameters as a function of  $D$ . This is shown in figure 6.13.

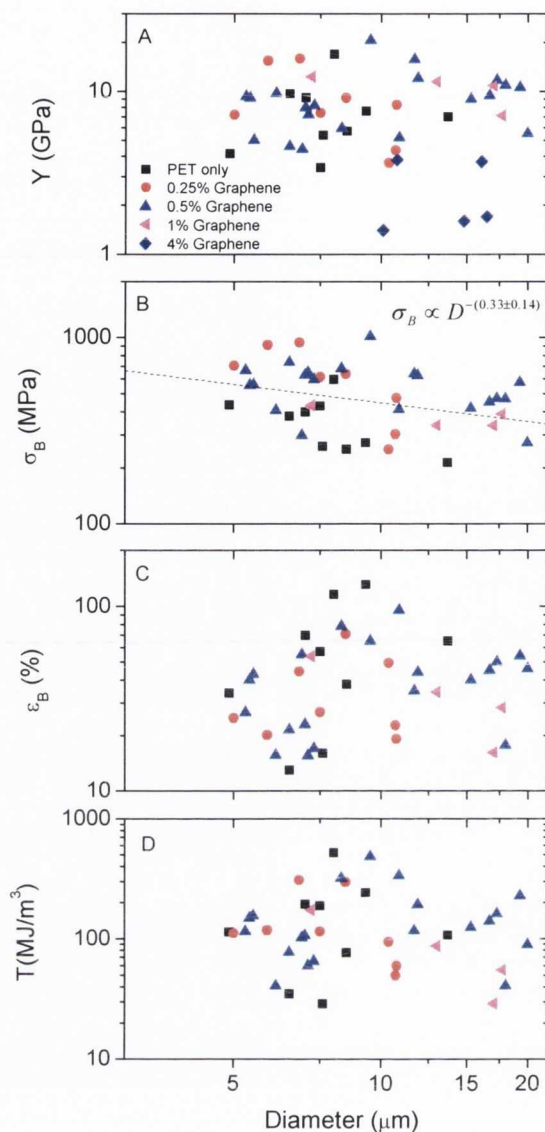


**Figure 6.13: Mechanical properties of PET-graphene fibres as a function of fibre diameter. For a given fibre the typical spread in the diameter is 7%. A) Young's modulus, B) ultimate tensile strength, C) strain at break and D) tensile toughness. The graphene contents are given as wt%. The line in B is a power law fit to the entire data set.**

The modulus data (figure 6.13A) is extremely scattered, hardly displaying any diameter dependence at all (i.e.  $Y \propto D^{-\alpha}$  with  $\alpha=0.1\pm 0.2$ , fit line not shown). This is perhaps not surprising for a planar filler like graphene, as confinement due to small fibre diameter may not result in orientation as efficiently as it will for rodlike fillers. As a result the largest modulus observed was 21 GPa for a relatively large fibre with  $D=9.5 \mu\text{m}$ .

However, the strength data in figure 6.13B does display a diameter dependence, consistent with  $\sigma_B \propto D^{-(\alpha+\beta)}$  where  $\alpha+\beta=0.33\pm 0.14$ . Ultimately, this means that  $\beta=0.2\pm 0.3$ , a value entirely consistent with defect limited strength.<sup>23</sup> As with modulus, the strongest fibre had  $D=9.5\ \mu\text{m}$  and had  $\sigma_B=1.0\ \text{GPa}$ . The strain at break data is plotted as a function of  $D$  in figure 6.13C. Here two things are of note. It is very clear that addition of graphene results in a reduction of ductility. Secondly, the peak in ductility observed previously, is much clearer here. The toughness, as shown in figure 6.13D, shows similar behaviour.

### 6.4.6 Comparison of mechanical properties with previous work on PET-nanotube composites

The mechanical properties found here can be compared to literature values. As mentioned in the introduction and background, there are only a handful of papers describing composites of PET and nanotubes. For these papers, the best results are plotted in terms of strength as a function of modulus in figure 6.14. In addition, the same data is plotted for all of the fibres in this work.

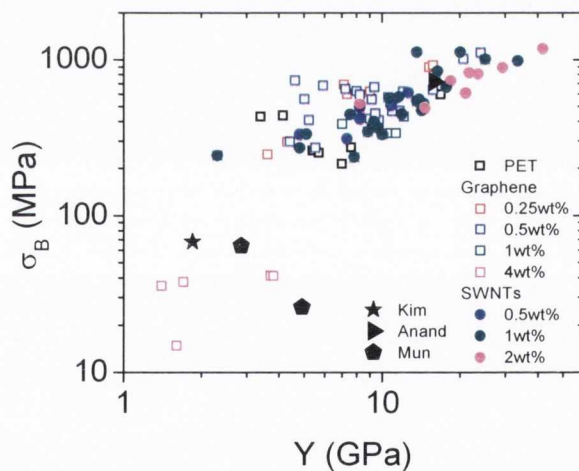


**Figure 6.14: Summary of strength and stiffness data for all the fibres measured in this work. For comparison, the best data from three papers in the literature are also included.**

Of the literature data, by far the highest strength and modulus values were those of Anand et al.<sup>28</sup> who attained values of  $Y=16\ \text{GPa}$  coupled with  $\sigma_B=720\ \text{MPa}$ . By comparison, the PET-nanotube (2wt%) and PET-graphene (0.5wt%) composites in this work show maximum moduli of 42 GPa and 21 GPa respectively and maximum strengths

of 1.2 GPa and 1.0 GPa respectively. It can be suggested that the data in this chapter is superior largely because of the use of an extremely good dispersion of the filler in the matrix (except for high graphene contents). This is almost certainly due to the fact that the filler is dispersed in NMP prior to mixing, guaranteeing minimal aggregation. In addition, it is worth noting that the best values of modulus and strength in this work are competitive with the best polyester fibres reported to date ( $Y=26$  GPa,  $\sigma_B=1.3$  GPa for  $D\approx 20$   $\mu\text{m}$ )<sup>5</sup>.

The results in this chapter can be put in context with other fibres which are currently produced such as coagulation spun fibres, PET only fibres and high performance fibres (figure 6.15). Figure 6.15 shows the UTS Vs Young's modulus and the toughness Vs strain at break for PET-nanotube and PET-graphene fibres in comparison with high performance fibres like Kevlar<sup>51,74</sup>, Xylon<sup>75,76</sup> and Spectra<sup>75</sup>, with other PET-nanotube composite fibres<sup>29,30,32</sup>, with PET fibres<sup>29,30,32</sup>, with nanotube fibres<sup>77-81</sup> and also with coagulation spun fibres<sup>13,21,25,51,82-90</sup>. A data point at each concentration studied is shown here. The best modulus and toughness were sometimes obtained for different fibres. For this reason, the best strength is plotted with its corresponding Young's modulus but the toughness values reported for each fibre batch are not necessarily for the same fibre as for the strength value.

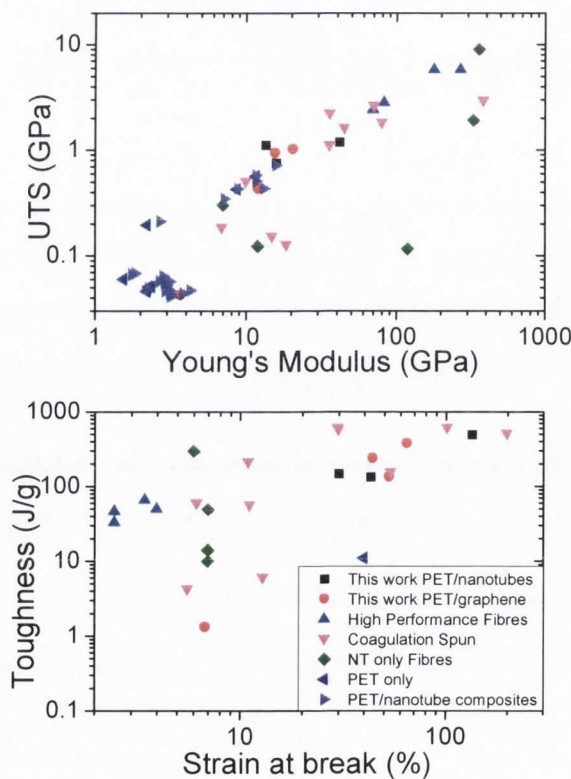


**Figure 6.15. Comparison of mechanical properties of this work with other fibres from literature**<sup>13,20,21,25,29-31,75-78,80,82-93</sup>.

The PET-nanotube and PET-graphene composites show maximum strengths of 1.19 GPa and 1.01 GPa respectively. PET-nanotube composites also have maximum Young's modulus value of 41.7 GPa while PET-graphene composites have a maximum Young's modulus of 20.56 GPa. These fibres have a higher strength and Young's modulus than other PET-nanotube composites reported in literature with the next highest being 0.7 GPa<sup>29,30,32</sup>. They also show higher values than PET only fibres which have a maximum strength of 0.426 GPa<sup>29,30,32</sup>. While some nanotube only fibres show lower strengths than the composites produced in this work, some show superior strengths and Young's modulus values than the composites reported here<sup>77-81</sup>. Windle et al. produced nanotube only fibres with impressive strengths of 9 GPa<sup>80</sup>. These PET composites also lie in the mid range of coagulation spun composites<sup>13,21,25,51,82,84,85,87,89,90</sup> but have the advantage of industrial style processing in comparison with these composites. While the strength and Young's modulus values of the composites prepared in this work are below that of high performance composites like Kevlar<sup>74</sup> and Xylon<sup>75,76</sup>, they can be processed at a much lower cost than these fibres.

PET-nanotube composites display higher toughness values than PET-graphene composites with values of 490 J/g and 372 J/g respectively. Both types of composites in this work show higher toughness values than high performance fibres such as Kevlar (33 J/g)<sup>51,74</sup>, Xylon (66 J/g)<sup>75,76</sup> and Spectra (50 J/g)<sup>75</sup>. Along with this, some fibres are also tougher than nanotube only fibres<sup>77-79</sup>. They show similar toughness values to the highest toughness coagulation spun fibres (max 600 J/g)<sup>13,21,51,83-88</sup> into which extensive research has been carried out.

## 6.5 Conclusions

A method has been developed to produce PET-nanotube and PET-graphene fibres by combining solution and melt processing. These fibres have exceptional mechanical properties, similar to the best polyester fibres ever reported. For low loadings of both filler types, the modulus and strength increased linearly with volume fraction with slopes far in excess of rule of mixtures predictions, suggesting the presence of filler-induced crystallinity. For nanotube based composites, the diameter dependence of the composites suggest the modulus to be limited by nanotube orientation while the strength is limited by orientation and defects. However, for PET-graphene composites, the modulus was relatively invariant with D suggesting orientation to be relatively unaffected by diameter reduction. While the strength did depend on fibre diameter, the dependence was much weaker than for the nanotube fibres. This is consistent with orientation playing virtually

no role and the strength being controlled largely by defects. It is noted that the ability to successfully reinforce commodity plastics with graphene is significant for purely economic reasons. For example the cost of graphite is <€5/kg. This means the material cost of adding 0.5wt% (i.e. where the maximum mechanical reinforcement is observed) graphene to a PET fibre is <0.03 c per km for a fibre with D=100 µm (c.f. PET fibre costs ~1-3 c per 1000 km). As the cost of high quality SWNT is ~€500/g, the cost per km of adding 2wt% SWNT is approximately €100. In reality, the cost of exfoliation/mixing etc will increase these estimates somewhat. However, reinforcement using graphene may be economically viable in a way that nanotubes never could be.

## 6.8 References

- 1 Sesto, B., Yoneyamam, M. & Xiaoxiong, H. Polyester Fibers. *Chemical Economics Handbook Report* (2010).
- 2 Gupta, V. B. & Kothari, V. K. *Manufactured Fibre Technology*. (Chapman & Hall, 1997).
- 3 Hansen, S. & Atwood, K. B. in *Kirk-Othmer Encyclopedia of Chemical Technology*. (John Wiley and Sons, 2005).
- 4 Callister, W. D. *Materials Science and Engineering an Introduction*. (John Wiley and sons, 2007).
- 5 Chen, P., Afshari, M., Cuculo, J. A. & Kotek, R. Direct Formation and Characterization of a Unique Precursor Morphology in the Melt-Spinning of Polyesters. *Macromolecules* **42**, 5437-5441 (2009).
- 6 Chae, H. G. & Kumar, S. Rigid-rod polymeric fibers. *Journal of Applied Polymer Science* **100**, 791-802 (2006).
- 7 Breuer, O. & Sundararaj, U. Big returns from small fibers: A review of polymer/carbon nanotube composites. *Polymer Composites* **25**, 630-645 (2004).
- 8 Coleman, J. N., Khan, U., Blau, W. J. & Gun'ko, Y. K. Small but strong: A review of the mechanical properties of carbon nanotube-polymer composites. *Carbon* **44**, 1624-1652 (2006).
- 9 Saheb, D. N. & Jog, J. P. Natural fiber polymer composites: A review. *Advances in Polymer Technology* **18**, 351-363 (1999).
- 10 Padawer, G. E. & Beecher, N. On Strength and Stiffness of Planar Reinforced Plastic Resins. *Polymer Engineering and Science* **10**, 185 (1970).
- 11 Rosenthal, J. A Model For Determining Fiber Reinforcement Efficiencies And Fiber Orientation In Polymer Composites. *Polymer Composites* **13**, 462-466 (1992).
- 12 Hull, D. & Clyne, T. W. *An introduction to composite materials*. (Cambridge University Press, 1996).
- 13 Minus, M. L., Chae, H. G. & Kumar, S. Interfacial Crystallization in Gel-Spun Poly(vinyl alcohol)/Single-Wall Carbon Nanotube Composite Fibers. *Macromolecular Chemistry and Physics* **210**, 1799-1808 (2009).
- 14 Belytschko, T., Xiao, S. P., Schatz, G. C. & Ruoff, R. S. Atomistic simulations of nanotube fracture. *Physical Review B* **65** (2002).
- 15 Li, C. Y. & Chou, T. W. A structural mechanics approach for the analysis of carbon nanotubes. *International Journal of Solids and Structures* **40**, 2487-2499 (2003).

- 16 Lu, J. P. Elastic properties of single and multilayered nanotubes. *Journal of Physics and Chemistry of Solids* **58**, 1649-1652 (1997).
- 17 Lu, J. P. Elastic properties of carbon nanotubes and nanoropes. *Physical Review Letters* **79**, 1297-1300 (1997).
- 18 Yakobson, B. I., Campbell, M. P., Brabec, C. J. & Bernholc, J. High strain rate fracture and C-chain unraveling in carbon nanotubes. *Computational Materials Science* **8**, 341-348 (1997).
- 19 Yu, M. F., Files, B. S., Arepalli, S. & Ruoff, R. S. Tensile loading of ropes of single wall carbon nanotubes and their mechanical properties. *Physical Review Letters* **84**, 5552-5555 (2000).
- 20 Dalton, A. B. *et al.* Super-tough carbon-nanotube fibres - These extraordinary composite fibres can be woven into electronic textiles. *Nature* **423**, 703-703 (2003).
- 21 Miaudet, P. *et al.* Hot-drawing of single and multiwall carbon nanotube fibers for high toughness and alignment. *Nano Letters* **5**, 2212-2215 (2005).
- 22 Minus, M. L., Chae, H. G. & Kumar, S. Single wall carbon nanotube templated oriented crystallization of poly(vinyl alcohol). *Polymer* **47**, 3705-3710 (2006).
- 23 Young, K. *et al.* Strong Dependence of Mechanical Properties on Fiber Diameter for Polymer-Nanotube Composite Fibers: Differentiating Defect from Orientation Effects. *Acs Nano* **4**, 6989-6997 (2010).
- 24 Kearns, J. C. & Shambaugh, R. L. Polypropylene fibers reinforced with carbon nanotubes. *Journal of Applied Polymer Science* **86**, 2079-2084 (2002).
- 25 Vigolo, B. *et al.* Macroscopic fibers and ribbons of oriented carbon nanotubes. *Science* **290**, 1331-1334 (2000).
- 26 Ma, H., Zeng, J., Realff, M. L., Kumar, S. & Schiraldi, D. A. Processing, structure, and properties of fibers from polyester/carbon nanofiber composites. *Composites Science and Technology* **63**, 1617-1628 (2003).
- 27 Chang, J.-H., Kim, S. J., Joo, Y. L. & Im, S. Poly(ethylene terephthalate) nanocomposites by in situ interlayer polymerization: the thermo-mechanical properties and morphology of the hybrid fibers. *Polymer* **45**, 919-926 (2004).
- 28 Anand, K. A. *et al.* PET-SWNT Nanocomposite Fibers through Melt Spinning. *International Journal of Polymeric Materials* **59**, 438-449 (2010).
- 29 Kim, J. Y., Park, H. S. & Kim, S. H. Multiwall-carbon-nanotube-reinforced poly(ethylene terephthalate) nanocomposites by melt compounding. *Journal of Applied Polymer Science* **103**, 1450-1457 (2007).
- 30 Mun, S. J., Jung, Y. M., Kim, J.-C. & Chang, J.-H. Poly(ethylene terephthalate) nanocomposite fibers with functionalized multiwalled carbon nanotubes via in-situ polymerization. *Journal of Applied Polymer Science* **109**, 638-646 (2008).
- 31 Li, Z., Luo, G., Wei, F. & Huang, Y. Microstructure of carbon nanotubes/PET conductive composites fibers and their properties. *Composites Science and Technology* **66**, 1022-1029 (2006).
- 32 Anand K, A., Agarwal, U. S. & Joseph, R. Carbon nanotubes-reinforced PET nanocomposite by melt-compounding. *Journal of Applied Polymer Science* **104**, 3090-3095 (2007).
- 33 Hernandez, Y. *et al.* High-yield production of graphene by liquid-phase exfoliation of graphite. *Nat Nano* **3**, 563-568 (2008).
- 34 Khan, U., O'Neill, A., Lotya, M., De, S. & Coleman, J. N. High-Concentration Solvent Exfoliation of Graphene. *Small* **6**, 864-871 (2010).
- 35 Khan, U. *et al.* Solvent-Exfoliated Graphene at Extremely High Concentration. *Langmuir* **27**, 9077-9082 (2011).
- 36 Bergin, S. D. *et al.* Towards Solutions of Single-Walled Carbon Nanotubes in Common Solvents. *Advanced Materials* **20**, 1876-1881 (2008).

- 37 Coleman, J. N. Liquid-Phase Exfoliation of Nanotubes and Graphene. *Advanced Functional Materials* **19**, 3680-3695 (2009).
- 38 Giordani, S. *et al.* Debundling of Single-Walled Nanotubes by Dilution: Observation of Large Populations of Individual Nanotubes in Amide Solvent Dispersions. *The Journal of Physical Chemistry B* **110**, 15708-15718 (2006).
- 39 Khan, U., O'Neill, A., Lotya, M., De, S. & Coleman, J. N. High-Concentration Solvent Exfoliation of Graphene. *Small* **6**, 864-871 (2010).
- 40 Blond, D. *et al.* Enhancement of Modulus, Strength, and Toughness in Poly(methyl methacrylate)-Based Composites by the Incorporation of Poly(methyl methacrylate)-Functionalized Nanotubes. *Advanced Functional Materials* **16**, 1608-1614 (2006).
- 41 Amornsakchai, T., Cansfield, D. L. M., Jawad, S. A., Pollard, G. & Ward, I. M. The Relation between Filament Diameter and Fracture Strength for Ultra-High-Modulus Polyethylene Fibers. *Journal of Materials Science* **28**, 1689-1698 (1993).
- 42 Arinstein, A., Burman, M., Gendelman, O. & Zussman, E. Effect of supramolecular structure on polymer nanofibre elasticity. *Nat. Nanotechnol.* **2**, 59-62 (2007).
- 43 Chae, H. G., Choi, Y. H., Minus, M. L. & Kumar, S. Carbon nanotube reinforced small diameter polyacrylonitrile based carbon fiber. *Composites Science and Technology* **69**, 406-413 (2009).
- 44 Ji, Y., Li, B. Q., Ge, S. R., Sokolov, J. C. & Rafailovich, M. H. Structure and nanomechanical characterization of electrospun PS/clay nanocomposite fibers. *Langmuir* **22**, 1321-1328 (2006).
- 45 Wagner, H. D. Dependence of Fracture-Stress Upon Diameter in Strong Polymeric Fibers. *Journal of Macromolecular Science-Physics* **B28**, 339-347 (1989).
- 46 Wagner, H. D. Stochastic Concepts in the Study of Size Effects in the Mechanical Strength of Highly Oriented Polymeric Materials. *Journal of Polymer Science Part B-Polymer Physics* **27**, 115-149 (1989).
- 47 Blighe, F. M. *et al.* The Effect of Nanotube Content and Orientation on the Mechanical Properties of Polymer-Nanotube Composite Fibers: Separating Intrinsic Reinforcement from Orientational Effects. *Advanced Functional Materials* **21**, 364-371 (2011).
- 48 Coleman, J. N. *et al.* High-performance nanotube-reinforced plastics: Understanding the mechanism of strength increase. *Advanced Functional Materials* **14**, 791-798 (2004).
- 49 Coleman, J. N. *et al.* Reinforcement of polymers with carbon nanotubes. The role of an ordered polymer interfacial region. Experiment and modeling. *Polymer* **47**, 8556-8561 (2006).
- 50 Wang, Z., Ciselli, P. & Peijs, T. The extraordinary reinforcing efficiency of single-walled carbon nanotubes in oriented poly(vinyl alcohol) tapes. *Nanotechnology* **18**, 455709 (2007).
- 51 Dalton, A. B. *et al.* Super-tough carbon-nanotube fibres. *Nature* **423**, 703-703 (2003).
- 52 Haggemueller, R., Gommans, H. H., Rinzler, A. G., Fischer, J. E. & Winey, K. I. Aligned single-wall carbon nanotubes in composites by melt processing methods. *Chemical Physics Letters* **330**, 219-225 (2000).
- 53 Lee, C., Wei, X., Kysar, J. W. & Hone, J. Measurement of the Elastic Properties and Intrinsic Strength of Monolayer Graphene. *Science* **321**, 385-388 (2008).

- 54 Hu, H. W. & Chen, G. H. Electrochemically Modified Graphite Nanosheets and Their Nanocomposite Films with Poly(vinyl alcohol). *Polymer Composites* **31**, 1770-1775 (2010).
- 55 Jiang, L., Shen, X. P., Wu, J. L. & Shen, K. C. Preparation and Characterization of Graphene/Poly(vinyl alcohol) Nanocomposites. *Journal of Applied Polymer Science* **118**, 275-279 (2010).
- 56 Miller, S. G. *et al.* Characterization of epoxy functionalized graphite nanoparticles and the physical properties of epoxy matrix nanocomposites. *Composites Science and Technology* **70**, 1120-1125 (2010).
- 57 Putz, K. W., Compton, O. C., Palmeri, M. J., Nguyen, S. T. & Brinson, L. C. High-Nanofiller-Content Graphene Oxide-Polymer Nanocomposites via Vacuum-Assisted Self-Assembly. *Advanced Functional Materials* **20**, 3322-3329 (2010).
- 58 Ramanathan, T. *et al.* Functionalized graphene sheets for polymer nanocomposites. *Nat. Nanotechnol.* **3**, 327-331 (2008).
- 59 Steurer, P., Wissert, R., Thomann, R. & Mulhaupt, R. Functionalized Graphenes and Thermoplastic Nanocomposites Based upon Expanded Graphite Oxide. *Macromolecular Rapid Communications* **30**, 316-327 (2009).
- 60 Yang, X. M., Li, L. A., Shang, S. M. & Tao, X. M. Synthesis and characterization of layer-aligned poly(vinyl alcohol)/graphene nanocomposites. *Polymer* **51**, 3431-3435 (2010).
- 61 Zhao, X., Zhang, Q. H., Chen, D. J. & Lu, P. Enhanced Mechanical Properties of Graphene-Based Poly(vinyl alcohol) Composites. *Macromolecules* **43**, 2357-2363 (2010).
- 62 Gomez-Navarro, C., Burghard, M. & Kern, K. Elastic properties of chemically derived single graphene sheets. *Nano Letters* **8**, 2045-2049 (2008).
- 63 Gong, L. *et al.* Interfacial Stress Transfer in a Graphene Monolayer Nanocomposite. *Advanced Materials* **22**, 2694 (2010).
- 64 May, P., Khan, U., O'Neill, A. & Coleman, J. N. Approaching the theoretical limit for reinforcing polymers with graphene. *Advanced Materials (submitted)* (2011).
- 65 Bourlinos, A. B., Georgakilas, V., Zboril, R., Steriotis, T. A. & Stubos, A. K. Liquid-Phase Exfoliation of Graphite Towards Solubilized Graphenes. *Small* **5**, 1841-1845 (2009).
- 66 Catheline, A. *et al.* Graphene solutions. *Chemical Communications* **47**, 5470-5472 (2011).
- 67 Green, A. A. & Hersam, M. C. Solution Phase Production of Graphene with Controlled Thickness via Density Differentiation. *Nano Letters* **9**, 4031-4036 (2009).
- 68 Khan, U., May, P., O'Neill, A. & Coleman, J. N. Development of stiff, strong, yet tough composites by the addition of solvent exfoliated graphene to polyurethane. *Carbon* **48**, 4035-4041.
- 69 Lotya, M. *et al.* Liquid Phase Production of Graphene by Exfoliation of Graphite in Surfactant/Water Solutions. *Journal of the American Chemical Society* **131**, 3611-3620 (2009).
- 70 Lotya, M., King, P. J., Khan, U., De, S. & Coleman, J. N. High-Concentration, Surfactant-Stabilized Graphene Dispersions. *ACS Nano* **4**, 3155-3162 (2010).
- 71 Nuvoli, D. *et al.* High concentration few-layer graphene sheets obtained by liquid phase exfoliation of graphite in ionic liquid. *Journal of Materials Chemistry* **21**, 3428-3431 (2011).
- 72 O'Neill, A., Khan, U., Nirmalraj, P. N., Boland, J. J. & Coleman, J. N. Graphene Dispersion and Exfoliation in Low Boiling Point Solvents. *The Journal of Physical Chemistry C* **115**, 5422-5428 (2011).

- 73 Vadukumpully, S., Paul, J. & Valiyaveetil, S. Cationic surfactant mediated exfoliation of graphite into graphene flakes. *Carbon* **47**, 3288-3294 (2009).
- 74 Dubin, R. A., Callegari, G. C., Kohn, J. & Neimark, A. V. Carbon nanotube fibers are compatible with mammalian cells and neurons. *Ieee Transactions on Nanobioscience* **7**, 11-14 (2008).
- 75 O'Connor, I., Hayden, H., Coleman, J. N. & Gun'ko, Y. K. High-Strength, High-Toughness Composite Fibers by Swelling Kevlar in Nanotube Suspensions. *Small* **5**, 466-469 (2009).
- 76 Hearle, J. W. S. High Performance Fibres. (Woodhead Publishing, 2001).
- 77 Ericson, L. M. *et al.* Macroscopic, Neat, Single-Walled Carbon Nanotube Fibers. *Science* **305**, 1447-1450 (2004).
- 78 Razal, J. M., Gilmore, K. J. & Wallace, G. G. Carbon nanotube biofiber formation in a polymer-free coagulation bath. *Advanced Functional Materials* **18**, 61-66 (2008).
- 79 Liu, Phang, I. Y., Shen, L., Chow, S. Y. & Zhang, W.-D. Morphology and Mechanical Properties of Multiwalled Carbon Nanotubes Reinforced Nylon-6 Composites. *Macromolecules* **37**, 7214-7222 (2004).
- 80 Koziol, K. *et al.* High-Performance Carbon Nanotube Fiber. *Science* **318**, 1892-1895 (2007).
- 81 Fang, F. Z., Xu, Z. W., Dong, S. & Zhang, G. X. High Aspect Ratio Nanometrology using Carbon Nanotube Probes in Atomic Force Microscopy. *CIRP Annals - Manufacturing Technology* **56**, 533-536 (2007).
- 82 Barisci, J. N. *et al.* Properties of carbon nanotube fibers spun from DNA-stabilized dispersions. *Advanced Functional Materials* **14**, 133-138 (2004).
- 83 Dalton, A. B. *et al.* Continuous carbon nanotube composite fibers: properties, potential applications, and problems. *Journal of Materials Chemistry* **14**, 1-3 (2004).
- 84 Granero, A. J., Razal, J. M., Wallace, G. G. & Panhuis, M. I. H. Spinning Carbon Nanotube-Gel Fibers Using Polyelectrolyte Complexation. *Advanced Functional Materials* **18**, 3759-3764 (2008).
- 85 Munoz, E. *et al.* Multifunctional carbon nanotube composite fibers. *Advanced Engineering Materials* **6**, 801-804 (2004).
- 86 Munoz, E. *et al.* Highly conducting carbon nanotube/polyethyleneimine composite fibers. *Advanced Materials* **17**, 1064 (2005).
- 87 Neri, W. *et al.* Surfactant-free spinning of composite carbon nanotube fibers. *Macromolecular Rapid Communications* **27**, 1035-1038 (2006).
- 88 Razal, J. M. *et al.* Arbitrarily shaped fiber assemblies from spun carbon nanotube gel fibers. *Advanced Functional Materials* **17**, 2918-2924 (2007).
- 89 Xu, X. *et al.* Fabrication of high strength PVA/SWCNT composite fibers by gel spinning. *Carbon* **48**, 1977-1984.
- 90 Zhang, X. *et al.* Gel spinning of PVA/SWNT composite fiber. *Polymer* **45**, 8801-8807 (2004).
- 91 Anand, K. A. *et al.* PET-SWNT Nanocomposite Fibers through Melt Spinning. *International Journal of Polymeric Materials* **59**, 438-449.
- 92 Mark, J. E. Polymer Data Handbook. (Oxford University Press).
- 93 Zhang, X. *et al.* Strong Carbon-Nanotube Fibers Spun from Long Carbon-Nanotube Arrays. *Small* **3**, 244-248 (2007).

# Chapter 7

## Conclusions and Future Work

### 7.1 Conclusions

A method to control and measure the nanotube volume fraction in poly(vinyl) alcohol-nanotube fibres has been developed. The effect of nanotube volume fraction on the mechanical properties of fibres was studied, facilitating analysis using models such as the rule of mixtures. Both the fibre modulus,  $Y$ , and strength,  $\sigma_B$ , scale linearly with nanotube volume fraction up to  $V_f \sim 10\%$ , after which saturation occurs. A value of  $dY/dV_f = 254$  GPa and  $d\sigma_B/dV_f = 2.8$  GPa was measured in the linear region. By drawing fibres with  $V_f < 10\%$ , these values could be increased to  $dY/dV_f = 600$  GPa and  $d\sigma_B/dV_f = 7$  GPa. Raman measurements show the Herman's orientation parameter,  $S$ , to increase with drawing, indicating that significant nanotube alignment occurs. Raman spectroscopy also shows that the nanotube effective modulus,  $Y_{Eff}$ , increases with drawing, due to the increased alignment. As expected for simple two-phase composites, the undrawn samples display  $dY/dV_f = Y_{Eff}$ . However, for draw ratios above 22%,  $dY/dV_f > Y_{Eff}$ , suggesting that drawing induces polymer crystallinity. An empirical relationship between Krenchel's nanotube orientation efficiency factor,  $\eta_o$ , and  $S$  was calculated. Data showing  $Y_{Eff}$  versus  $S$  was fitted, confirming that the fibre modulus scales linearly with  $\eta_o$ . In addition, the Young's modulus of the nanotubes used in this work was estimated to be  $Y_{NT} = 480$  GPa. This value is about half of the expected value of 1 TPa, suggesting that these composites are limited either by an imperfect polymer-nanotube interface or that the nanotubes are less stiff than expected. It was shown that the fibre strength also scales linearly with  $\eta_o$ . The effective interfacial shear strength and critical length could be calculated to be 40 MPa and 1250 nm respectively.

The mechanical properties of polymer-nanotube fibres as a function of fibre diameter were characterised. A strong dependence of fibre modulus and strength with diameter was observed. This  $D$  dependence was attributed to a combination of the effects of nanotube orientation and surface defects. The balance of these effects was determined and showed that orientation effects are dominant for fibre diameters between 4 and 50  $\mu\text{m}$ . While the defect contribution to the diameter dependence is relatively small ( $D^{-0.29}$ ), this could probably be reduced dramatically by improving the spinning process. The orientation contribution to the diameter dependence is larger ( $D^{-0.64}$ ). However, it should be possible to change  $\gamma$  by changing the processing conditions. A reduction of  $\gamma$ , possibly by optimisation of needle and pipe diameters and flow rates, would reduce the orientation contribution to the diameter dependence. Such improvements could result in extremely high stiffness and strength for higher diameter fibres. For low diameter fibres where the nanotubes are well aligned, fibres have been prepared with moduli approaching 250 GPa and strength of 2.9 GPa.

An alternative method of composite fibre production was also described. PET-nanotube and PET-graphene fibres were produced using a combination of both solution processing and melt processing. This was the first time that fibres reinforced with graphene have been produced. A volume fraction study was also conducted to establish the most effective volume fraction for composite reinforcement. PET-nanotube fibres with a strength of 1.19 GPa and a Young's modulus of 41.7 GPa were produced. PET-graphene fibres had a maximum strength of 1.01 GPa and Young's modulus of 20.56 GPa. The use of graphene may provide a more economically viable method of composite reinforcement due to its extremely low cost and effectiveness in increasing polymer strength and modulus.

## 7.2 Future Work

The work presented in this thesis shows that very strong composite fibres can be produced by reinforcing polymers with carbon nanotubes and graphene. However, there is still room for improvement and potentially very strong, stiff composites could be produced for a larger range of diameters. It is known that PVA fibres with different molecular weights result in fibres with very different strengths. Other brands of PVA could be investigated and molecular weight dependencies on the mechanical properties of composites could be established. Fibres made from nanotubes of different lengths could be investigated. An increase in nanotube length should increase the mechanical properties of the PVA-nanotube fibres described in this thesis. The drawing technique could also be

improved. While it was seen that fibre drawing significantly improved the mechanical properties of PVA-nanotube fibres, hot drawing of fibres could also be investigated to see if further drawing and hence an improvement in mechanical properties is possible. A combination of such improvements could result in extremely high stiffness and strength for higher diameter fibres. Also, the possibility of nanotube templated crystallinity in these fibres must also be investigated further to establish if low diameter fibres have well aligned polymer chains, resulting in  $Y/V_f > dY/dV_f$  and  $\sigma_B/V_f > d\sigma_B/dV_f$ .

Surfactant free fibre spinning could also be studied. It is hoped that fibres prepared from functionalised nanotubes that do not require a surfactant to disperse can also be produced, optimised and fully characterised.

While there has been extensive research into coagulation spinning of PVA-nanotube fibres in literature, PET-nanotube and PET-graphene fibres were produced for the first time using the preparation method described in this thesis. Thus, there are many improvements on this system which could be investigated. The nanotube dispersion could be optimised further by sonicating for varying times resulting in fibres containing nanotubes of lengths. The graphene dispersion could also be improved. If the aspect ratio of the graphene flakes used for this work was increased, improvements in the mechanical properties of fibres should be expected. As with the case with PVA fibres, the use of hot drawing could also be investigated to see if further drawing is possible using this technique.

It would also be interesting to investigate the use of biosteel (spider silk) for fibre production. Spider silk is flexible and lightweight and has exceptional strength and toughness. Spider dragline have Young's modulus, strength and toughness values of 10GPa, ~1GPa and 123J/g respectively<sup>1</sup>. Native spider silk cannot be used experimentally due to failure to domesticate spiders. However recently, the production of silk by protein synthesis in mammalian cells has been achieved<sup>2</sup>. This silk (known as Biosteel) has already been used by Blond et al. in carbon nanotube composite films<sup>1</sup> and by Lazaris et al in coagulation spun fibres<sup>2</sup>. Investigation into the incorporation of carbon nanotubes into coagulation spun Biosteel composites should result in both strong and tough fibres.

It is hoped that, because of the advances made in this thesis that there is a better insight into what makes a fibre strong and into how the mechanical properties of fibres can be improved. It is hoped that building on this work will result in even stronger and stiffer composites and further advances in carbon nanotube reinforced fibres will be achieved using this work as a strong foundation.

### 7.3 List of Publications

- “High strength composite fibres from polyester filled with nanotubes and graphene” Umar Khan, Karen Young, Arlene O’ Neill and Jonathan N. Coleman. **In preparation** (2011).
- “Two-dimensional nano-sheets produced by liquid exfoliation of layered materials”, Jonathan N Coleman, Mustafa Lotya, Arlene O’ Neill, Shane D. Bergin, Paul J. King, Umar Khan, Karen Young et al., **Science**, 331 (6017), 568-571 (2011).
- ‘Strong Dependence of Mechanical Properties on Fibre Diameter for Polymer-Nanotube Composite Fibres: Differentiating Defect from Orientation Effects’, Karen Young, Fiona Blighe, Jonathan N. Coleman et al., **ACS Nano**, 4, 11, 6989-6997 (2010).
- ‘The Effect of Nanotube Content and Drawing on the Mechanical Properties of Polymer-Nanotube Composite Fibres: Separating Intrinsic Reinforcement from Orientational Effects’, Fiona Blighe, Karen Young, Jonathan N. Coleman **Advanced Functional Materials**, 21, 2, 364-371, (2010).
- ‘Strong, Tough, Electrospun Polymer-Nanotube Composite Membranes with Extremely Low Density’, David Blonde, William Walshe, Karen Young, Jonathan N. Coleman, et al. **Advanced Functional Materials**, 18, 17 (2008).
- ‘Chemical and Structural Diversity in Chiral Magnesium Tartrates and their Racemic and *Meso* Analogues’ Kinson Kam, Karen Young and Anthony K. Cheetham. **Crystal Growth & Design**, 7, 1522 (2007)

### 7.4 References

- 1 Blond, D., McCarthy, D. N., Blau, W. J. & Coleman, J. N. Toughening of Artificial Silk by Incorporation of Carbon Nanotubes. *Biomacromolecules* 8, 3973-3976 (2007).
- 2 Lazaris, A. *et al.* Spider Silk Fibers Spun from Soluble Recombinant Silk Produced in Mammalian Cells. *Science* 295, 472-476 (2002).